Contusion Progression in Traumatic Brain Injury

Mathew Rhys Guilfoyle

St. John's College

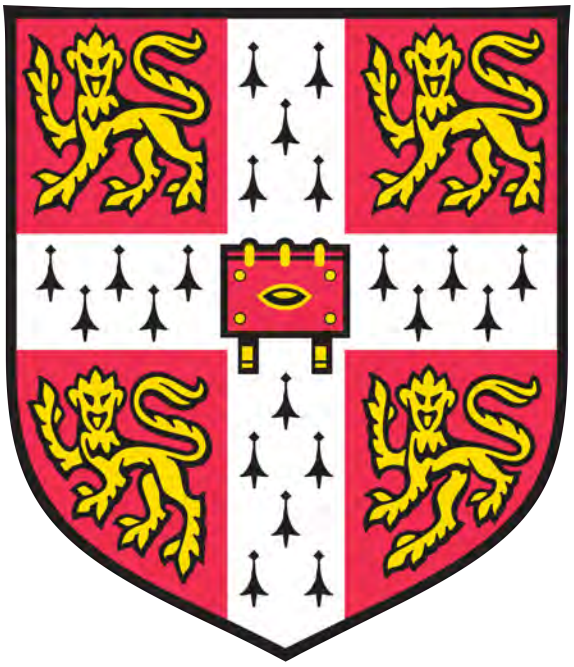

June 2019

This dissertation is submitted for the degree of Doctor of Philosophy

Declaration

This dissertation is the result of my own work and includes nothing which is the outcome of work done in collaboration except as declared in the Preface and specified in the text.

It is not substantially the same as any that I have submitted, or, is being concurrently submitted for a degree or diploma or other qualification at the University of Cambridge or any other University or similar institution except as declared in the Preface and specified in the text. I further state that no substantial part of my dissertation has already been submitted, or, is being concurrently submitted for any such degree, diploma or other qualification at the University of Cambridge or any other University or similar institution except as declared in the Preface and specified in the text

It does not exceed the prescribed word limit for the Degree Committee of the Faculties of Clinical Medicine and Veterinary Medicine.

Abstract

Contusion Progression in Traumatic Brain Injury

Mathew Rhys Guilfoyle

Cerebral contusions that result from brain trauma have the propensity to enlarge over the days following injury, including extension of the haemorrhage core and swelling of the surrounding peri-contusional brain. This secondary injury increases the likelihood of death and severe disability, and interventions to prevent or limit contusion progression may improve clinical outcomes. In preclinical studies a number of pathophysiological process have been identified that contribute to brain oedema including blood brain barrier (BBB) disruption, neuroinflammation, and cerebral metabolic dysfunction. This work has set out to measure and quantify contusion progression in TBI patients, characterise BBB permeability with computed tomography imaging, and identify key mediators of this process using intracerebral microdialysis.

- **Study I**: A robust and effective stereological method for measuring the volume of brain lesions was validated and applied to a cohort of TBI patients to examine the temporal course of contusion progression. Intracranial pressure and brain lactate/pyruvate ratio were found to be associated with the magnitude of contusion expansion.
- **Study II**: Dynamic contrast enhanced computed tomography (DCE-CT) was applied in patients with brain contusions to quantify BBB permeability. The imaging showed profound reduction in cerebral blood flow associated with contusions but did not show evidence of contrast extravasation or BBB permeability.
- **Study III**: Paired microdialysis catheters, one inserted in proximity to a contusion and another in non-injured brain, were used to characterise the peri-contusional inflammatory response with a multiplex assay of 42 cytokines, chemokines, and growth factors. Peri-contusional tissue was found to exhibit an early pro-inflammatory signature.

- **Study IV**: A paired microdialysis study of pericontusional expression of matrix metalloproteinases (MMP). Specific increase in the expression of MMP-9 was identified in pericontusional brain

- **Study V**: Nitric oxide (NOx) concentrations were assayed in pericontusional and uninjured brain with paired microdialysis. NOx levels were lower in pericontusional brain and exhibited significant correlations with brain glucose, pyruvate, and lactate.

- **Study VI**: Microdialysis data from 619 TBI patients with collated to explore the physiological correlates of deranged metabolism and elevated LPR. Cerebral glucose was found to a key determinant of LPR.

The implications of these findings in the context of existing knowledge of BBB permeability, inflammation, and cerebral metabolism in TBI are discussed. Future investigations to clarify the mechanisms highlighted, and potential therapeutic studies directed at reducing contusion progression and brain oedema are suggested.

Acknowledgements

I wish thank my supervisor Prof Peter Hutchinson for his direction and advice throughout this project. I also greatly appreciate the many helpful discussions with Dr Keri Carpenter, Mr Adel Helmy, and Prof David Menon.

I am indebted to my parents for their unfailing support at all times. This work would not have been possible without the encouragement, patience, and understanding of Allanah, Imogen, and Ted, for which I am very grateful.

Publications

Papers

- Guilfoyle MR, Carpenter KL, Helmy A, Pickard JD, Menon DK, Hutchinson PJ. Matrix Metalloproteinase Expression in Contusional Traumatic Brain Injury: A Paired Microdialysis Study. Journal of Neurotrauma. 2015;32(20):1553-9. doi: 10.1089/neu.2014.3764

Conference Abstracts

- Guilfoyle MR, Donnelly J, Stovell MS, Timofeev I, Helmy A, Carpenter KL, Menon DK, Smielewski P, Czosnyka M, Hutchinson PJ. Lactate/pyruvate ratio in traumatic brain injury: assessing prognostic impact and defining therapeutic strategies. Society of British Neurological Surgeons, London, September 2018 (Oral Presentation Prize)

- Guilfoyle MR, Timofeev I, Helmy A, Carpenter KL, Menon DK, Smielewski P, Czosnyka M, Hutchinson PJ, Time course and physiological determinants of brain lactate/ pyruvate ratio following traumatic brain injury. Congress of Neurological Surgeons, Boston, October 2017

- Guilfoyle MR, Timofeev I, Helmy A, Carpenter KL, Czosnyka M, Menon DK, Hutchinson PJ, Physiological determinants of brain lactate/ pyruvate ratio following traumatic brain injury. Society of British Neurological Surgeons, Oxford, March 2017

- Guilfoyle MR, Helmy A, Carpenter KLH, Menon DK, Pickard JD, Hutchinson PJ. Matrix Metalloproteinase Expression in Focal Traumatic Brain Injury Society of British Neurological Surgeons, Southampton, April 2015

- Guilfoyle MR, Helmy A, Carpenter KLH, Menon DK, Pickard JD, Hutchinson PJ. Matrix metalloproteinase 9 levels are increased in peri-contusional brain: a paired microdialysis study. International Neurotrauma Society Meeting, Budapest, March 2014 (Poster Prize)

Abbreviations

ABP	Arterial Blood Pressure
AIF	Arterial Input Function
ATP	Adenosine Triphosphate
BBB	Blood Brain Barrier
CBF	Cerebral Blood Flow
CBV	Cerebral Blood Volume
CO_2	Carbon Dioxide
CPP	Cerebral Perfusion Pressure
CSF	Cerebrospinal Fluid
CT	Computed Tomography
DCE	Dynamic Contrast Enhanced
GAMM	Generalised Additive Mixed Model
GCS	Glasgow Coma Score
GOS	Glasgow Outcome Scale
ICH	Intracerebral Haemorrhage
ICP	Intracranial Pressure
IL	Interleukin
IQR	Interquartile range
LPR	Lactate Pyruvate Ratio
MCP	Monocyte Chemoattractant Protein
MIP	Maximum Intensity Projection
MMP	Matrix Metalloproteinase
MNI	Montreal Neurological Institute
MRI	Magnetic Resonance Imaging
MTT	Mean Transit Time
MWCO	Molecular Weight Cut-Off

NOS Nitric Oxide Synthase

NOx Nitric Oxide products (combined NO_2 and NO_3)

PCA Principal Components Analysis

PET Positron Emission Tomography

PLS Partial Least Squares

$PbtO_2$ Brain tissue oxygen tension

PRx Pressure Reactivity index

ROS Reactive Oxygen Species

ROC Receiver Operating Characteristic

ROI Region of Interest

SEM Standard Error of the Mean

SPECT Single Photon Emission Computed Tomography

TBI Traumatic Brain Injury

TCA Tricarboxylic Acid

TJ Tight Junction

TTP Time to Peak

TTS Time to Start

TTD Time to Drain

VEGF Vascular Endothelial Growth Factor

VOI Volume of Interest

Contents

Chapter 1

General Overview

1.1 Traumatic Brain Injury

1.1.1 Incidence and Outcome

Traumatic Brain Injury (TBI) remains the leading cause of death and disability amongst young people (i.e age <40 years), and the annual incidence has continued to increase over the last decade[1]. In the UK in 2014-15, TBI was the principal cause for over 175,000 admissions to hospital and necessitated around 5000 intensive care unit (ICU) admissions.

Mortality for patients presenting with severe TBI i.e. Glasgow Coma Score (GCS) <8, is 20-40% [168, 55, 139] Furthermore, 50-70% of patients survive with significant cognitive and physical disability [139]. Together these result in TBI having major social and economic impact, both for patients themselves and their families and relatives, and there is a self-evident motive for continued investigation into understanding the pathophysiology of TBI and identifying therapeutic strategies to improve outcomes.

1.1.2 Primary vs. Secondary Injury

The neurological outcome from TBI is determined both by the severity of the primary injury i.e. the degree of immediate irreversible axonal disruption and cell loss due to mechanical forces at the time of impact, and the ensuing secondary insults that exacerbate the extent of tissue destruction over the subsequent hours and days. The major secondary insults that are known to impact

[1]UK Hospital Episode Statistics http://www.hscic.gov.uk; useful summary by the Headway TBI support group: https://www.headway.org.uk/media/2881/brain-injury-statistics-methodology-injury-categories-and-further-notes.pdf

on survival and functional outcome include systemic hypotension and hypoxia, raised intracranial pressure, and cerebral dysautoregulation, all of which ultimately result in inadequate tissue perfusion and ischaemia [35, 91]. Current medical and surgical management of severe TBI is fundamentally based on maintaining these parameters within normal physiological ranges during the first several days following injury when the traumatised brain is particularly vulnerable. In particular, avoidance of raised intracranial pressure (ICP) and reduced cerebral perfusion pressure (CPP) is the key target of modern goal-directed tiered neurocritical care protocols, involving escalation of increasingly intensive medical treatment and, ultimately, surgical decompressive craniectomy for patients with refractory intracranial hypertension (Fig 1.1).

Within the fixed confines of the skull the principal variables that contribute to intracranial pressure, in the context of TBI, are extra- and intra-axial mass lesions (i.e. extradural, subdural or intraparenchymal haematomas), hydrocephalus, cerebral blood volume, and the accumulation of brain water content distributed between the interstitial and intracellular spaces as different forms of cerebral oedema. The latter of these factors is the most challenging to directly treat. Mass lesions and hydrocephalus can be rectified with surgery, and intracranial blood volume can be, within limits, readily manipulated through control of ventilation and arterial CO_2 tension. In contrast, brain oedema may be refractory to all interventions [177].

1.2 Cerebral Contusions and Brain Oedema

Around 8% of all TBI patients and over a third of those with severe TBI have haemorrhagic parenchymal mass lesions or contusions [81]. Concomitant with the disruption of neurons and glia the transfer of kinetic energy at the moment of impact causes shearing of microvessels and extravasation of blood. Exposure of intracellular substances and the products of early cellular necrosis are key instigators of a multitude of secondary injury processes which, although representing highly conserved 'normal' responses to injury, frequently have deleterious effects on cells and tissues that survived the primary injury [96]. Breakdown products from haemolysis of extravasated erythrocytes are also highly toxic to neurons and other CNS cells, via both excitotoxic and haem-dependent mechanisms [167]. Furthermore, microvascular rupture also results in localised loss of tissue perfusion and ischaemia, further compounding secondary injury within surrounding pericontusional tissue.

Consequences of continued microvascular disruption and dysfunction include further escape of

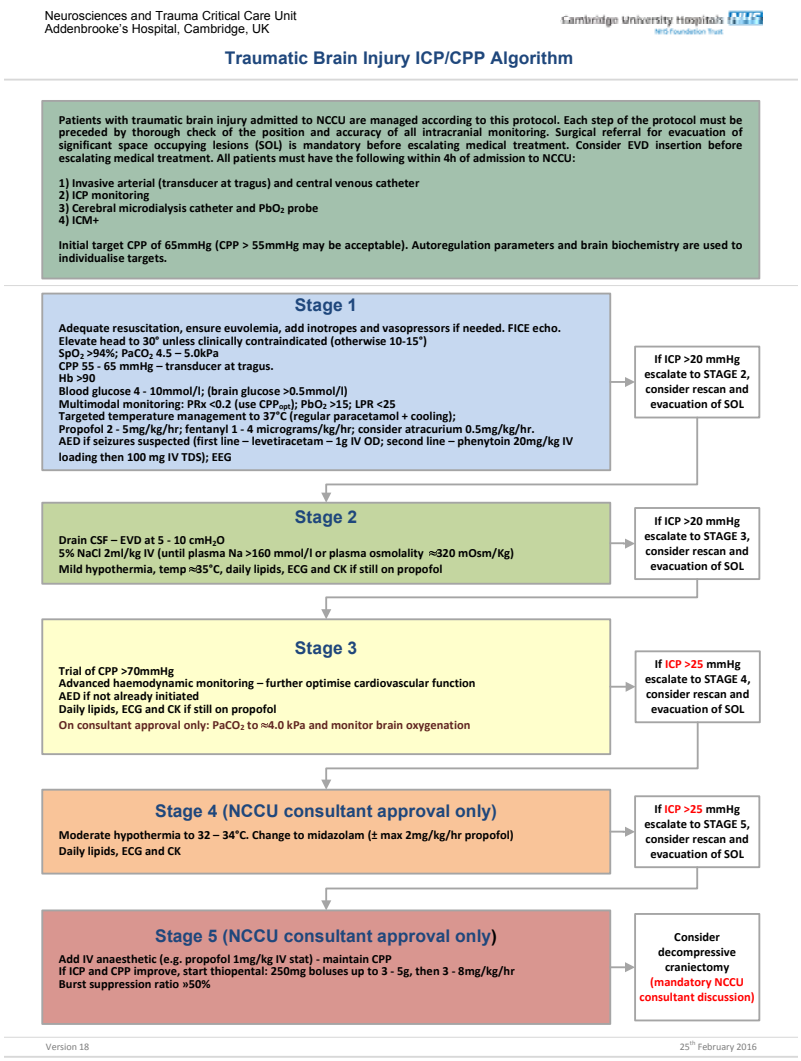

Figure 1.1: Addenbrooke's Hospital Neurocritical Care Unit (NCCU) ICP/CPP Protocol

blood in to the intersitial space, endothelial ischaemia and swelling causing microvessel thrombosis or occlusion, loss of integrity of the blood-brain barrier, and progressive oedema [154]. The mass effect of an expanding volume of contusion and oedema further compromises local perfusion and contribute to raised intracranial pressure affected global cerebral perfusion and herniation syndromes.

Prospective studies suggest 30-50% or more of patients develop progressive haemorrhagic injury (PHI) manifest as a volume expansion of the core haemorrhagic lesion on serial imaging studies [126, 122]. Typically this is also associated with concomitant increase in peri-haematoma oedema and brain swelling, collectively contributing to reduced intracranial compliance and increased pressure.

PHI is predominantly an early phenomenon that occurs within the first 24 hours following injury. As a corollary of this a higher incidence of PHI is observed the earlier an initial CT scan is performed. Increased age and lower admission GCS are both independent risk factors for PHI [126]. Larger contusions and traumatic parenchymal haematomas are also more likely to display further progression [2]. Patients on therapeutic anticoagulation at the time of injury are at significantly higher risk of sustaining larger extra- and intra-axial haematomas and of suffering PHI [204]. The evidence for a similar effect of anti-platelet therapy is less concrete; aspirin therapy alone does not appear to increase the risk of PHI. Coagulopathy on admission also predisposes to PHI [126, 204, 53].

1.2.1 Classification of Brain Oedema

Although further expansion of the haemorrhagic contusion core can be an important component of raised ICP, it is typically pericontusional swelling and oedema that has a more major impact after the first 24h from injury. The mechanisms by which the brain can accumulate tissue water and swell remain a subject of debate, no more so that which predominates in traumatic injury. Cerebral oedema may be broadly classified as cytotoxic (cellular) or vasogenic (extracellular)(Fig 1.2) [46, 117]. Cytotoxic oedema is characterised by redistribution of water from the interstitial to intracellular compartment as a result of osmotic imbalance, typically attributed to failure of Na/K and other energy-dependent membrane pumps. Importantly, though cytotoxic oedema is associated with marked cellular dysfunction, it does not produce a gain in total brain water and therefore, by itself, cannot generate gross brain swelling or raised ICP. As the term implies, vasogenic oedema is a shift of water from the intravascular space to the brain interstitium, and generally entails both a degree of increased permeability of the blood-brain or brain-CSF barriers and an osmotic or hydrostatic gradient driving water extravasation. Primary disruption of the blood brain barrier (BBB) allows plasma macromolecules to leak into the interstitial space and their subsequent breakdown generates an osmotic gradient and fluid shift. An alternative model of vasogenic oedema that may be relevant in TBI has been proposed by Katayama, wherein neuronal and glial cell death (e.g. in a contusion) releases intracellular molecules which produce an osmotic gradient that draws water from plasma without gross BBB disruption.[89]

There remains longstanding controversy as to the relative importance of the different types of cerebral oedema and the role of BBB permeability in the context of acute TBI. Early MRI studies by Marmarou and colleagues, both in animal models and TBI patients, have been interpreted

as showing an early but transient period of BBB permeability and vasogenic oedema over the first few hours after injury, followed by a period of several days increasing brain water content but predominantly cytotoxic oedema reflected in reduction of the apparent diffusion coefficient (ADC) [14, 15, 17, 82, 113]. However, ADC is a net measure of the relative magnitude of vasogenic and cytotoxic oedema and hence does not preclude both coexisting. Moreover, to explain an increase in brain water content there must be flux from the intravascular to interstitial space (i.e. vasogenic oedema) with, presumably, a secondary redistribution into the intracellular compartment. Significantly, in animals subject to combined TBI and a secondary injury of hypoxia and hypotension the observed period of BBB permeability was extended. Detailed studies with tracers of varying molecular weights in focal and diffuse TBI models have shown that BBB permeability to large macromolecules is limited to the first <6 hours following injury, but that continued opening for molecules of size 4-10kDa is observed for several days [63, 109]. Corroborating these findings, a study of rabbits subject to TBI followed with serial dynamic contrast enhanced MRI showed evolving permeability beginning at 3 hours and peaking at 3 days both in the lesion core and surrounding brain [194].

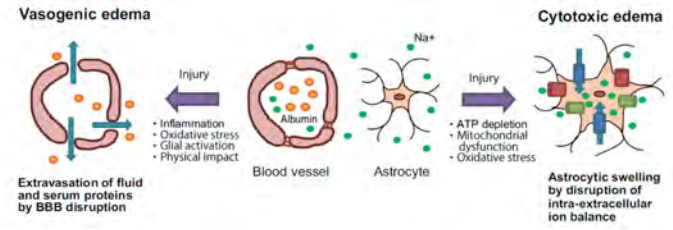

Figure 1.2: Schematic representation of vasogenic and cytotoxic oedema. Adapted under Creative Commons attribution licence from [117]

1.3 Imaging Blood Brain Barrier Permeability

All techniques for measuring or imaging BBB (dys)function share a common principle of quantifying the extravasation and parenchymal accumulation of a molecule to which the brain endothelium would normally be impermeable. Administration of contrast agents is routine practice in clinical computed tomography (CT) and magnetic resonance imaging (MRI), and highlight pathologies where the BBB is permeable (e.g. tumours or inflammatory lesions). However, with standard imaging protocols of single pre- and post-contrast scans only a qualitative assessment of permeability can be made. To quantify BBB permeability the time course of contrast influx and efflux within the vasculature and tissue is required, which necessitates rapid repeated serial imaging over the course of several minutes [28]. These imaging protocols are typically labelled as

'dynamic' or 'perfusion' imaging.

Dynamic MRI with gadolinium-based contrast agents, either employing dynamic contrast enhancement (DCE-MRI, T1-weighted) or dynamic susceptibility contrast (DSC-MRI, T2*-weighted) sequences are perhaps the most widely utilised imaging modalities for examining BBB permeability [73, 182]. Standard gadolinium chelates such as Gadopentetic Acid (Gd-DTPA) have molecular weight of approximately 550Da but for investigating the degree of permeability to macromolecules alternatives such as Gd-DTPA complexed with hyaluronic acid or dextran are available. Ultimately quantifying the permeability coefficient (usually termed K-trans) requires fitting one of a number of alternative pharmacokinetic models to the time-course data from individual voxels, with the Tofts and Patlak models the most commonly used [73, 182, 158].

Dynamic contrast enhanced CT (DCE-CT, often synonymously called perfusion CT) is analogous to DCE-MRI and can be performed on most modern multislice CT scanners that are able to acquire serial volume scans of the brain with sufficient temporal resolution, using standard ionic or non-ionic iodinated contrast agents injected as a rapid bolus. Compared with MRI, the linear relationship between CT Hounsfield unit density with contrast concentration simplifies pre-processing of the images [182]. In general, permeability is quantified either by non-linear optimisation of a two compartment model with a permeability term (e.g. modified Tofts model), or employing the Patlak plot which essentially arrives at the permeability coefficient as the gradient of the straight line fit to the plot of the ratio between voxel density and that in a reference artery, against the integral of the density in the reference artery divided by the current density in the reference artery, for all time points [158]. In addition to assessing permeability these imaging protocols provide per-voxel quantitation of cerebral blood flow, blood volume, and other haemodynamic parameters, typically through deconvolution with the arterial input function, i.e. the time course of the contrast bolus within one of the major cerebral arteries [92].

DCE-MRI has been favoured in most clinical and research contexts given the superior anatomical fidelity of MR structural imaging, the additional advanced MR sequences such as diffusion tensor imaging that can be performed in the same imaging session, and the avoidance of ionising radiation. However, in the context of imaging permeability in acute conditions, such as stroke or TBI, the better availability and more rapid acquisition of CT is a potential major advantage, particularly when patients may be imaged on a number of occasions.

DCE-MRI and DCE-CT have shown evidence of increased permeability related to a number of pathologies including intrinsic brain tumours (both primary and metastatic), multiple sclerosis plaques, infection, and small vessel disease [73, 182]. In stroke, permeability imaging has emerged as having a number of potentially important clinical implications, specifically early increases in BBB permeability identified by both DCE-MRI and DCE-CT have been found to predict the likelihood of infarct extension, cerebral swelling, haemorrhagic transformation, and mortality [134, 145].

In a pre-clinical diffuse impact-acceleration TBI model, dynamic MRI did not show evidence of significant BBB permeability [18]. However, more recent studies in focal injury models have shown regions of increased permeability in proximity to the contusion lesion, that BBB dysfunction starts within three hours of injury but progresses to reach its peak at around three days, and that the degree of permeability correlates with final lesion volume [193, 105, 195]. Several studies have utilised DCE-MRI to examine the prevalence of chronic changes in BBB permeability in patients with TBI of varying severity. However, there is little data on the acute temporal course and spatial pattern of BBB permeability in human TBI patients.

1.4 Pathophysiology of Blood Brain Barrier Dysfunction Following TBI

The blood brain barrier (BBB) is formed by the neurovascular unit, consisting of an endothelial monolayer, basal lamina, associated support cells including pericytes and smooth muscle, and astrocyte foot process which cover 98-99% of the vascular wall [12, 67, 106] (Fig 1.3A). Apart from small (<400Da) lipophilic molecules, the BBB tightly regulates the exchange of all substances between plasma and the brain interstitium. Ion homeostasis and uptake into the brain of small molecules, such as glucose and amino acids, is conducted via specific endothelial membrane channels and solute carriers. Larger peptides and proteins are transported by endo- or transcytosis pathways within caveolae and clathrin-coated microvesicles (Fig 1.3B, *right*). Importantly, paracellular diffusion is highly restricted by tight junctions (TJ) between the apical regions of adjacent endothelial cells which are composed of the transmembrane proteins claudin and occludin linked to the cytoskeleton by the intracellular scaffolding proteins zona occludens (ZO)-1 to -3 [12] (Fig 1.3C).

Brain injury may result in excess BBB permeability through increased caveolae formation and transcytosis, or by disruption of tight junction protein expression and assembly permitting unregulated passive diffusion across the endothelium [106]. This latter mechanism is proposed to play the predominant role in cerebral vasogenic oedema following TBI [154].

The temporal course of experimental BBB disruption after injury is typically biphasic, with an immediate or early phase of hyperpermeability, followed by temporary restoration of BBB function, and subsequently a delayed and more prolonged period of opening [11, 183]. The early period of permeability is presumed to reflect the extent of direct mechanical disruption of brain microvessels by the primary impact. Brain parenchymal cells are then exposed to blood-borne factors that are normally shielded from the CNS, promoting a number of inflammatory pathways which have been implicated in the later delayed phase of BBB permeability. Exacerbating this process is intravascular thrombosis as a consequence of endothelial disruption, which sets up a localised ischaemic response and inflammatory signalling triggered by thrombin, which rapidly activates astrocytes and microglia; this phenomenon has been confirmed in experimental TBI and in human patients [146, 162]. Crucially, while the immediate transient BBB opening may be difficult to prevent, the secondary phase of permeability potentially offers a therapeutic window and practical opportunity to intervene and limit the extent of swelling.

A plethora of intercellular signalling pathways have been reported to be involved in delayed BBB opening (Fig 1.4). Here we have focused on a subset that have been most strongly implicated as having pivotal roles in vasogenic oedema in TBI patients.

1.4.1 Pro-inflammatory cytokines and chemokines

In contrast to long established doctrine that the central nervous system is an immune privileged organ, there is now widespread recognition that the brain inflammatory response to injury is a key part of the pathophysiology of TBI, including BBB disruption. Early following TBI, prototypic pro-inflammatory cytokines, such as IL-1b and TNFa, are rapidly expressed, alongside chemokines that induce immune cell migration into the brain parenchyma. The initiators of this cascade are disease- (or danger-) associated molecular patterns (DAMPs), which are essentially cytosolic or nuclear proteins, nucleic acids, and other macromolecules which are exposed on the cell surface or released into the interstitium following traumatic tissue disruption and activate inflammatory signalling predominantly via toll-like receptors [131]. IL1b and TNFa have been shown in vitro to promote permeability of brain endothelial cells, both by inducing cytoskeletal

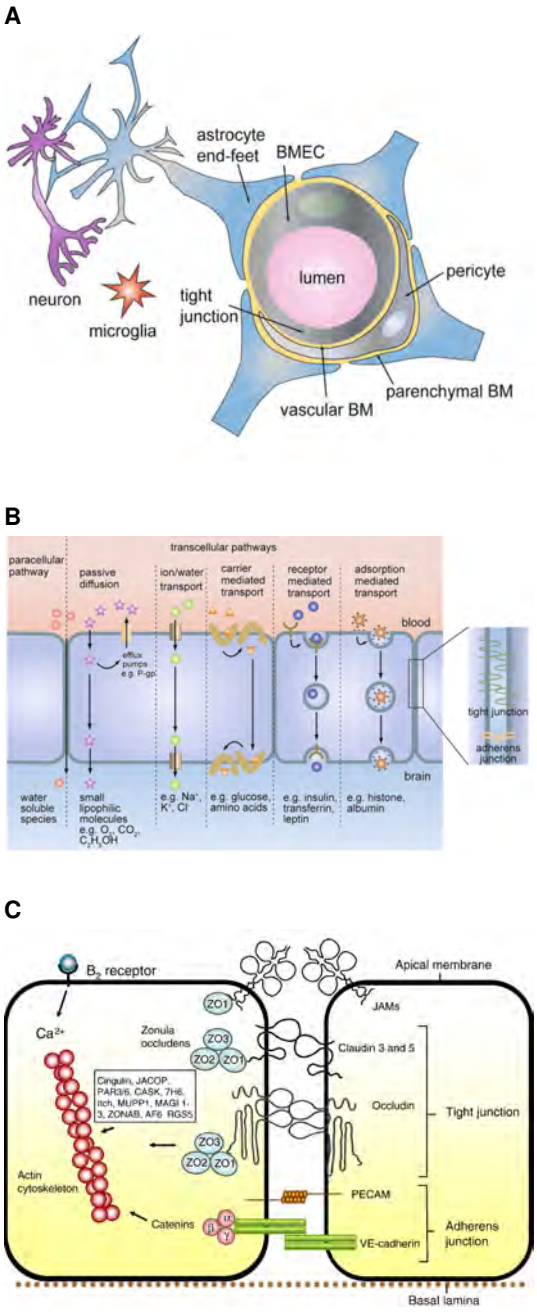

Figure 1.3: (**A**) schematic representation of cellular components of the neurovascular unit, (**B**) representation of the multiple regulated pathways for transport of different molecules across the healthy BBB, (**C**) detailed structure of apical tight junctions and cytoskeleton, which form the primary barrier to paracellular diffusion.

changes that cause cellular retraction, downregulation of tight junction protein synthesis, and disruption of cell membrane associated with tight junctions [42, 197, 110, 104]. At least some part of the IL-1b induced permeability may be VEGF-dependent (see below) [22, 6].

Furthermore, pro-inflammtory cytokines also initiate the upregulation of cellular adhesion molecules, such as intercellular adhesion molecules (ICAM), vascular cell adhesion molecules (VCAM), and

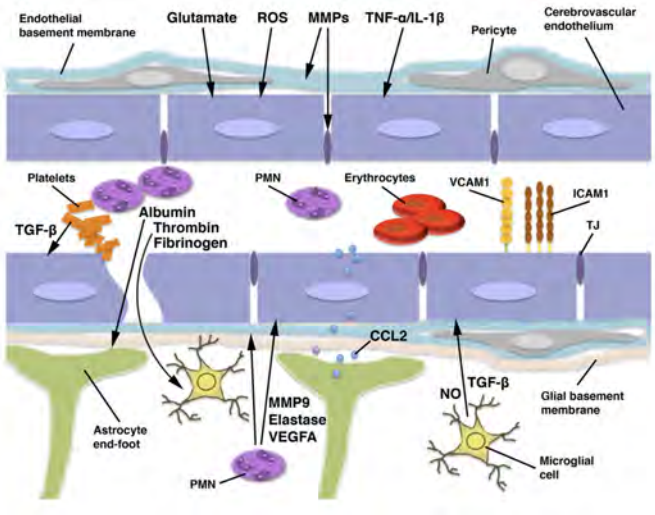

Figure 1.4: Pathways affecting BBB permeability following TBI. Adapted under Creative Commons attribution licence from [37]

E-selectin, at the brain endothelial surface [198, 65] and increase expression of chemokines that induce migration of neutrophils, monocytes, and macrophages. This latter effect is crucial as, while there is extravasation of red blood cells in the process of early mechanical BBB disruption, there is minimal leuocyte infiltration without the additional signalling of chemotactic factors. This, again, suggest a potentially feasible therapeutic window in which to effect reduction in the migration of neutrophils and macrophages that are highly toxic to neurons.

Prominent chemokines that have been implicated in TBI and other acute brain injury models are Monocyte Chemoattractant Protein-1 (MCP-1, also known as CCL2), and MCP-3 (CCL7), and IL-8 (CXCL8). Sustained MCP-1 expression has been assayed in CSF of TBI patients, and mice deficient in MCP-1 have lower total lesion volume in experimental focal brain injury [148]. Correspondingly, mice over-expressing CCL2 were found to have massive neutrophil recruitment into the brain with prolonged BBB disruption [54]. The initial influx of inflammatory cells as a result of chemokine production by astrocytes and endothelial cells, is subsequently exacerbated by further production of chemokines by neutrophils and monocytes themselves. Further, chemokines also amplify the severity of vasogenic oedema via a direct effect on BBB permeability through endothelial cell actin cytoskeleton eorganisation and inhibiting expression of claudin and other tight junction proteins [160, 161].

IL-8 is a chemokine has been shown to promote neutrophil infiltration and consequently increase blood brain barrier permeability and may be activated upstream by IL-1b [88, 200]. Levels of IL-8 were previously found to be markedly elevated in CSF following TBI and are associated with

increased blood brain barrier permeability measured by serum:CSF albumin quotient [93, 196] and the current data corroborate elevated interstitial levels. In one study IL-8 CSF concentrations were significantly higher in subsequent fatalities [98].

1.4.2 Vascular Endothelial Growth Factor

Several lines of evidence suggest that Vascular Endothelial Growth Factor and related mediators play a major role in the development of BBB permeability associated with a range of pathologies, including TBI. VEGF-A through -D and Placental Growth Factor (PlGF) are key regulators of endothelial proliferation and angiogenesis, and have potent effects on vascular permeability [50]. VEGF-A (usually referred to simply as VEGF) is the most prominent in the adult vascular system and is the best characterised. VEGF-B is a regulator of embryonal vasculogenesis and VEGF-C and ?D are involved in the development of lymph vessels. VEGFs exert their action via at least three receptor tyrosine kinases: VEGFR1 (Flt-1), VEGFR2 (Flk-1 or KDR) and VEGFR3 (Flt-4) [50].

Alternative splicing of the primary transcript from the 8-exon VEGFA gene yields isoforms and variants with divergent expression patterns and biological activity [50, 66]. Alternative splicing of exons 6 and 7, the latter of which codes a heparin binding domain, produces assorted isoforms containing 121 to 206 residues which vary considerably in their affinity to cell membranes and extracellular matrix (ECM). VEGF121 is acidic and freely diffusible in the extracellular space whereas the more basic VEGF189 and VEGF206 are strongly bound to cell surface proteoglycans. VEGF165, typically the most abundant isoform, has intermediate affinity and exists in both bound and soluble fractions. Matrix metalloproteinases (MMPs) and other enzymes including urokinase and plasmin can cleave bound VEGF and release active fragments that are recognised by VEGF receptors [50].

In vitro, VEGF increases the permeability of brain microvascular endothelial cell (BMEC) monolayers by downregulation of tight junction proteins, including ZO-1, claudin and occludin, which disrupts cell-cell adhesion and results in endothelial fenestrations [209, 190, 7]. In other endothelial models, including brain-tumour interfaces, VEGF also increases expression of caveolin and mobilizes exisiting calveolae, thereby increasing permeability by accelerating the transcytosis system [31]. One of the principal upstream regulators of VEGF is hypoxia inducible factor (HIF), a transcription factor that is stabilised under conditions of cellular hypoxia and which promotes VEGF expression. Correspondingly, BMEC cultured under hypoxic conditions show a two-fold increase of both VEGF and VEGFR1 expression and become hyperpermeable, an effect that is

abolished independently by anti-VEGF antibodies and inhibitors of nitric oxide synthesis.[52]

In animal transient or permanent cerebral artery occlusion studies there is upregulation of VEGF and VEGFR1 expression in astroglia, endothelium, and neutrophils commencing between 1-48 hours following ischaemia, dependent on the specific model parameters [95, 38], which is associated with reduced expression and proteolysis of tight junction proteins, the latter via activation of matrix metalloproteinases (MMP-9) [59, 16]. Further, studies have demonstrated that interventions to interrupt this pathway significantly attenuate permeability and cerebral oedema following ischaemia-reperfusion in vivo, including pharmacological inhibition of HIF, sequestration of VEGF with soluble receptors, and MMP antagonists [179, 203, 142].

Alternative pathways may activate the HIF-VEGF axis under non-hypoxic conditions. For example, intracerebral injection of IL-1beta is associated with BBB permeability and oedema and there is evidence from inflammatory lesion models that this effect is mediated by upregulation of HIF and VEGF, a pathway that may also be relevant in the context of the inflammatory response to TBI [22, 6].

In focal cortical impact studies increased HIF, VEGF, and VEGF receptor expression is observed in astrocytes within the contusion and perilesional tissue, as well as amongst infiltrating neutrophils and macrophages, and is maximal at around day 4 after injury [36, 155]. In one contusion model VEGF expression was inversely correlated with expression of SMI-71, a marker of BBB integrity [155]. Similarly, following cold/freeze injury endothelial and astrocyte expression of VEGF peaks at day 4, in concert with evidence of BBB disruption measured by extravasation of albumin or fibronectin, and the degree of oedema can be reduced by VEGF receptor antagonists [120, 128]. However, the efficacy of such direct anti-VEGF strategies in more clinically relevant TBI models (e.g. controlled cortical impact) has not been studied.

Together, these studies strongly suggest a role for VEGF in the delayed phase of BBB permeability and vasogenic oedema observed in patients with ischaemic and traumatic brain injury. Increased VEGF has been shown in the circulation and penumbral brain tissue of stroke patients [156], and microdialysis studies have demonstrated significantly raised intracerebral VEGF concentration in patients following diffuse TBI and SAH [115, 69]. Crucially, microdialysate levels exceed those of paired serum samples implying central production as opposed to passive influx from the circulation [69]. However, the relationship between VEGF expression and BBB permeability and

oedema, as well as the potential of anti-VEGF therapy, has yet to be determined.

It is important to recognise that in addition to potential deleterious actions, VEGF also has a neuroprotective role and is important in reparative angiogenesis following injury [191]. Upregulation of VEGF prior to transient ischaemia has a preconditioning effect and reduces final infarct volume [151]. However, when administrating exogenous VEGF as a neuroprotective strategy following a lesion, timing is critical: intravenous recombinant VEGF within one hour of transient ischaemia significantly exacerbates vasogenic oedema, whereas at 48 hours the same dose enhances angiogenesis in the ischaemic penumbra and significantly reduces final infarct volume [205].

1.4.3 Matrix Metalloproteinases

Matrix metalloproteinases (MMPs) are a family of over 20 extracellular endopeptidases that cleave a wide range of protein substrates in diverse signalling pathways [121]. In particular, the subfamily of gelatinases, MMP-2 (Gelatinase A) and MMP-9 (Gelatinase B), have been implicated as key mediators of proteolytic blood brain barrier (BBB) disruption associated with traumatic injury, ischaemia, and neuroinflammatory disorders [4, 9, 64].

In the rat cortical contusion model MMP-9 expression was increased in lesioned tissue compared with contralateral uninjured brain, and was associated with local BBB permeability and oedema [153]. Correspondingly, an MMP inhibitor (GM6001) reduced the degree of BBB leakage and the extent of oedema. In a similar mouse model, MMP-9 knockout animals were found to have smaller final lesion volume and better functional recovery compared to wildtype mice [64].

Tissue samples from patients requiring surgical resection of brain contusions have been shown to have significantly higher expression of MMP-9 compared with lobectomies performed for non-trauma indications [186]. Furthermore, in vivo microdialysis studies in TBI patients have also shown increased interstitial concentrations of MMP-9 and possibly MMP-2 early following injury, although it is unclear if this is a localised response to brain parenchymal injury, a reflection of a diffuse brain injury process, or potentially a consequence of a systemic inflammatory response to trauma [187, 138].

Mechanistically, MMPs have been shown to directly disrupt tight junctions (TJ) between endothelial cells through cleavage of the extracellular domains of critical structural proteins including claudin and occludin [202, 29]. This process dramatically alters the water reflectance and so-

lute permeability of the BBB, exacerbating vasogenic oedema, and also contributing to immune cell invasion into the CNS. These molecular events provide a framework for the microvascular failure which is thought to underlie contusion expansion [96]. Multiple upstream signalling molecules have been shown to have a role in regulating the expression and activation of MMP-9, including cytokines (e.g. IL-1b), growth factors (e.g. TGFb, VEGF), neurotransmitters and small molecules (e.g. histamine, nitric oxide), and hormones (e.g. epinephrine) [181]. In the wider experimental brain injury literature, MMPs have been identified as mediators of lesion expansion and perilesional oedema in models of ischaemic stroke and intracerebral haemorrhage [141, 84]. Importantly, recent evidence has highlighted the crucial roles that MMPs have in the subacute and chronic reparative processes following brain injury, such as neurovascular remodelling and migration of cells from the subventricular zone to damaged tissue [206, 140].

Grosslete et al. and Zheng at el. have previously reported elevated levels of MMP-9 in CSF sampled acutely from TBI patients via ventriculostomy, with comparable temporal profiles demonstrating greatest concentrations in the first sample at 24 hours post-injury followed by a decline, but remaining higher than control CSF for at least 72 hours [206, 140]. Vilalta et al. studied four patients with diffuse brain injury using microdialysis and found similar early elevation of cerebral MMP-9 concentrations [187]. More recently, Roberts et al. conducted a single site microdialysis study of MMP-1, -2, -3, -7, -8, and -9 in eight TBI patients with a mixture of diffuse and focal injuries; similarly to the present study, they found MMP-9 was increased early following injury and thereafter declined [138].

1.4.4 Nitric Oxide

Nitric Oxide (NO) is a highly diffusable radical gas molecule that is synthesised from the amino acid L-arginine by the nitric oxide synthase (NOS) family of enzymes [57]. NO has a variety of roles in neurotransmission and synaptic modulation, intracellular signalling, neuroinflammatory cascades, and in the regulation of cerebrovascular tone and cerebral blood flow [57, 34]. Three NOS isoforms have been identified in humans: endothelial NOS (eNOS), neuronal NOS (nNOS), and inducible NOS (iNOS). Both eNOS and nNOS are constitutively expressed in the brain whereas iNOS is upregulated in response to injury [175, 57].

Broadly, cerebral autoregulation comprises mechanoregulation (maintenance of constant flow with varying systemic arterial blood pressure) and chemoregulation (maintenance of flow in response to changing CO_2 concentrations due to metabolic pertubations and during hypoxia) [57].

NO is a key mediator of both CO_2 chemoregulatory pathways [102] and is necessary for augmenting blood flow in response to hypoxia [166]. In the context of TBI this would suggest a beneficial role for NO in maintaining constant CBF under the stress conditions following injury, and that relative NO depletion may be a factor in post-injury ischaemia and loss of flow-metabolism coupling [57].

However, excess NO may be a factor in post-traumatic dysautoregulation, vasoplegia and vasodilatation, and hyperaemia, with consequent raised intracranial pressure, and has also been identified as a component of the pathway resulting in blood-brain barrier breakdown by VEGF [52, 34, 147, 188]. Furthermore, following cerebral insults, it has been shown that eNOS can become uncoupled from its cofactor tetrahydrobiopterin, resulting in the alternative production of superoxide, a radical that is neurotoxic. Superoxide may in turn react with NO to form peroxynitrite that is also neurotoxic and depletes available NO.

NO itself is difficult to assay in clinical samples owing to its short half life. However, assaying concentrations of stable NO metabolites nitrite and nitrate (NO_2 and NO_3, collectively NOx) is a validated method of indirectly quanitfying endogenous NO synthesis [137]. In humans, NOx have been assayed in CSF and microdialysate of diffuse-injury pattern TBI patients. A series of eleven TBI patients who underwent regular CSF sampling suggested a peak in NOx at approximately 24h following injury [178]. The concentration of NO was correlated with that of IL-8, suggesting that NO levels may reflect the degree of post-TBI inflammatory burden [178]. In a pilot study of twelve brain injury patients (11 TBI), studied with microdialysis, extracellular NOx concentration was found to be correlated with higher cerebral glucose and lower lactate/pyruvate ratio, suggesting a beneficial metabolic effect of higher NO concentrations [24]. However, a more recent microdialysis study in eleven TBI patients found significantly higher NO concentrations within the first 48h from injury amongst patients who died compared with survivors, suggesting that NO is a either a marker of more severe primary insult or that it potentially contributes to secondary injury and likelihood of poor outcome [174].

1.5 Metabolic Dysfunction Following Traumatic Brain Injury

Metabolic dysfunction has been described in acute brain injury of various aetiology, including TBI, ischaemic stroke, and intracerebral haemorrhage, and has an important role in secondary injury cascades such as the induction of pro-inflammatory cytokine signalling and microvascular

breakdown causing blood brain barrier permeability [111, 167]. Metabolic crisis in astrocytes and neurons will potentiate the activation of IL-1b and VEGF axes and their downstream effectors of BBB opening. Metabolic crisis induced within endothelial cells has been shown to directly result in increased permeability [45].

Manipulation of systemic and, directly or indirectly, cerebral energy metabolism may therefore be a potential therapeutic avenue to limit or reduce BBB opening and vasogenic oedema in TBI patients. However, this requires a suitable classification of the differing states of metabolic derangement so that appropriate interventions are applied with the aim of correcting or normalising cerebral metabolism. Various categories of cerebral metabolic dysfunction have been hypothesised and demonstrated in evidence accrued from cell culture and tissue models, and in animal and human studies. Broadly, these can be organised under three terms: cellular substrate deficiency (as a consequence of tissue ischaemia or local diffusion barriers), aerobic glycolysis, or, lastly, a failure of oxidative phosphorylation that has been dubbed 'mitochondrial dysfunction' [27]. Distinguishing these dynamic states within individual TBI patients *in vivo* over time is important as potentially simple interventions, such as improving cerebral perfusion and supplementing systemic glucose or oxygenation, may be sufficient to overcome local deficiency or provide hyperglycolitic tissue with sufficient substrate. In contrast, mitochondrial dysfunction would not be expected to respond to these manoeuvres and experimental alternatives such as direct succinate supplementation into the Krebs cycle may may be appropriate [171, 164].

Cerebral microdialysis is an invasive neuromonitoring technique that permits continuous real-time sampling of brain extracellular fluid and assessment of cerebral metabolism in the intensive care unit [79]. Standard metabolites assayed on bedside analyzers include glucose, lactate, pyruvate and glutamate, which permit characterisation of glycolysis and oxidative phosphorylation (Fig 1.5). There is a body of observational evidence to support absolute values, ratios, and temporal trends of specific metabolites as indicators of cerebral metabolic dysfunction. The most extensively studied parameter is the lactate/pyruvate ratio (LPR), generally accepted to be an index of cellular redox state and the balance between oxidative and anaerobic metabolism.

Patients with average or prolonged LPR above thresholds of 25 or 40 are more likely to die or have unfavourable outcome following TBI [79]. Low cerebral glucose has similarly been associated with worse outcome both in observational series and interventional studies comparing alternative glycaemic control regimens [172]. Identically LPR values can potentially result from

an infinite range of combinations of absolute lactate and pyruvate concentrations wherein one or both may be higher or lower than their respective normal range. Similar increases in LPR resulting from very different changes in lactate and/or pyruvate will likely reflect distinct states of energy compromise, for instance ischaemia or subtrate deficiency as opposed to aerobic hyperglycolysis. Thus, there as been much recent work on defining classifications of lactate, pyruvate, and LPR values that are proposed to map to various metabolic states [144]. A further aspect crucial to interpreting glucose, pyruvate, and lactate concentrations, and their trends in vivo, is that they are not independent variables and display strong covariance and autocorrelation, a fact that is often overlooked or not explicitly addressed in the microdialysis literature [123]. Characterising the functional form (i.e. linear or non-linear) of the relationships between these metabolites is fundamental to understanding how they change in concert and in forecasting the response to therapeutic interventions. Moreover, characterising the typical metabolic derangements localised to pericontusional brain is key to designing treatment that attempts to support or normalise metabolism in these brain regions to limit the development of vasogenic oedema and further ischaemia.

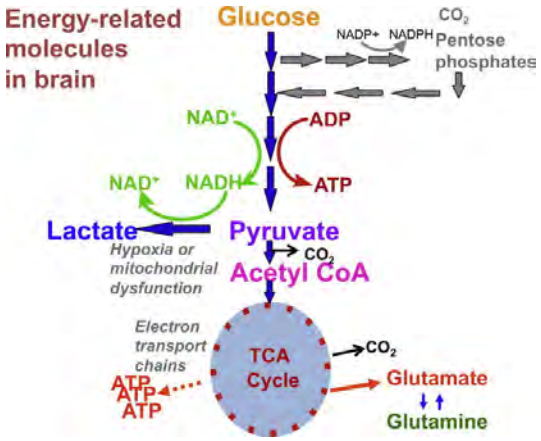

Figure 1.5: Schematic of the major metabolic pathways in the brain. Glucose is converted through glycolysis to pyruvate, which then enters the tricarboxylic acid (TCA) or Krebs' cycle in mitochondria after forming acetyl-CoA. Alternatively pyruvate may be converted to lactate. The pentose phosphate pathway is an alternative source of reducing agents. Reproduced under Creative Commons attribution licence from [25]

1.6 Summary and Objectives

In vitro and pre-clinical studies have suggested a number of pathophysiological processes are initiated following brain injury that can ultimately contribute to increased permeability of the BBB, progression of vasogenic oedema, and lesion expansion. Identifying which of these are salient

in patients with contusional TBI is an important goal to refine the development and targeting of therapies to limit contusion progression.

The principal objectives of this work are threefold: firstly, to establish a robust methodology to assess the temporal course of contusion progression in TBI patients; secondly, to interrogate the localised response of key mediators of BBB permeability directly in the pericontusional brain of TBI patients; and thirdly, to characterise the cerebral metabolic dynamics in brain injury patients.

1.7 Hypotheses

- **Study I:** Measuring Contusion Volume
  - H1: Stereology is an accurate method for measuring volume of brain lesions of variable morphology
  - H2: Contusion volume expansion predominantly occurs in the first 72h following injury.
- **Study II:** Quantifying Blood Brain Barrier Permeability
  - H3: Dynamic contrast enhanced computed tomography can quantify the severity of BBB permeability in the vicinity of brain contusions.
  - H4: Maximal BBB permeability is observed at around 72h following injury.
- **Study III:** Peri-contusional Inflammation
  - H5: Pericontusional brain exhibits a pro-inflammatory signature following TBI.
  - H6: Vascular Endothelial Growth Factor exhibits higher expression in pericontusional brain following TBI.
- **Study IV:** Matrix Metalloproteinases in Peri-contusional Brain
  - H7: MMP-9 shows increased expression early following TBI and is primarily localised to pericontusional brain.
  - H8: MMP-2 shows delayed increase in expression following TBI that is also primarily localised to pericontusional brain.
- **Study V:** Nitric Oxide in Peri-Contusional Brain
  - H9: NO concentrations are higher in pericontusional brain following TBI.

  - H10: NO is correlated with energy metabolites in both pericontusional and radiologically normal brain.

- **Study VI:** Cerebral Metabolism following TBI
  - H11: Cerebral metabolic parameters predict neurological outcome following TBI
  - H12: Derangements in LPR and cerebral glucose are different in radiologically normal and contused brain following TBI.
  - H13: There are defined functional relationships between the principal energy molecules assayed with microdialysis, namely glucose, pyruvate, and lactate.

Chapter 2

Generic Methods

2.1 Microdialysis

Microdialysis is a technique that is unique in allowing *in vivo* sampling of interstitial fluid from any accessible tissue or organ. All components of the microdialysis system used in this research are approved for clinical application.

2.1.1 Microdialysis Catheter

The microdialysis catheter consists of a concentric dual lumen tube of 0.5mm outer diameter. The terminal 10mm of the outer tube is formed by a semipermeable membrane. Fluid (*perfusate*) is continuously pumped by a microinfusion syringe-driver pump via the inflow catheter into the outer tube towards the catheter tip. The returning fluid (*dialysate* or *microdialysate*) passes via the inner tube and outflow catheter to be collected in a vial that is changed at regular intervals (Fig 2.1).

The semipermeable membrane of the catheter rests in the brain parenchyma and molecules diffuse from the intersistium/extracellular fluid into the perfusate and can then be assayed in the dialysate. From the perspective of examining the role of intercellular messengers such as cytokines and matrix metalloproteinases, the extracellular space is compartment in which these mediators are secreted, are at highest concentration, and where they act on their cognate receptors or substrates.

The size of the pores in the semipermeable membrane determine a nominal molecular weight cut-off (MWCO) for the catheter. For clinical applications the available catheters generally either have either a MWCO in the region of 20kDa or 100kDa. For assaying small molecules (e.g. glucose) either MWCO is acceptable but high MWCO catheters (i.e. 100kDa) are required to effectively recover larger molecules, including proteins.

For the retrospective studies presented here the earlier patients received 20kDa CMA70 catheters but more recently 100kDa CMA71 catheters have been routinely inserted. For all studies of cytokines and MMPs the CMA71 100kDa MWCO catheters were used.

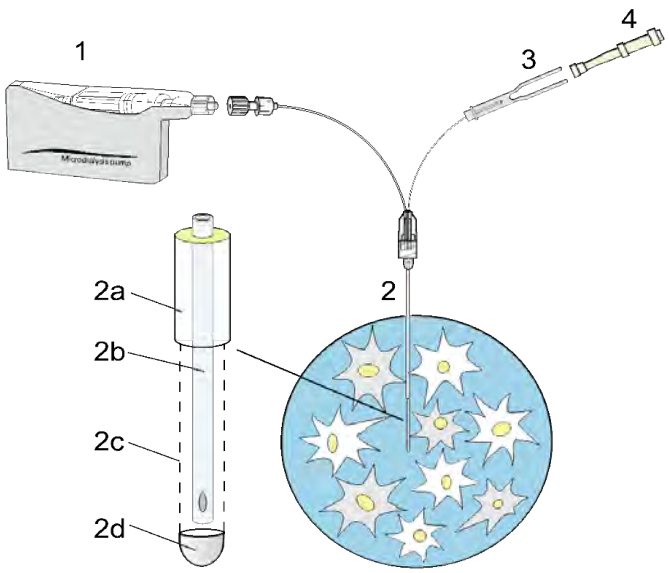

Figure 2.1: Schematic representation of the microdialysis apparatus: (1) Battery powered micropump, (2) Microdialysis catheter implanted in tissue. The catheter consists of concentric outer (2a) and inner (2b) tubes and semipermeable membrane extending 10mm at the distal end (2c). The golden tip (2d) on each catheter facilitates visualisation on CT. (3) Microvial holder, with needle that on insertion of the vial penetrates its lid. (4) Microvial for collection of dialysate. Reproduced from [62]

2.1.2 Relative Recovery

The ratio of the concentration of a diffusible substance recovered in the microdialysate compared with its true external concentration is termed the *relative recovery (RR)*. Several factors influence the RR, including catheter material and porosity (i.e. the MWCO), the molecular weight and ionic charge of the molecule of interest, and flow rate of the perfusate. Generally, the RR of any given substance is improved with lower flow rates, at the expense of recovering lower volumes of dialysate and reducing the temporal resolution of the technique. The RR of any molecule of

interest can be measured *in vitro* but this may not necessarily accurately reflect the *in vivo* RR. It is not usually possible to directly assess RR *in vivo* but it can be estimated by measuring concentrations recovered at two or more flow rates and extrapolating to the 'zero-flow' intercept.

2.1.3 Perfusate

The standard perfusion fluid for clinical microdialysis is an isotonic aqueous solution with similar electrolyte composition to the brain extracellular space (ECF): NaCl 147mM, KCl 2.7mM, $CaCl_2$ 1.2mM, and $MgCl_2$ 0.85mM. To improve the RR of larger molecules, specifically proteins, the perfusate can be supplemented with a macromolecule such as dextran or albumin. Previous studies in our group have shown that standard perfusate solution with the addition of 3.5% Human Albumin Solution (HAS) improves the *in vitro* recovery of a range of cytokines. This 'colloid' perufsate is manufactured and tested at the Ipswich Hospital Manufacturing Pharmacy Unit, Ipswich, UK. All studies examining the concentration of proteins used the 3.4% HAS supplemented perfusion fluid. Irrespective of the type of perfusate all studies were conducted at a constant flow rate of 0.3 microL/min

2.1.4 Microdialysate collection and bedside analysis

In routine clinical application the collection vials are changed at hourly intervals and then placed immediately on a bedside CMA600 or Iscus analyser to quantify the concentrations of glucose, pyruvate, lactate, glutamate, and glycerol. Reference values for these analytes in normal brain have been reported [136] and are shown in Table 2.1. An assay for urea is also available but not used in our centre. The bedside analyzers both employ a standard voltametric assay. The timecourse data of the analytes are displayed for the clinical team to use as a guide to clinical management. For the protein studies the remaining microdialysate following the bedside analysis was collected and stored as soon as possible at -80°C for later analysis. In vitro studies indicate that cytokines are relatively stable in microdialysate solution at body and room temperature for several hours [68].

Analyte	Concentration in Normal Brain
Glucose (mmol/L)	1.7 +/- 0.9
Pyruvate (micromol/L)	166 +/- 47
Lactate (mmol/L)	2.9 +/- 0.9
Lactate:Pyruvate Ratio (LPR)	23 +/- 4
Glycerol (micromol/L)	35 +/- 11
Glutamate (micromol/L)	16 +/- 16

Table 2.1: Reference values for standard clinical microdialysis analytes assayed in normal brain [136]

2.2 Additional Monitoring

2.2.1 Intracranial Pressure Monitoring

All patients in the included studies had intracranial pressure continuously monitored using a intraparenchymal strain gauge sensor (Codman, Raynham, MA, USA). Prior to insertion the sensor is zeroed to atmospheric pressure in sterile saline and then inserted to a depth of 2-3cm into the brain white matter. The ICP waveform is continuously displayed at the bedside.

2.2.2 Brain Tissue Oxygen Tension

Brain tissue oxygen ($PbtO_2$) was measured up to the year 2007 using the Neurotrend probe (Codman, Raynham, MA, USA) which utilises an optical technique to quantify tissue oxygen tension. Since then all $PbtO_2$) monitoring has been performed using the Licox probe (Integra LifeSciences, Plainsboro, NJ, USA). This is provided pre-calibrated with a unqiue reference card that is inserted into the bedside monitor.

2.2.3 Arterial Blood Pressure

All patients managed according to the ICP/CPP protocol require continuous invasive arterial blood pressure monitoring using standard intra-arterial catheters placed typically in the radial or brachial artery. The ABP monitor was zeroed at the level of the right atrium until 2014, and thereafter the clinical protocol changed to zeroing at the level of the tragus.

2.2.4 Data Recording

Continuous arterial blood pressure (ABP), ICP, and $PbtO_2$), together with other signals from the ventilator (e.g. end-tidal CO_2) are digitised at 50-240Hz and recorded using ICM+ software on a

dedicated PC at the bedside.

2.3 Insertion of Intracranial Monitors

Adult patients admitted to the Neurosciences Critical Care Unit (NCCU) at Addenbrooke's Hospital with Traumatic Brain Injury (TBI) requiring invasive intracranial monitoring for clinical care were eligible for recruitment to the studies. As part of the standard ICP/CPP targeted care protocol (1.1), all patients received a triple-lumen cranial access device ('bolt', Techicam, Newton Abbott, UK) either placed at the bedside or in theatre. This is a magnetic resonance imaging (MRI)-compatible device that is secured to the skull and incorporates three equidistant obliquely-angled ports that permits sterile insertion of compatible monitors. A variety of attachments are provided to accommodate different monitors and it facilitates easy verification or replacement of monitors without necessitating further surgery (Fig 2.2).

The standard battery of monitors placed via the bolt includes an intraparenchymal intracranial pressure transducer (Codman), a Licox tissue oxygen probe, and a CMA71100kDa MWCO gold-tipped microdialysis catheter (CMA Microdialysis). As these monitors are placed for clinical management they would normally be inserted by the emergency neurosurgical team. For all patients recruited to the two-site paired microdialysis study the additional monitors were placed by me.

By default the cranial access device is inserted in the right frontal region, anterior to the coronal suture, as this is the least eloquent region of brain. A left frontal position is suitable if there are scalp wounds, fractures or other reasons that the right frontal region is not preferred. The skin is prepared by clipping hair as required and then sterilising with liberal application of povidone-alcohol or chlorhexidine-alcohol solutions. A 1-2cm linear incision is made and the periosteum elevated and swept away to reveal the outer bone cortex. Using a custom drill bit with safety guide, a burrhole is drilled with a manual brace taking care not to suddenly breach the inner table of the skull and damage the underlying dura and brain. The dura is opened in a cruciate manner and the pial surface coagulated. The bone channel is then reamed to create a screw thread which allows the access device to be secured in place. Each of the three channels is confirmed to be patent without resistance at the cortical surface to deflect the pliable catheters and then the monitors are inserted in turn. The skin around the access device is approximated with 3-0 nylon sutures. Once monitoring is completed the monitors and access device are removed at the bed-

side and the scalp closed with 3-0 silk or nylon.

For patients who require craniotomy or craniectomy to evacuate mass lesions or achieve decompression, monitors can be inserted at the time of surgery by tunnelling through the scalp at the edge of the craniotomy, insertion into the brain under direct vision, and then secured to the scalp with 3-0 silk. ICP sensors and microdialysis catheters are suitable to be inserted by this method but the Licox probe is difficult to secure satisfactorily. The advantage of tunnelled catheters is the ability to precisely locate the monitor in visibly injured or perilesional brain; the disadvantage is the inability to change or replace the catheter if it fails or is inadvertently removed without further surgery.

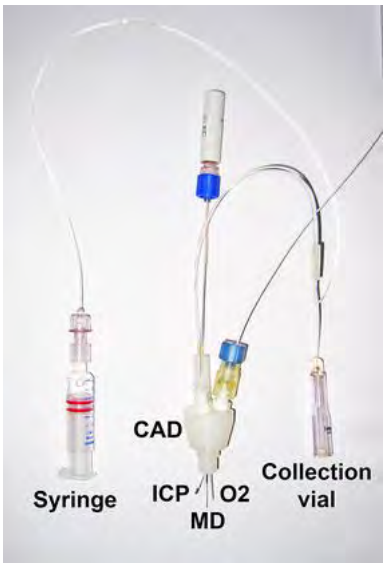

Figure 2.2: The cranial access device (CAD) with associated monitors place in the three available lumen: microdialysis (MD), intracranial pressure transducer (ICP), and brain tissue oxygen probe (O_2). The CAD is threaded to allow it to be secured to the burrhole fashioned in the skull. Reproduced from [149] under Creative Commons attribution licence

2.4 Ethical Approval and Procedures

The two-site microdialysis studies reported here were conducted following ethical approval for the insertion of additional monitoring (for up to ten days following injury) and performing the dynamic contrast enhanced computed tomography (DCE-CT) imaging. This research protocol was approved by the East of England NHS Research Ethics Committee, reference 11/EE/0075. Acutely, relatives were approached for written assent to enrol a patient in the research prior to any procedures being performed. If patients subsequently recovered sufficiently and regained

competence, the research was again discussed directly with them to seek affirmation of consent; if refused the patient would be withdrawn from the study.

For larger cohort study, microdialysis catheters were inserted and samples collected as part of routine care. Retention of this data for research purposes was approved by the Cambridgeshire Local Research Ethics Committee as part of an ongoing 'Blood flow, swelling and metabolism after head injury' project (Protocol 30).

Chapter 3

Study I - Measuring Contusion and Oedema Progression

3.1 Introduction

Haemorrhagic expansion and progression of perilesional oedema are the critical features of intracerebral haematomas and traumatic brain contusions that can result in tissue destruction, raised intracranial pressure and cerebral hypoperfusion, herniation, and ultimately death or more severe disability [135]. Therefore, a method that provides accurate and efficient estimation of the volume of intracerebral haematoma or contusions and perilesional oedema is an essential tool for studies examining the pathophysiology of these lesions and those assessing the efficacy of therapeutic interventions.

In the context of stroke, intracerebral haemorrhage (ICH) accounts for 10-15% of all presentations and haematoma volume is amongst the main prognostic factors that influence outcome and clinical decision-making [23]. Probably the most widely used estimator of ICH volume in both clinical practice and research studies is the ABC/2 formula [23, 94]. This is an approximation to the volume of an ellipsoid where A and B are the maximal orthogonal dimensions (length and width) measured on the axial imaging slice displaying the largest area of ICH, and C is the product of the number of slices on which the ICH appears and the slice thickness (i.e. 'height' or maximal rostro-caudal dimension). Studies in TBI have also adopted this heuristic methodology for estimating the volume of contusions and surrounding hypodensity or oedema.

Alternative techniques include planimetry, wherein the the lesion is manually outlined on each image slice and the total volume calculated by the sum of the respective areas multiplied by slice thickness [80]. However, this is a time consuming process and, particularly when the margins of the lesion are diffuse or poorly defined (e.g. oedema), the interobserver variation may be substantial given the potentially infinite degrees of freedom inherent in the approach.

Automated and semi-automated segmentation techniques for radiological images is a well developed field, and delineation of brain lesions specifically has received much attention. Algorithms including region growing, watershed transform, and active contour level sets have been reported to be effective at isolating a variety of lesions, including primary and secondary tumours, stroke, and inflammatory plaques. However, these algorithms each have a number of parameters that need to be tuned precisely to the specific characteristics of the lesions of interest before any satisfactory results are obtained. Often the efficacy of the algorithm is very sensitive to a subset of these parameters and those that are refined on a given training set may perform poorly on what may appear to be a very similar test-set of scans.

A number of studies have shown that ABC/2 substantially overestimates volume of ICHs classified as irregular based on qualitative criteria [80, 207, 44]. This can be partially compensated by increasing the divisor to 3 (i.e. ABC/3) or by adopting the formula 2LC/3 where L is the largest surface area of ICH on any slice, and C is again height [207, 208]. However, particularly in the context of traumatic contusions which are often highly irregular, any of the methods that approximates to the volume of a regular solid will be less accurate than a technique which is agnostic to lesion shape.

Stereology is an established generic technique, developed primarily in microscopy, for estimating object volume from planar sections and involves estimating the cross sectional areas on parallel sections by counting the points that fall within the region fo interest using a regular counting grid - the so-called Cavalieri estimator [119]. Stereology can also be adapted to estimate the surface area of objects. As there are no underlying assumptions about shape or regularity, stereology should have predictable accuracy irrespective of lesion morphology. A small number of studies have reported applying stereology for quantification of anatomical structures on cross sectional imaging, including a study of five patients with brain contusions, with findings of good accuracy [85, 48].

The objectives of this study were, firstly, to quantitatively establish the relationship between morphology and the accuracy of cerebral haematoma volume determined using ABC/2, ABC/3 and 2LC/3 estimators. Secondly, we have assessed the comparative accuracy of estimating volume with a simple stereological grid technique. Lastly, the stereological approach has been applied to a cohort of patients with contusional TBI to characterise the temporal evolution of contusion volume.

3.2 Methods

3.2.1 Design

The first component of this study was performed using fifty standard axial non-contrast computed tomography scans demonstrating a discrete (spontaneous) intracerebral haemorrhage of variable size and morphology. Scans with ICH extending to the ventricles or subdural space were excluded. To objectively compare the accuracy of the formula estimators and a stereological approach an automated procedure was developed to apply both techniques without introducing user bias or error.

The second component of this study was performed on the set of clinical CT scans of fifty two patients with contusional TBI. The series of scans for each patient obtained within 14 days of injury were analysed using the stereological technique to estimate contusion and oedema volume.

3.2.2 Image processing

All image processing was performed using the SimpleITK (www.simpleitk.org) interface to the Insight Toolkit (ITK, www.itk.org). ITK is a free and mature open source library of image processing, registration, and segmentation component routines that can be composed in to a flexible analysis pipeline. SimpleITK is a layer over ITK that provides a simplified procedural interface to the majority of ITK functions and also has an R-language wrapper that allows rapid prototyping and interactive image analysis within the full R language environment.

Anonymised non-contrast 4-6mm slice thickness axial computed tomography scans DICOM files were imported and any gantry tilt corrected with a affine shear transform calculated from the

origins of the first two image slices - the DICOM header information regarding gantry tilt was found to be often absent or inaccurate when compared with calculated values from image coordinates. Ground truth segmentation of the ICHs was performed by first cropping the volume to a margin no less than 5mm around the haematoma in all planes. The image slices were then thresholded to a range of Hounsfield units representing acute blood, i.e. 45-100. The resulting binary mask of the haematoma was used as the reference and both volume and surface area were calculated. Regularity of each haematoma was quantified by calculating its sphericity S, according to $S = \pi^{1/3}(6V)^{2/3}/T$, with V the volume and T the surface area. Sphericity has values ranging between 0 and 1; a perfect sphere has $S = 1$ and this declines toward 0 as an object's shape becomes progressively more eccentric/non-spherical or irregular.

3.2.3 Volume Estimation by ABC/2, ABC/3, and 2SH/3

To objectively apply the three formula techniques as a clinician would, the area of the binary haematoma mask on each imaging slice was computed and the largest selected. On the selected slice the largest dimension of the haematoma (Feret diameter) was obtained and then the maximal orthogonal dimension calculated. The number of slices on which the haematoma mask was present was counted and thus all the required variables for the formula calculations were obtained.

3.2.4 Stereological Volume Estimation

Binary images of the same dimensions as the respective scan consisting of regular grids of voxels with point-spacing of 5, 10, or 20mm (equivalent to point area of 25, 100, and 400mm^2) with a random horizontal and vertical offset were generated for each haematoma. With a series of binary logical operations the grid points falling within the haematoma mask were segmented and then automatically counted. Haematoma volume estimates were then obtained by multiplying the total number of points within the ICH by the point-area (PA) and slice thickness. For each haematoma and at each point-spacing the process was repeated at ten random grid offsets (Fig 3.1).

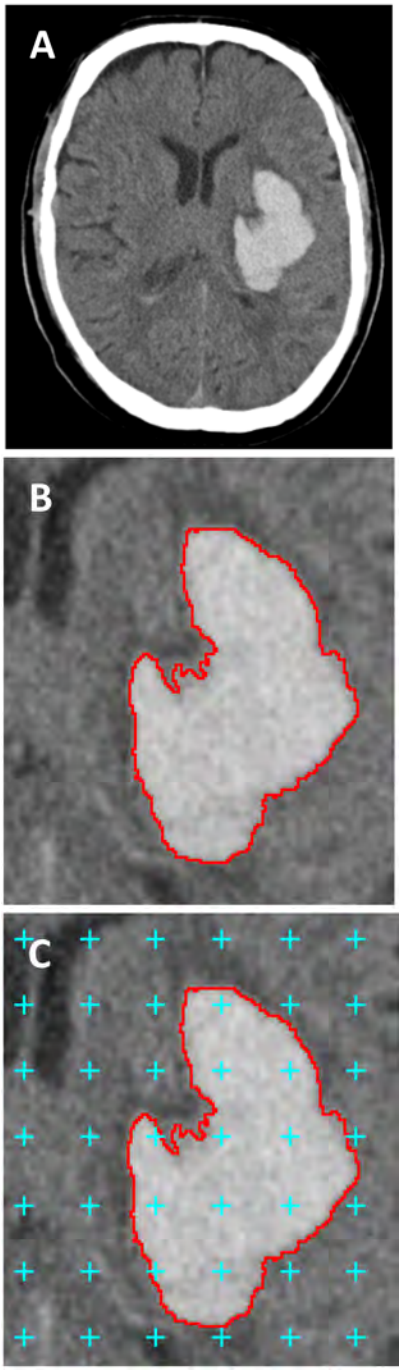

Figure 3.1: Segmentation and Stereological Procedure. A: An example of an ICH included in the study. B: Segmentation by thresholding (red line). C: Crosshair stereology grid with point-area of 100mm^2 (blue); crosses falling within the ICH were automatically counted, in this case n=11.

3.2.5 Contusion Stereology

To apply stereology volume estimation to scans from TBI patients, anonymised standard non-contrast soft tissue kernel CT images with 1-5mm slice thickness were imported and corrected for gantry tilt. The volumes were then resampled to 1mm isotropic voxel spacing with linear

interpolation and windowed to 1-100 Hounsfield Units. A contrasting three-dimensional grid of voxels with 10mm point spacing in three dimensions (i.e. a point volume of 1000mm^3, equivalent to 1cm^3 or 1ml) and with a random offset in each plane was then applied to the CT images. The slices on which the grid appeared were extracted from the full volume and saved; this subset of the isotropic volume was then reviewed and the grid points within regions of haemorrhagic contusion and pericontusional oedema were counted manually.

3.2.6 Statistical Analysis

Accuracy of volume estimation was quantified as the mean difference between estimated and reference volumes with 95% limits of agreement (LoA: Mean +/- 1.96SD) and visualised as a Bland-Altman plot. Correlation was measured with Pearson's r. Data are reported as mean (SEM) unless otherwise stated. The temporal course of contusion volume was characterised by fitting generalised additive models (GAM) separately for the haemorrhagic and oedema components, and the total lesion volume. Standard 10-knot cubic spline bases were used and a random effect (intercept) included for each patient to account for the variable initial contusion volumes. GAMs were fitted using the *mgcv* R package.

3.3 Results

3.3.1 ICH Characteristics and Reference Volumes

Fifty CT scans of patients presenting with acute ICH were selected, with slice thickness of 4-6mm. ICH reference volumes obtained by threshold segmentation ranged from 1.1 to 142.2cm^3 with mean 34.4 (5.3) cm^3. ICH sphericity ranged from 0.27 to 0.58, with mean 0.42 (SEM 0.01). ICH volume and sphericity were inversely correlated (r=-0.58, p<0.001; Fig 3.2).

3.3.2 ICH Volume Estimation by ABC/2. ABC/3, and 2LC/3

Difference plots (Fig 3.3) showed ABC/2 estimates exceeded the reference volume for all but two of the ICHs and there were progressively larger errors in in the ABC/2 estimates as ICH volume increased, correspondingly with wide LoA. Estimates of volume using ABC/3 and 2LC/3 were more accurate. However, estimates with all three formulae showed an inverse correlation with sphericity (Fig 3.4 ABC/2: r=-0.57, p<0.001; ABC/3: r=-0.33, p<0.05; 2LC/3: r=-0.49, p<0.001).

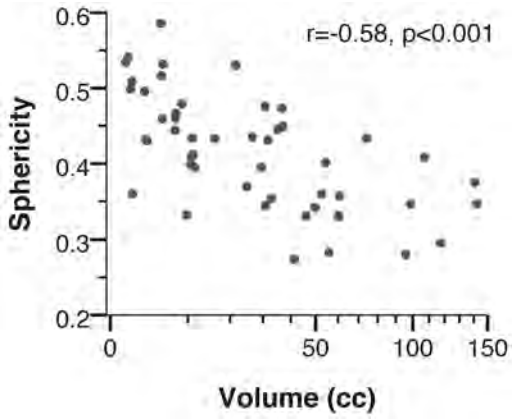

Figure 3.2: Scatter plot of sphericity and reference haematoma volume (cc=cm3); Horizontal axis is shown on a square root scale for clarity

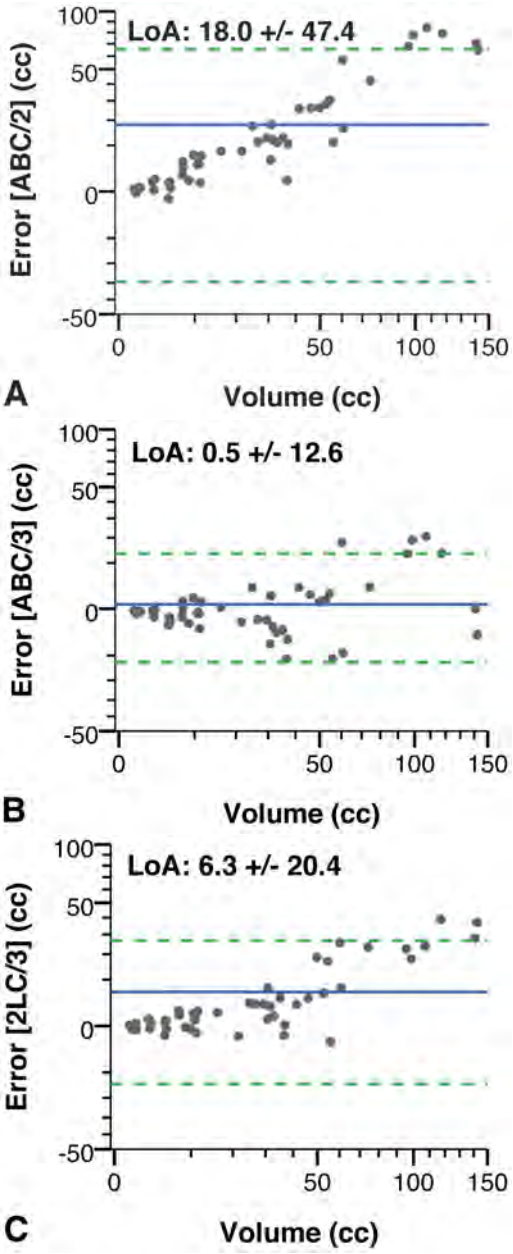

Figure 3.3: Accuracy of Formula-Based Volume Estimates. Difference plots of error vs. reference volume (cc=cm3). Error of A: ABC/2 estimates, B: ABC/3 estimates, C: 2LC/3 estimates. Axes are plotted on square root scales for clarity. Blue/solid line indicates mean error; green/dotted lines indicate 95%LoA.

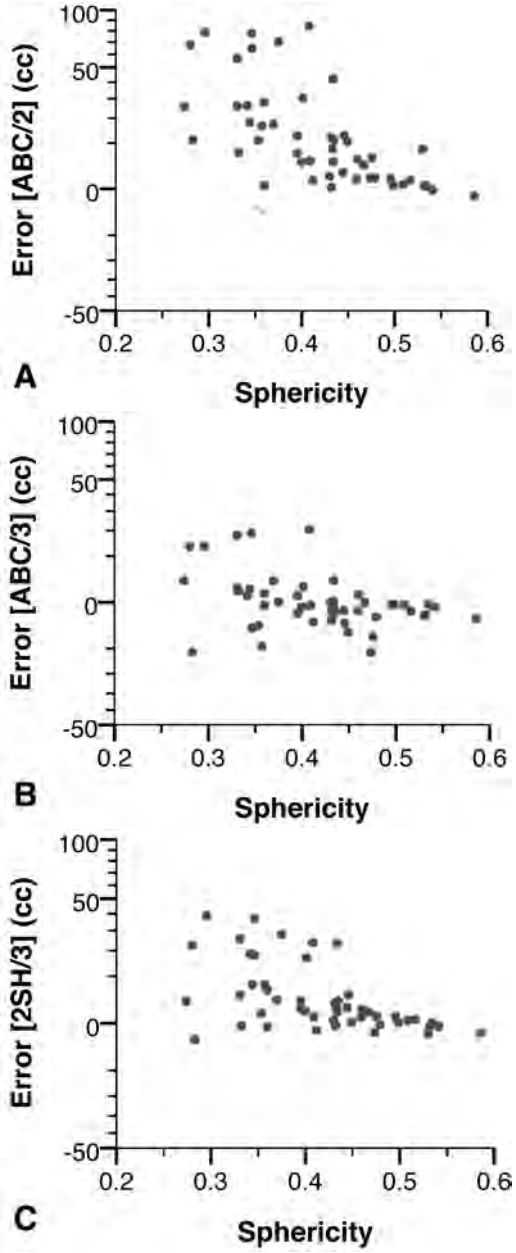

Figure 3.4: Relationship between the error of the formula-based estimates and the haematoma sphericity. Error of A: ABC/2 estimates, B: ABC/3 estimates, C: 2LC/3 estimates. Axes are plotted on square root scales for clarity.

3.3.3 Stereological Volume Estimation

Difference plots of the stereological volume estimates are shown in Fig 3.5. LoA widened with increasing PA but all were narrower than those for ABC/2, ABC/3, or 2LC/3. There were no correlations between stereology estimates and sphericity (all $r<0.05$, $p>0.1$).

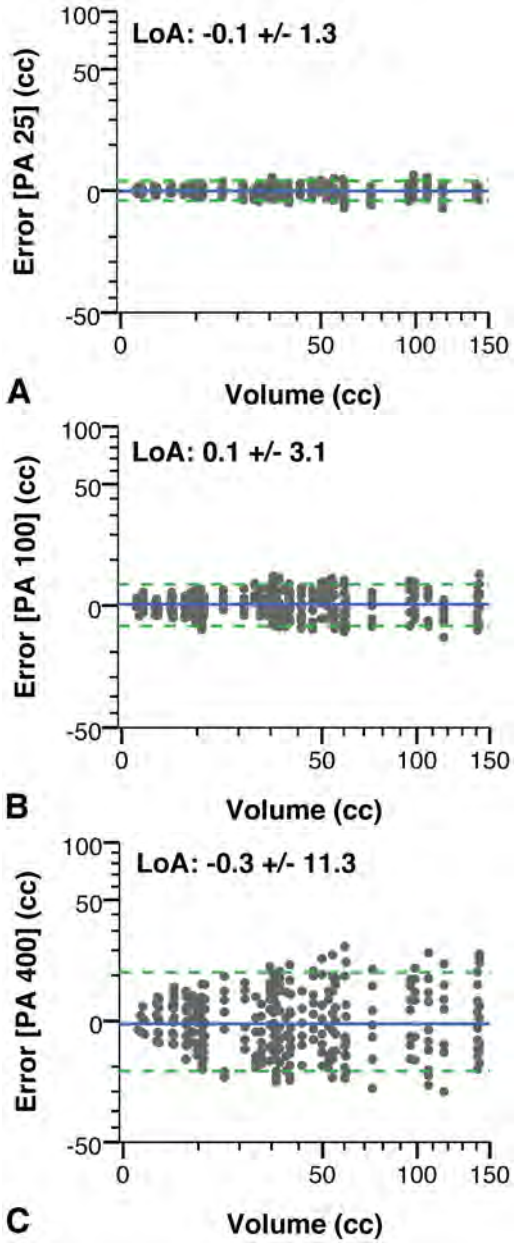

Figure 3.5: Accuracy of Stereology Volume Estimates. Difference plots of error vs. reference volume (cc=cm3). Error of stereology with A: PA=25mm2, B: PA=100mm2, C: PA=400mm2. Axes are plotted on square root scales for clarity. Blue/solid line indicates mean error; green/dotted lines indicate 95%LoA.

3.3.4 Contusion Volume Measurement and Temporal Progression

The stereological technique was applied to the non-contrast routine clinical CT head scans of 52 TBI patients with predominantly contusional TBI (Table 3.1). Patients with a high-velocity diffuse injury pattern or primarily extra-axial haematomas were excluded. All patients required intensive care management of their traumatic brain injury; the median best pre-inubation GCS was 8. All patients were monitored with a standard clinical triple lumen cranial access device,

A total of 252 scans were analysed; each patient had between two and nine suitable scans within 14 days of injury with median number of five.

On the presenting CT scans mean haemorrhagic contusion volume was 20.2ml (SEM 2.7ml, range 1-86ml), and the mean initial oedema volume was 18.0ml (SEM 3.2ml, range 0-112ml; Fig 3.6).

Generalised additive mixed models with 10-knot cubic splines and per-patient random effects were generated to model the temporal course of haemorrhagic contusion volume, oedema volume, and combined total lesion volume (Fig 3.8). This showed that contusion progression was most rapid within the first 72h following injury. Expansion of the haemorrhagic core reached its maximum at around 4 days from injury, whereas pericontusional oedema continued to accumulate at a slower rate until approximately ten days from injury, and thereafter plateaued or slowly declined.

Characteristic		Total N = 52
Age		*(median [IQR] years)*
		48 [31-62]
Sex		*(N [%])*
	Male	42 [80.8]
	Female	10 [19.2]
GCS		*(N [%])*
	3-8	26 [50]
	9-12	12 [23]
	13-15	12 [23]
	N.A.	2 [4]
Pupils		*(N [%])*
	Both reactive	42 [80.7]
	Unilateral unreactive	5 [9.6]
	Bilateral unreactive	0 [0]
	N.A.	5 [9.6]
Mechanism of Injury		*(N [%])*
	Assault	8 [15.4]
	Fall	24 [46.2]
	Cyclist	8 [15.4]
	Pedestrian RTA	2 [3.8]
	Occupant RTA	10 [19.2]

Table 3.1: Admission baseline characteristics of the patient cohort analysed for contusion progression. *IQR, interquartile range; GCS, Glasgow Coma Scale; N.A., not available.*

3.3.5 Contusion Progression, Intracranial Pressure, and Metabolism

There was a significant correlation between maximum contusion expansion i.e. the change in total volume of contusion, incorporating both haemorrhage and oedema, from baseline, and mean ICP over the period of monitoring (Pearson r=0.49, p=0.0012; Fig 3.9A). There was a similar trend to association between contusion expansion and mean LPR (Fig 3.9B). Dividing the patient group in

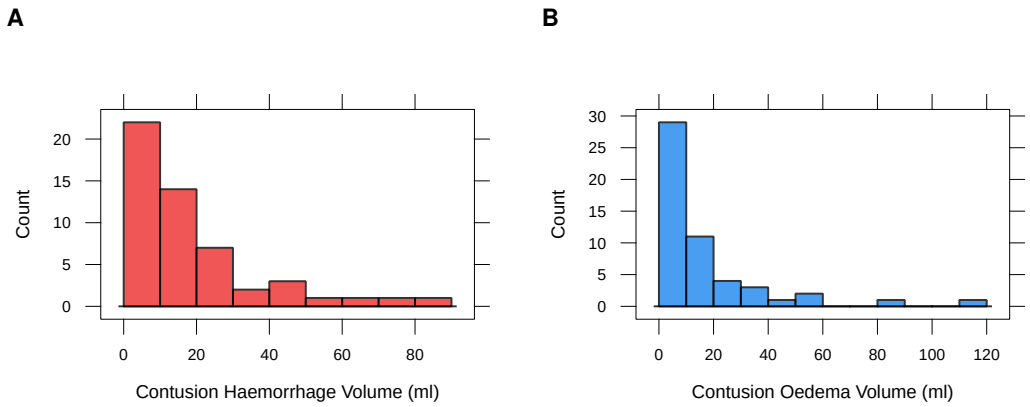

Figure 3.6: Histograms of the (**A**) core haemorrhage contusion volume and (**B**) pericontusional oedema volume on the first available CT for each patient

to those with mean LPR <25 and >25 showed that patients with metabolic dysfunction (i.e. LPR >25) also had significantly greater volume expansion of their contusions (76.5 vs 53.4 ml, t=-2.13, p=0.038; Fig 3.9C)

3.4 Discussion

3.4.1 Validation of the stereology technique

This study provides an objective and quantitative comparison of the accuracy of alternative techniques for estimating brain lesion volumes and demonstrates that stereology is a simple and effective method that can applied to lesions of any shape or size. This finding accords with intuition as in the limit of grid point spacing equal to the image resolution stereology, would be identical to counting the number of voxels within a lesion. At spacings greater than the image resolution stereology will remain accurate at the expense of a degree of precision and tuning the spacing to the particular application defines the magnitude of this trade-off.

To assess stereology and commonly used heuristic formulae for estimating lesion volume the reference or ground-truth volume measurements were obtained by a fixed thresholding operation, hence discrepancies in estimated volumes represented systematic error associated with the specific techniques being tested, rather than inter- or intra-observer variation or user bias. The significant findings are that volume estimates using the ABC/2, ABC/3, and 2LC/3 formulae all suffer increasing error as lesion volume increases and their regularity decreases. ABC/3 was least susceptible and provided the most precise estimates. The findings indicate that larger intracerebral haematomas have more irregular morphology and therefore the assumption of ellipsoidal

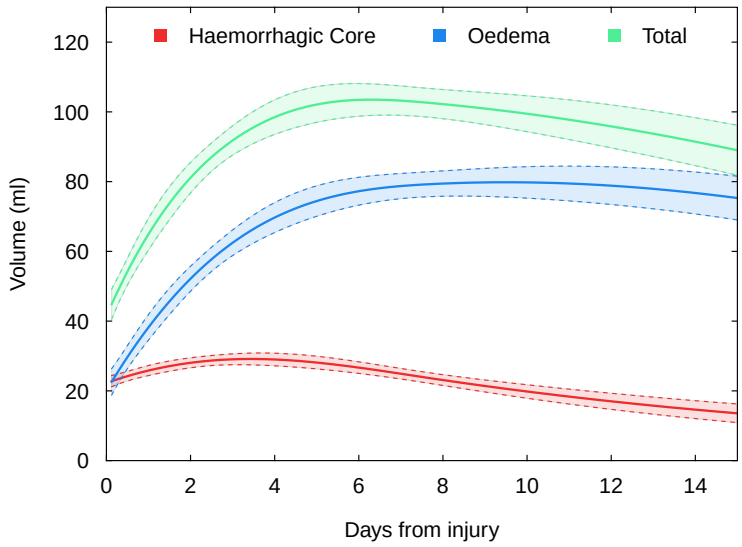

Figure 3.8: Generalised additive modelling of mean contusion volume, pericontusional oedema volume, and total lesion volume over the first two weeks following injury, quantified using stereology; n=52 patients. Per-patient random effect (intercept) included, dashed lines indicate the 95% confidence interval of the mean trend

shape loses its validity.

These data are consistent with earlier reports that ABC/2 overestimates ICH volume, particularly for irregular haematomas, although the magnitude of error observed in the present study was greater. Previously, ICH shape has only been qualitatively assessed as 'regular' or 'irregular' using subjective and study-specific criteria, rather than described by a quantitative metric such as sphericity. As in prior studies of ABC/3 and 2LC/3 we found them to be more accurate than ABC/2, but the degree of error remained dependent on ICH morphology [80, 207, 44].

In comparison to the three formulae, stereological estimates had excellent accuracy and narrower limits of agreement at all grid spacings. Clearly, the relative accuracy of the technique will diminish for objects or lesions of size close to, and certainly below, the point-area. However, a clinically relevant spectrum of ICH size was included in this study and the accuracy was maintained within acceptable limits for all spacings chosen. Depending on the application, grid spacing can be adjusted to maintain a suitable balance between precision and the efficiency of point counting. The point spacing can be reduced to achieve an arbitrary level of precision if required for a particular study. The superior accuracy of stereology over volume estimates based on approximating anatomical structures as ellipsoids has previously been shown in other radiology contexts, for example measuring the volume of the uterus on MR images [85].

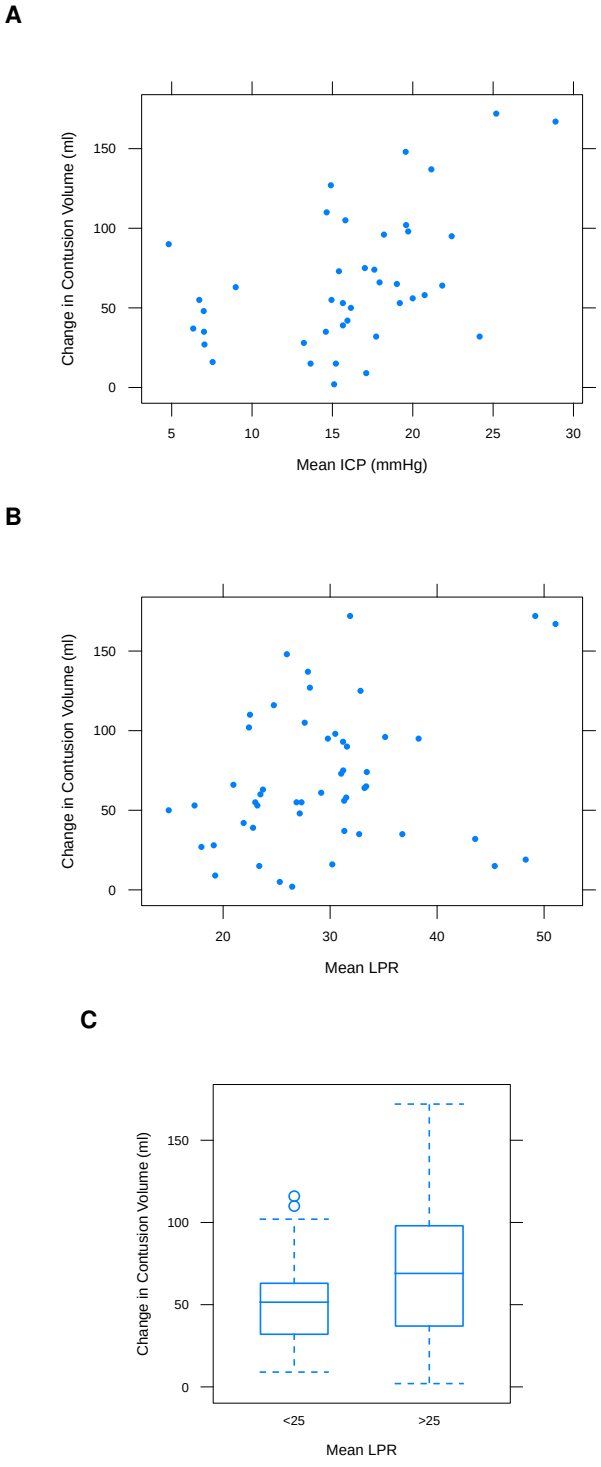

Figure 3.9: Association between contusion progression (i.e. difference between baseline and maximal volume of the total contusion including haemorrhage and oedema) and intracranial monitoring. (**A**) contusion expansion and ICP, (**B**) contusion expansion and LPR (**C**) contusion expansion in patients with mean LPR <25 and >25.

Importantly, the volume estimates with stereology showed no correlation with sphericity, reflecting that stereology is inherently agnostic of object morphology. For this reason, stereology should be equivalently accurate for measuring the volume of any lesion, irrespective or morphology, e.g. extra-axial haematomas, intraventricular haemorrhage, or tumours. Similarly, the volume of multifocal lesions, such as traumatic brain contusions, could be estimated using a technique such as ABC/2 on each individual region of haemorrhage, but this would both be a time consuming process and prone to similar systematic errors as described in this study. In contrast stereology can be applied to multifocal lesions with the expectation of comparable accuracy as for the estimation of volume of solitary objects.

3.4.2 Contusion progression

The existing literature on contusion progression suffers from a lack of consensus in terminology and methodology, and consequent ambiguity as to the specific phenomenon under investgation. Various descriptions include 'progressive haemorrhagic injury', 'delayed intracerebral haemorrhage' and 'haemorrhagic progression of contusion'. Further, studies have tended to examine only the evolution of the haemorrhagic component of contusions from presenting CT to the next available scan within 24-72h, rather than the full temporal course as examined in the present study, and often set arbitrary thresholds, for example 30% relative increase or an absolute increase by 10ml, which can nullify or inflate changes that are clinically important or silent, respectively [3]. Lastly, the focus has typically been solely on the volume of haemorrhage without assessing the co-evolution of pericontusional oedema, which, as this study shows, usually accounts for the greater proportion of total lesion volume.

In a selection of fifty-two patients with contusional brain injury, stereology was employed to characterise the temporal course of contusion volume, comprising of both the haemorrhagic core and pericontusional oedema. The mean non-parametric function fit to the data using a generalised additive mixed model showed that both contusion core and oedema expand principally over the first 72h following injury. Of note, over this period there an approximately linear increase in oedema volume was observed, thereafter expanding at a slower rate and plateauing at around ten days following injury. The mean time course for the haemorrhagic core reached its peak at around day 3-4 and thereafter the hyperdense component of contusions reduced in volume. This presumably reflects both a proportion of the haematoma breakdown products being

absorbed and the changing CT attenuation of blood in the subacute phase as it becomes more isodense with brain. Combined, the overall lesion volume exhibited the most rapid increase over the first 72h following injury, peaking between 5 and 7 days, and then gradually decreasing. These findings accord with the familiar clinical experience that the majority of patients that develop significant cerebral oedema do so over the first several days following admission to intensive care, with intracranial pressure and compliance subsequently improving towards the end of the first week.

The observed association between contusion expansion and intracranial pressure is not unexpected, as lesion expansion is one of the major contributors to raised ICP in this patient population. However, determining the true strength of association between contusion expansion and ICP is confounded by intensity of treatment directed at ICP control. The finding of more pronounced metabolic dysfunction in this patient group suggests that this may a potential cause of more aggressive contusion expansion and thus treatment aimed at correcting LPR could attenuate increases in oedema. However, the cause-and-effect relationship here is uncertain and contusion progression resulting in raised intracranial pressure and impaired cerebral perfusion may be source of the association.

3.4.3 Limitations

Although the inherent accuracy and precision of the stereology technique can be calculated with reference to grid size used, the inter-rater reliability of applying this to the specific measurement of contusions has not been determined and would be the subject of further study. However, a prior study utilising the stereological technique to determine total intracranial volume showed the interobserver coefficient of variation was 4.0% [114].

3.5 Summary and Context

This study has validated a simple, robust, and generalisable technique for volume quantification of intracerebral lesion including haematoma and oedematous brain. Using this method the temporal course of contusion and associated oedema progression was characterised. The majority of haemorrhagic expansion and increase in pericontusional oedema occurs within 72h from injury and thereafter plateaus before slowly receding.

3.5.1 Hypotheses

- H1: Stereology is an accurate method for measuring volume of brain lesions of variable morphology

  Based on the current evidence this hypothesis is accepted.

- H2: Contusion volume expansion predominantly occurs in the first 72h following injury.

  Based on the current evidence this hypothesis is accepted.

Chapter 4

Study II - Dynamic Contrast Enhanced Computed Tomography Assessment of Blood Brain Barrier Permeability

4.1 Introduction

Reliable quantification of blood brain barrier permeability in vivo is an important tool for investigating the pathophysiology of barrier disruption and vasogenic cerebral oedema, and to measure the effects of therapeutic interventions targeted at preventing or limiting these processes. All radiological techniques for detection of BBB permeability have in common the use of intravascular (usually administered intravenously) tracer or contrast agent to which the BBB is normally impermeable and are thus able to label or highlight regions of abnormal permeability. The molecular size of the compounds can be varied to assess the severity of barrier disruption; most are small molecules that are able to diffuse via paracellular routes when there is any degree of tight junction breakdown between endothelial cells, alternatively contrast agents have been complexed with molecules of several kiloDaltons (e.g. albumin) such that contrast extravasation indicates significant BBB opening to proteins and other endogenous macromolecules.

Radioligand-based tracer techniques including SPECT and PET have been validated for quantita-

tive measurements of BBB permeability, however, semiquantitative techniques based on dynamic contrast enhanced computed tomography (DCE-CT; iodinated contrast) and magnetic resonance imaging (gadolinium-based contrast) are cheaper and more widely available and have been introduced into routine clinical practice [182, 28]. Permeability maps from both MRI T1-based dynamic contrast enhancement and T2-based dynamic susceptibility imaging have been shown to be effective at differentiating intrinsic tumour types and also in prediction of haemorrhagic transformation of ischaemic stroke. Similarly, now that whole-head DCE-CT perfusion imaging is routinely available for acute stroke decision making, permeability maps have been shown to be independent predictor of stroke progression and haemorrhagic transformation [134, 145].

This study sought to establish whether DCE-CT is able to show localised BBB permeability related to contusions and/or pericontusional brain in TBI patients, and whether there are consistent temporal changes in the extent of any permeability visualised.

4.2 Methods

4.2.1 Design

Adult patients (>16 years) admitted with contusional TBI and requiring intubation, sedation, and invasive neuromonitoring were selected and informed assent was obtained from relatives. Monitoring and intensive care management was otherwise as per standard local clinical protocols. To assess temporal progression in permeability each patient was enrolled with the intention of being scanned within 48 hours of injury and then scanned again between 3 and 6 days following injury. However, if a patient was clinically too unstable to be transferred to the CT scanner the second scan was not performed unless a scan also required for clinical purposes.

4.2.2 Computed Tomography Imaging

Dynamic contrast enhanced computed tomography imaging was performed on a Siemens Somatom Definition Flash Dual-Energy Spiral CT scanner. An initial standard non-contrast scan was performed immediately prior to each perfusion sequence. For the perfusion imaging, thirty uniformly spaced sequential volume acquisitions with 10cm coverage, centered over the supratentorial compartment, were obtained at 80kV and 200mA over 45 seconds (i.e. every 1.5s) with

an additional further five volumes obtained at 13.5s intervals. Total scanning time was therefore 113s. The maximum scan time permitted by the scanner was 120s. A 50ml volume of iodinated contrast (Iodopam 300) was injected in two phases: 5 ml/s for 6s followed by 1ml/s for a further 20s, with a 50ml saline chaser, via a large bore peripheral venous cannula. Radiation exposure for each perfusion scan was calculated as no more than 7 milliSieverts.

Initial image processing was performed according to manufacturer's instructions on a Siemens SyngoCT workstation with the VolumePCT software module. Raw volume data was reconstructed into 5mm slices with a H20f kernel function. Following application of a 4D denoising algorithm and automatic segmentation of the intracranial compartment, regions of interest (ROI) were placed on a reference artery (typically the anterior cerebral artery) and vein (sagittal sinus). Based on the maximal intensity observed in the reference vessels further automatic Hounsfield unit thresholding was performed to exclude larger vessels from the parameter maps.

The software provides two algorithms for determining permeability based on Patlak analysis [30, 129] or a proprietary Siemens model. The Patlak approach assumes a two compartment model of the intravascular (IV) and extracellular (EC) space with unidirectional permeability of the contrast agent from the IV to EC space but no backflux [129]. The arterial input function is defined as the Hounsfield number in the selected arterial ROI over time, denoted $a(t)$. The corresponding contrast-time function for a given voxel is denoted $r(t)$. The relationship between dynamic enhancement observed in the voxel and AIF is

$$r(t) = P \int a(t)dt + V \cdot a(t) \tag{4.1}$$

where P represents the permeability or rate constant of contrast efflux from intravascular to the extracellular/interstitial space, and V is the volume of distribution of the contrast in the voxel or ROI. Dividing by $a(t)$ gives:

$$\frac{r(t)}{a(t)} = P\frac{\int a(t)dt}{a(t)} + V \tag{4.2}$$

From this equation, the standard Patlak approach is to obtain P and V as the gradient and intercept, respectively, of the line fit to the plot of $\frac{r(t)}{a(t)}$ against $\frac{\int a(t)dt}{a(t)}$, which can both be determined directly from the CT image.

The alternative proprietary manufacturer method involves modelling the voxel contrast enhance-

ment as:

$$r(t) = r_0 + F_{in} \int_{-\infty}^{t} a(t' - t_{in})\, dt' - F_{out} \int_{-\infty}^{t} a(t' - t_{out})\, dt' \tag{4.3}$$

Where F_{in} and t_{in} are the rate at which contrast arrives at the voxel/ROI (i.e. the CBF) and the time at which contrast first appears at the ROI, respectively. F_{out} and t_{out} are similarly defined for contrast leaving the ROI; r_0 is the baseline Hounsfield unit of the ROI. The algorithm then iteratively identifies values of these variables that minimise the cost function:

$$\sum_{n} \left(r_m(t_n) - r_t(t_n)\right)^2 \tag{4.4}$$

where $r_m(t_n)$ and $r_t(t_n)$ are the measured and theoretical profiles of contrast enhancement in the ROI. In this model permeability is then defined as:

$$P = F_{in} - F_{out} \tag{4.5}$$

For this study the parameter maps obtained were cerebral blood flow (CBF, ml/100g/min), cerebral blood volume (CBV, ml/100g), time to start (TTS, seconds), mean transit time (MTT, seconds), and permeability (PMB, ml/100g/min) using both the proprietary and Patlak methods .

4.2.3 Image Analysis

Areas of haemorrhagic contusion were manually segmented on the non-contrast axial CT scan using Fiji/ImageJ and saved as a binary volume of interest (VOI). The non-contrast CT head was then registered with a rigid affine transform to a reference template CT head in standardised Montreal Neuroimaging Institute (MNI) space and resampled to 1mm isotropic voxels using the SimpleITK imaging toolbox suite in the R programming language. Using the transform obtained in this registration as a starting input, the MIP image was then registered to MNI space and similarly resampled. This final transform was then applied to the respective parameter maps and VOI and resampled to 1mm isotropic spacing using nearest-neighbour algorithm to avoid artefacts of interpolation of 'empty' voxels.

A series of VOIs were generated for each scan using mathematical morphology operations provided in SimpleITK functions. The contusion VOI was eroded by spherical structuring elements with 1mm, 2.5mm, and 5mm radii and then the original VOI was subtracted to give three VOIs

of the periphery of the intracontusional tissue of increasing volume. Similarly, the initial contusion VOI was dilated with the same structuring elements, from which the original VOI was subtracted, to give three VOIs of increasing volume of the pericontusional/oedematous tissue (Fig 4.1). Finally, a VOI of the the totality of the non-contusional tissue was also generated. Therefore there was a total eight VOIs for each scan: Contusion VOI, 2mm, 5mm, and 10mm Contusion Edge (CE) VOIs, 2mm, 5mm, and 10mm Pericontusional Tissue (PT) VOIs and a Non-Contusional VOI). Each of these VOI masks was applied in turn to their respective parameter maps and the mean value of the parameter within each VOI was determined.

The mean parameter value in each VOI was analysed in a linear mixed model analysis with the VOI as a factor and incorporating nested random effects for patient and scan. Pairwise comparisons between VOI were obtained with post-hoc tests corrected for multiple comparisons. All statistical analysis was performed in R (v 3.4.3)

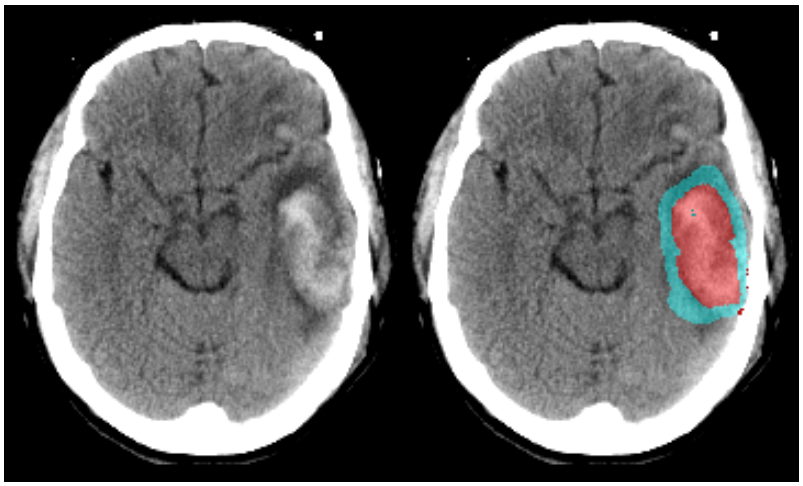

Figure 4.1: Left: unlabelled image. Right: Volume of Interest (VOI) manually circumscribed around the left temporal contusion (red). A VOI for the pericontusional oedema was then generated by morphological dilatation of the original VOI with a 5mm diameter spherical structuring element and the original contusion VOI is subtracted (green). Similar VOIs were generated using 1mm and 2.5mm radius elements and corresponding eroded VOIs were generated for the periphery of the contusion.

4.3 Results

4.3.1 Patients

Ten patients (9 males, 1 female) were enrolled to the study and underwent a total of sixteen CT perfusion scans. All the scans were well tolerated and there were no attributable adverse events due to the imaging or intravenous contrast. Median age of the participants was 51 years and median best pre-intubation GCS was 10 (Table 4.1). The timing of the CT perfusion scans for each

patient is shown in Fig 4.2.

Age	Sex	Mechanism	GCS	Pupils	Marshall	GOS
59	F	Fall	13	Reactive	2d	1
31	M	Fall	10	Reactive	2d	5
29	M	Assault	10	Reactive	2d	6
65	M	Fall	11	Reactive	3	6
48	M	Assault	8	Reactive	2d	1
66	M	Cyclist	14	Reactive	2d	7
48	M	Pedestrian	7	Unilateral	3	7
31	M	Fall	5	Unilateral	3	6
62	M	Fall	9	Reactive	2d	6
55	M	Pedestrian	8	Reactive	3	8

Table 4.1: Demographics of patients in the CT permeability study. Marshall Category 2d indicates bilateral contusions, and Category 3 indicates contusions with basal cistern effacement. GCS: Glasgow Coma Scale, GOS: Glasgow Outcome Score

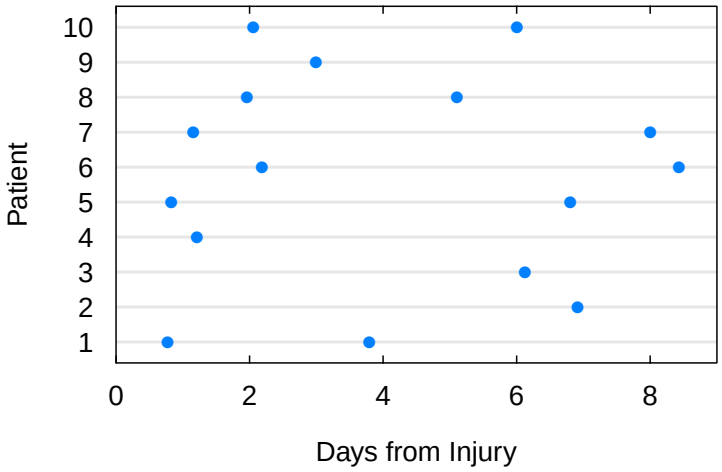

Figure 4.2: Time relative to injury of the CT perfusion scans for each patient in the study.

4.3.2 Qualitative Findings

Uniformly amongst the acquired scans there were profound matched reductions in CBF and CBV corresponding to regions of haemorrhagic contusion. Correspondingly, TTS, TTD, and MTT were also all delayed within these regions and in many voxels no temporal parameters could be calculated. Within the regions of pericontusional oedema (i.e. hypodensity surrounding the haemorrhagic component) there was also reduced CBF and CBV, though not to the same severity as within the contusion core, and MTT, TTS, and TTD were moderately delayed. In the 'non-injured' brain the CBF and CBV maps corresponded to normal white and grey matter values. Somewhat surprisingly, the permeability maps did not show any discernible increase within the haemorrhagic contusion, at the periphery of the contusion or at the boundary between haemor-

rhagic tissue and oedema. Furthermore, there was no apparent increase in permeability within the oedematous brain. Comparing the parameter maps in those patients who had two CTP scans the regions of abnormal CBF and CBV evolved corresponding with the change in contusion size and progression of oedema. However, there was no qualitative difference in permeability between scans performed with 48h and those performed later. A typical example of a scan in this study is shown in Figs 4.3 to 4.7

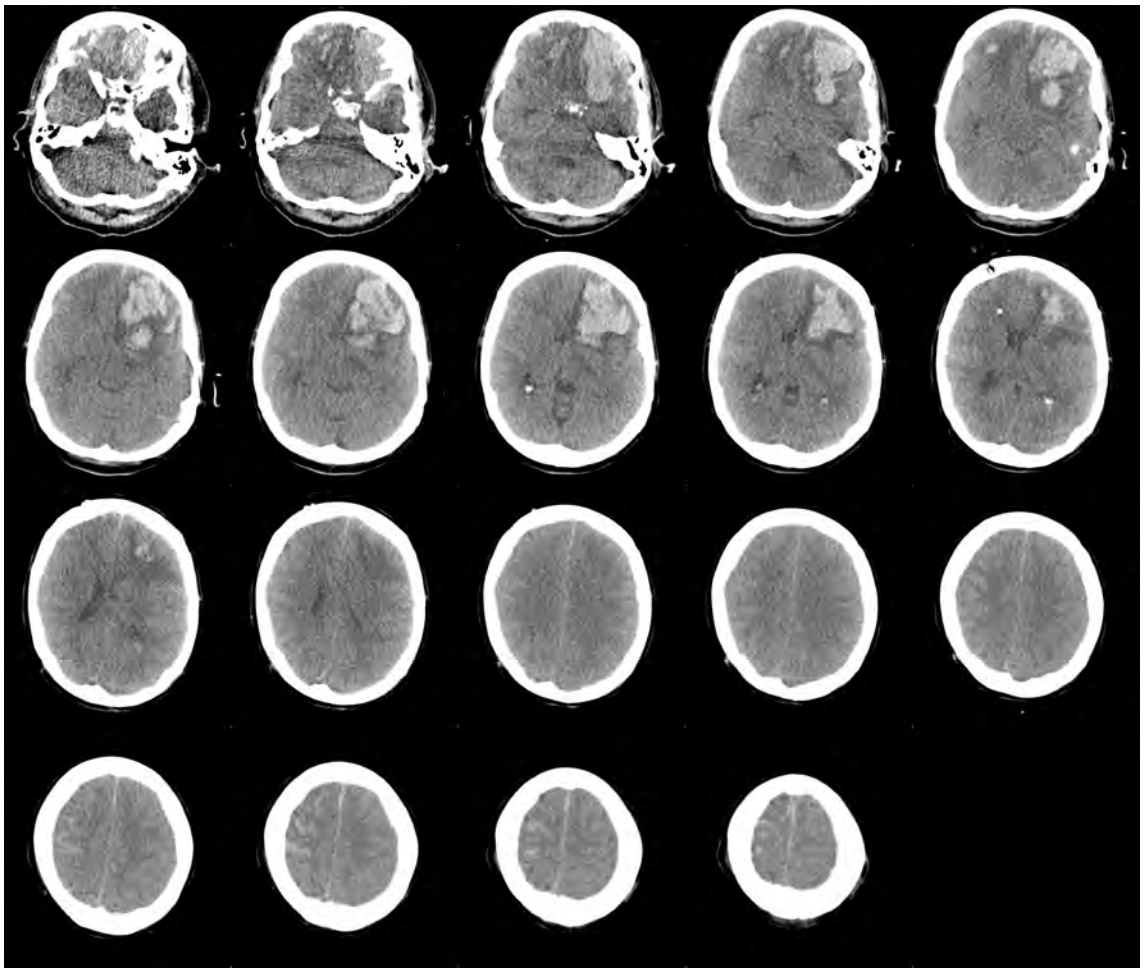

Figure 4.3: Montage of the non-contrast CT head showing large left frontal contusion and smaller right frontal contusions

4.3.3 Quantitative Analysis

Mean parameter values within each of the eight VOIs were obtained for each scan, giving 128 measurements of each parameter. Figures 4.8 to 4.11 show the comparison between VOIs for each parameter. Pairwise comparisons (Bonferroni corrected for multiple comparisons) found no difference in permeability between any of the VOIs (all p=1.0). This finding was unchanged when the analysis was restricted to scans performed within 48 or 72 hours of injury only. A repeat anal-

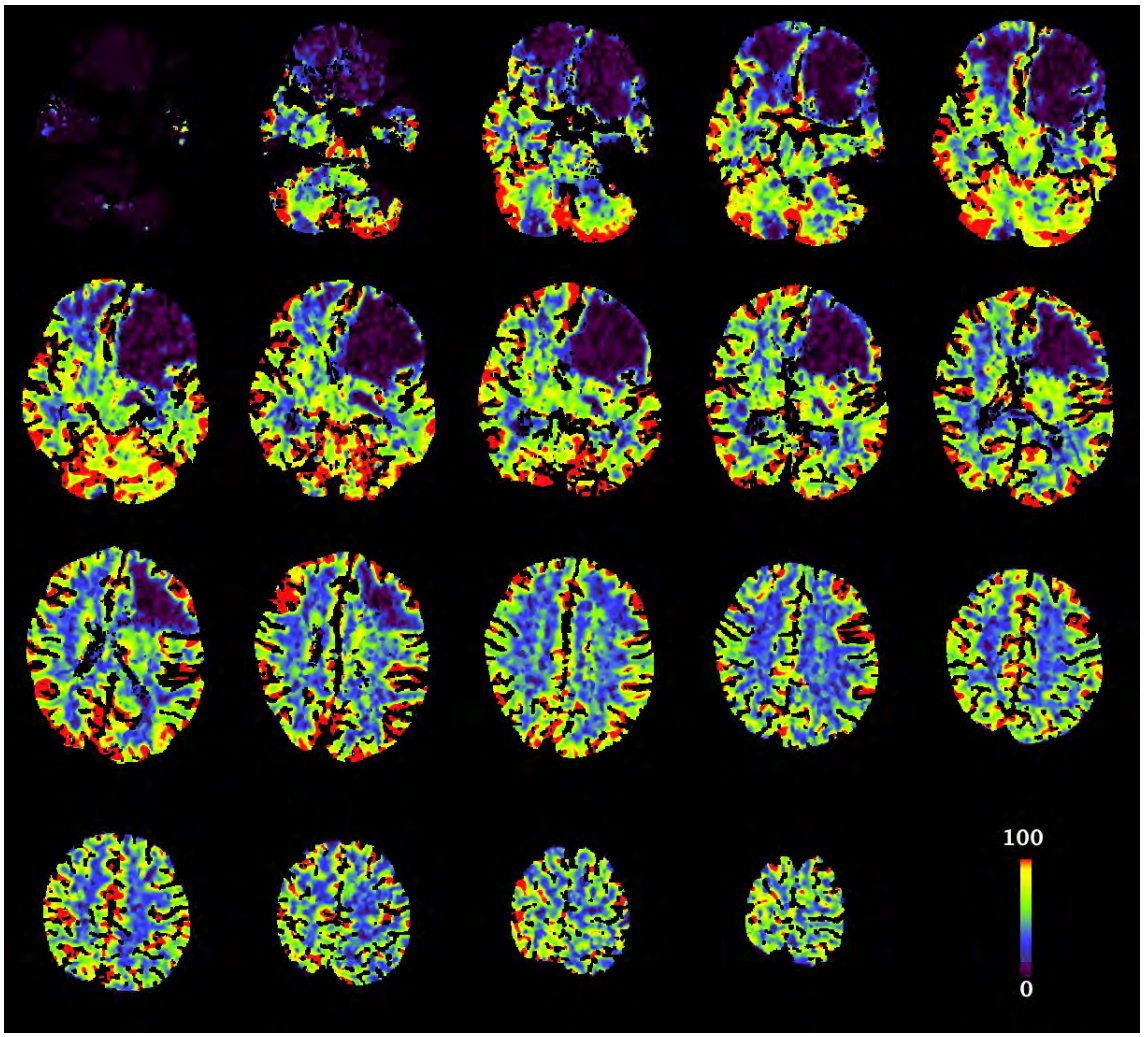

Figure 4.4: Montage of the cerebral blood flow (CBF) parameter map for the same patient shown in Fig 4.3. Units: ml/100g/min

ysis using permeability maps derived with the Patlak method showed similar findings.

For CBF and CBV there were no significant differences amongst the four intra-contusional VOIs or amongst the three peri-contusional VOIs, however both CBF and CBV were significantly higher in pericontusional VOIs compared with contusional VOIs ($p=0.015$ to 10^{-11}) and significantly higher in the non-contusional brain as a whole ($p=10^{-16}$). Correspondingly, MTT was significantly delayed in the contusional VOIs compared with pericontusional VOIs (p<), and both were delayed compared to the non-contusional brain.

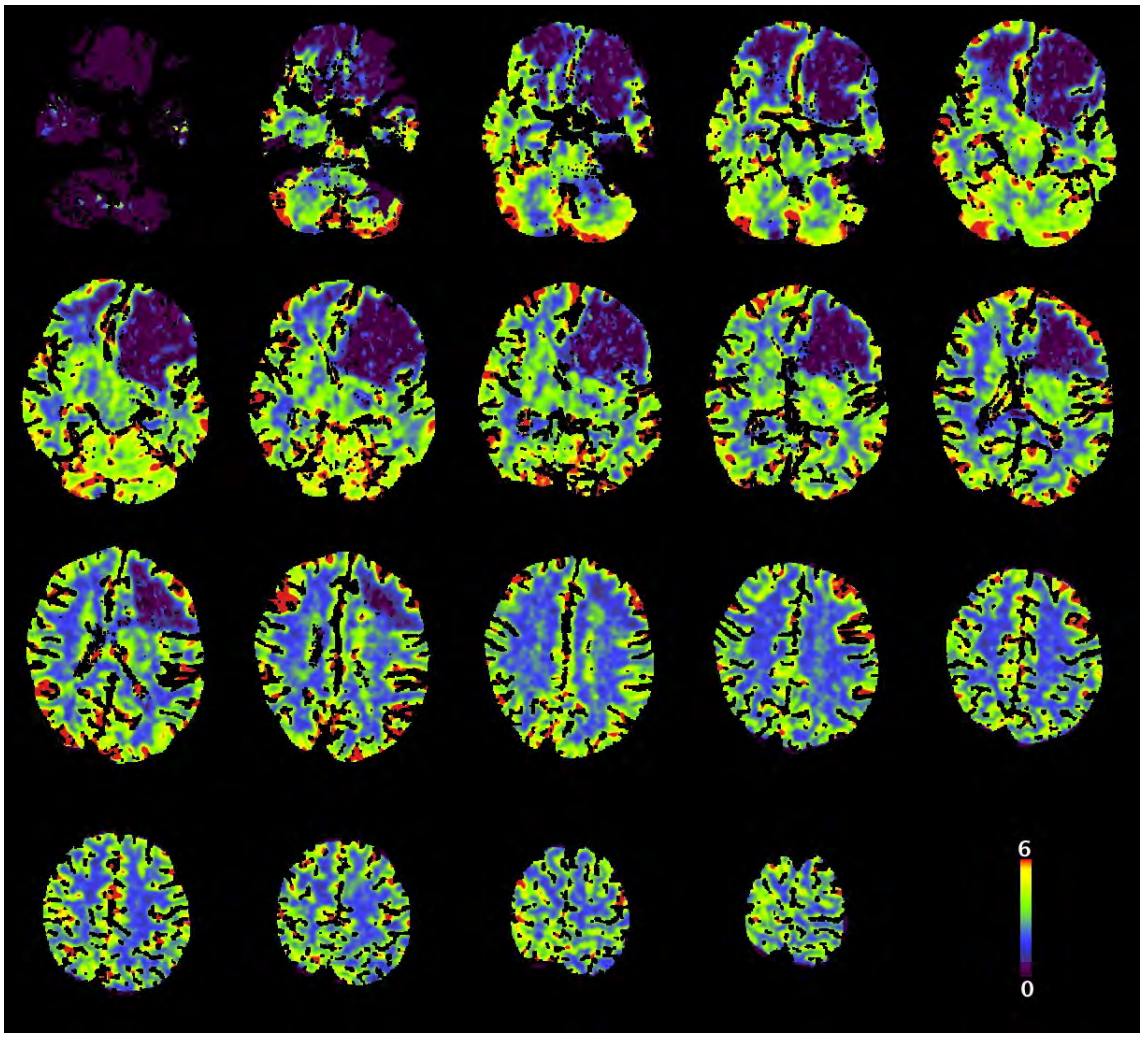

Figure 4.5: Montage of the cerebral blood volume (CBV) parameter map for the same patient shown in Fig 4.3. Units: ml/100g

4.4 Discussion

This study has examined whether dynamic contrast enhanced CT (CT perfusion) is able to demonstrate regions of blood brain barrier permeability in patients with traumatic brain contusions. The analysis sought to identify whether there was an increase in BBB permeability within the haemorrhagic contusion core and in the pericontusional hypodensity that is typically assumed to represent tissue with vasogenic oedema. Both on qualitative assessment and quantitative analysis of permeability maps there was no evidence of increased permeability within contusions or the surrounding tissue. This finding was true of scans performed within 72h and those acquired later following injury.

There are a number of potential explanations for the absence of observable BBB permeability in

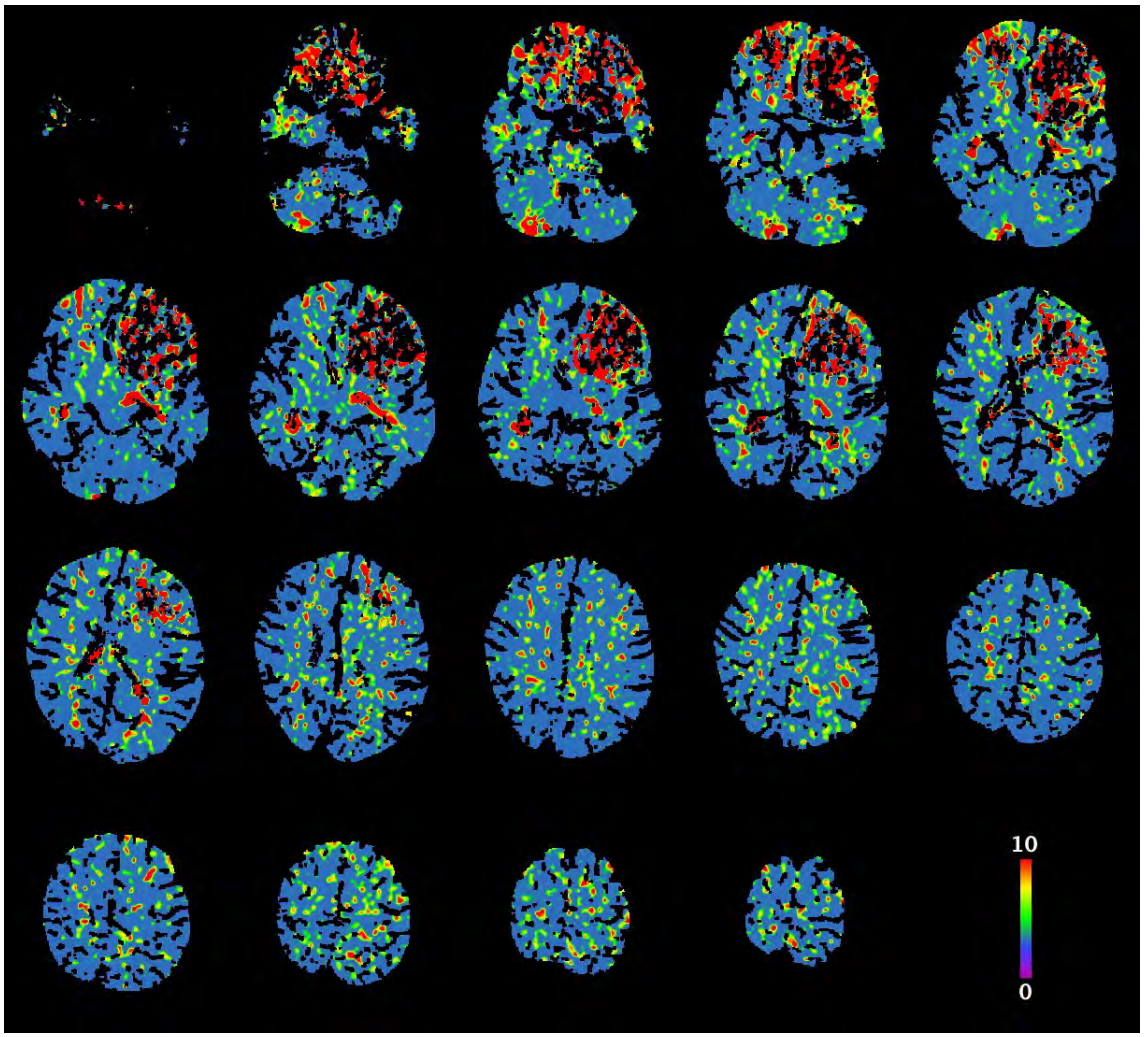

Figure 4.6: Montage of the mean transit time (MTT) parameter map for the same patient shown in Fig 4.3. Units: seconds

the present study. As has been argued previously, BBB disruption and the classical picture of vasogenic oedema may not be the primary mechanism of brain swelling following TBI [112, 177]. Alternatively, it could be the general imaging paradigm of contrast extravasation is not sufficiently sensitive to test for permeability in lesions with very low cerebral blood flow as was quantified here with perfusion parameters. Iodopam, the contrast agent used in this study, has a molecular weight of 820Da - while it is conceivable that BBB permeability may have been present but with pore sizes sufficient to transmit only molecules with a lower molecular weight, this would contrast sharply with the much more profound disruption permitting passage of macromolecules of many kDa and infiltrating inflammatory cells that is observed in preclinical models [154]. Lastly, it is possible that the specific imaging protocol and analysis in this study may have been poorly tuned for demonstrating increased pericontusional permeability.

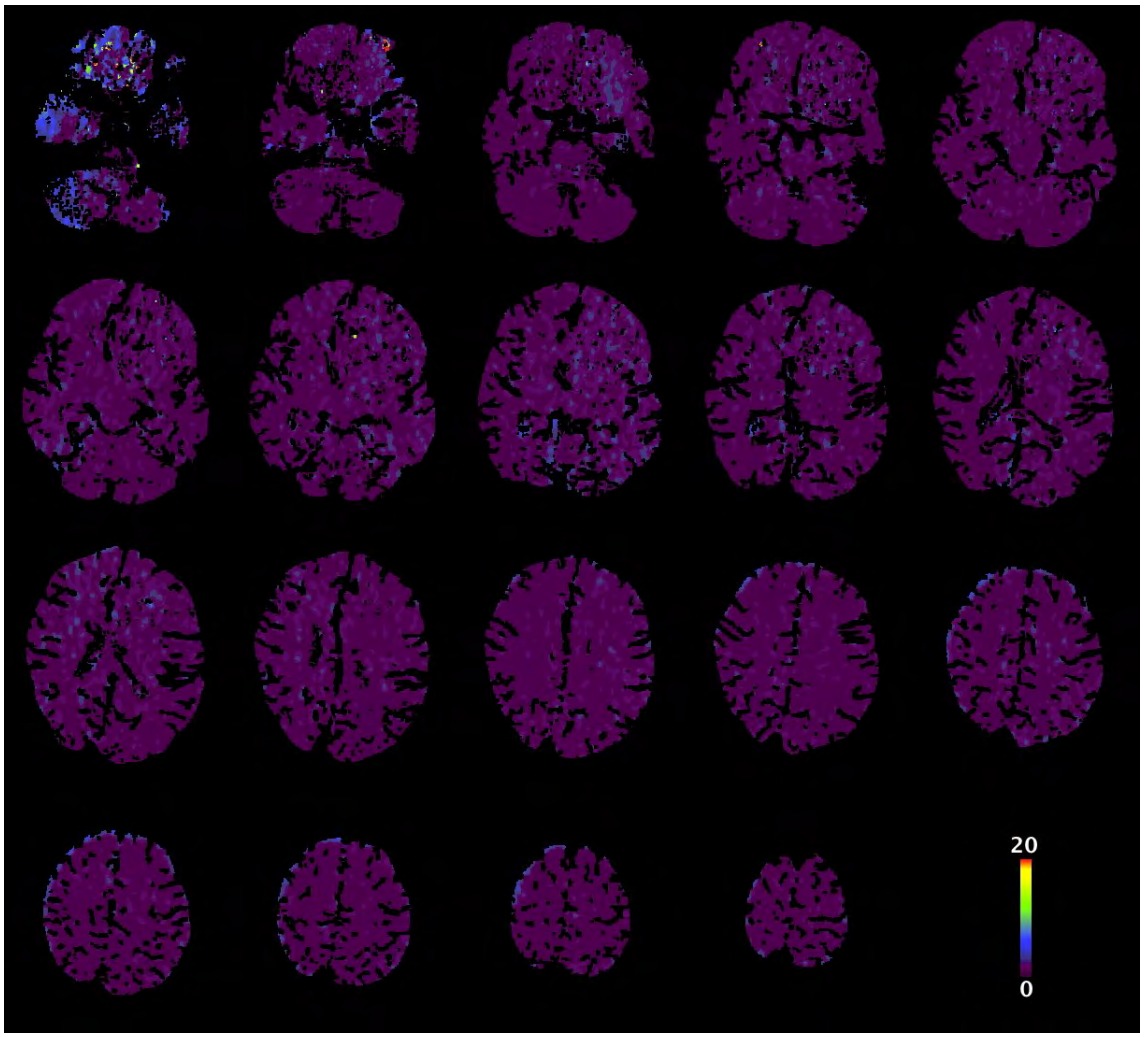

Figure 4.7: Montage of the permeability (PMB) parameter map for the same patient shown in Fig 4.3. Units: ml/100g/min

Whereas the preclinical literature contains a large number of reports demonstrating BBB disruption in a variety of TBI models using both histological and radiological quantification of contrast extravasation, there is a relative paucity of clinical studies examining BBB integrity in TBI patients. Early studies using gadolinium contrast enhanced magnetic resonance imaging in patients with contusional TBI reported inconsistent findings. This form of imaging is not a dynamic scanning technique wherein there are a series of acquisitions but a standard single pre- and post-contrast scan are performed. Lang et al [100] examined ten TBI patients with Gd-DPTA contrast MRI but found no evidence of contrast extravasation in those imaged within four days of injury, whereas the three patients who were imaged later that day six did show perilesional enhancement indicative of contrast extravasation. A subsequent study by Kushi et al. [97] also studied ten patients with Gd-DTPA MRI between 24-48h following injury but with post-contrast image was delayed to 2 and 4 hours following Gd-DPTA administration; contusions in all patients exhibited some

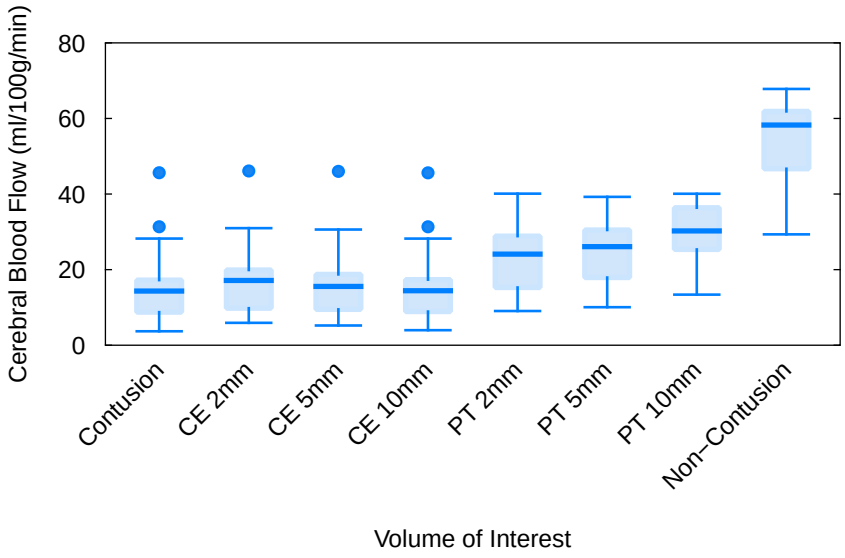

Figure 4.8: Comparison of cerebral blood flow amongst the VOIs

degree of enhancement. These qualitative studies suggest that BBB disruption is common following contusional TBI but that demonstration of the phenomenon may be vary dependent on scan protocols.

The much more extensive literature on dynamic contrast enhanced perfusion CT in the context of ischaemic stroke provides some useful insight into the current study [30]. Perfusion CT is now standard practice in the diagnosis and management planning of ischaemic stroke and increased peremeability associated within infarct and penumbra territories has been consistently shown to predict haemorrhagic transformation and propensity to haemorrhage following thrombolysis treatment [76]. The observation of permeability in ischaemic and oligaemic tissue following stroke suggests that perfusion CT is able to demonstrate permeability in tissue with low blood flow.

However, there is evidence that the duration of perfusion CT scans is important in the accuracy of permeability calculations. This arises from the fact that the contrast will arrive later at voxels in regions of low blood flow compared with the reference AIF and therefore calculations based on the 'first-pass' (<90s) of contrast will be misleading. More accurate permeability quantification can be achieved when additional scan volumes beyond 90s are incorporated and the contrast level in blood is quasi-steady state. Specifically, Dankbaar et al. [41] have shown that acqusitions of further scan volumes to 240s following contrast injection improves the reliability of permeability

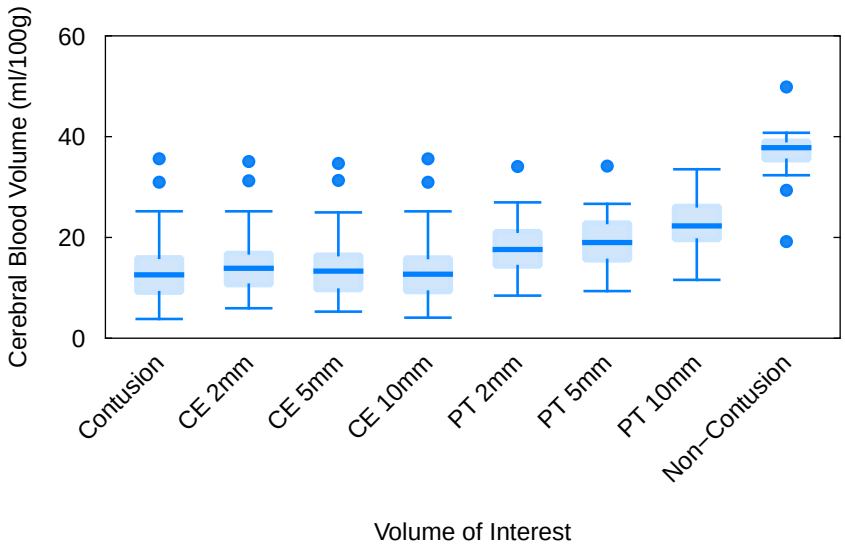

Figure 4.9: Comparison of cerebral blood volume amongst the VOIs

calculations compared with those based on the first-pass of contrast at up to 90s. However, the permeability values determined from first-pass are typically in excess of those obtained from inclusion of the additional delayed scans and correspondingly a technique developed by the same authors to correct perfusion scans limited to first-pass acquisitions was shown to decrease the estimated permeability. In a study from a separate group, permeability parameters from first-pass and delayed acquisition were shown to be reasonably well correlated with each other (r=0.67), with the latter being generally higher. These studies suggest that the scans used in the present investigation, with a total acquisition time of under 120s, would be expected to over-estimate permeability. A software lock on the CT scanner control console prevented developing an imaging protocol exceeding 120s. Conceivably, additional scan volumes could be obtained by concatenating a second protocol incorporating a series of delayed acquisitions. However, these additional scans would have been incompatible with the perfusion CT software provided by the manufacturer and could not have been included in the analysis algorithm. The feasibility of a combined study to compare perfusion CT with alternative modalities including dynamic perfusion MRI and PET for assessing BBB permeability was also explored but administration of gadolinium based contrast agents is not permitted for research participants (unless there is also a clinical indication) and the necessary PET ligands and protocols were not established and would not have been possible to validate in a realistic time frame.

A further qualitative indicator of BBB permeability that may be observed on either perfusion

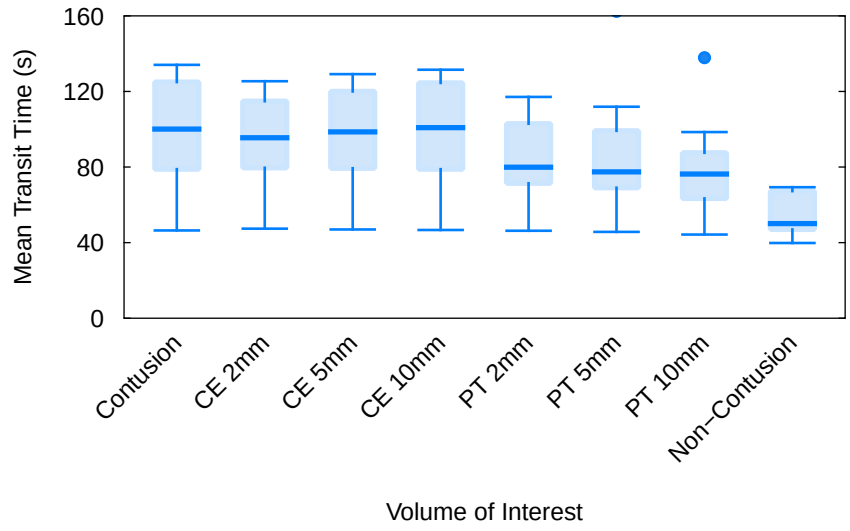

Figure 4.10: Comparison of mean transit time amongst the VOIs

CT or CT angiography is the so-called 'spot sign', described as a focal area of perilesional contrast extravasation that is presumed to indicate microvascular disruption and contrast extravasation. Similar to quantitative permeability maps, the presence of the spot sign in stroke patients is a predictor of haemorrhagic transformation and of progression of intracerebral haemorrhages [189]. In a series of 22 TBI patients studied with perfusion CT scan within six hours of injury, 9 were reported to show contrast extravasation and this subset of patients had a higher incidence of haemorrhagic contusion progression and greater oedema volume at 24h post-injury [77].

Although the primary objective of this study was to examine BBB permeability the perfusion parameters associated with contusions were also of interest. Profound reductions in cerebral blood flow and blood volume were observed within contusions and to a lesser degree in pericontusional brain. Previous studies have shown that perfusion CT can identify contusions that are not visible on plain non-contrast CT and that reductions in CBF have prognostic implications [116, 20]. The graduated concentric pattern of CBF reduction from contusion core through pericontusional tissue to normal brain has been previously observed in TBI patients studied with a number of perfusion imaging modalities and the volume of hypoperfused tissue, or the mean brain CBF has been associated with outcome [143]. CBF thresholds for infarction are dependent on duration and metabolic demand but CBF below approximately 16-18 ml/100g/min results in arrest of neuronal electrical activity and infarction after several hours; CBF below 12 ml/100g/min is associated with loss of membrane function and ion homeostasis [13]. In the present study median

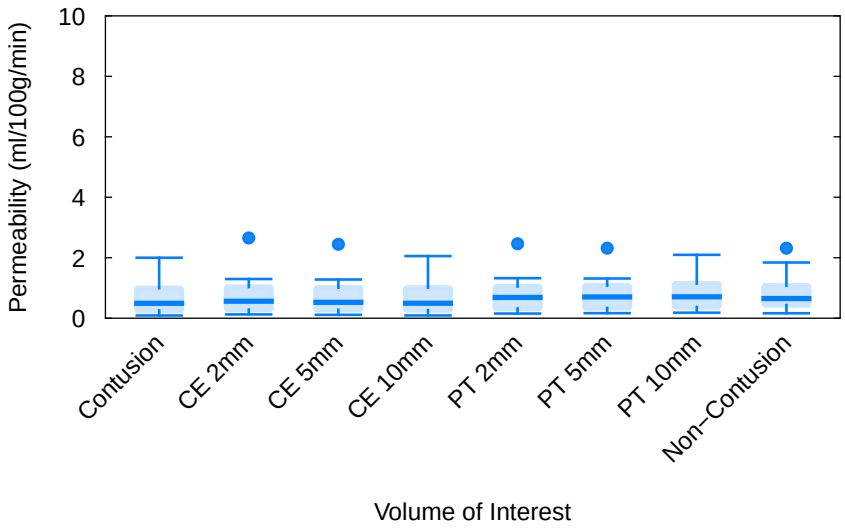

Figure 4.11: Comparison of permeability amongst the VOIs

CBF in the contusion VOI was around the 18ml/100g/min threshold suggesting that this tissue is at risk of infarction. CBF in pericontusional hypodense tissue VOI was significantly higher than in respective contusion VOI and approximately in the oligaemic range considered as penumbral tissue in the context of stroke; here cells may be inactive but remain viable and the tissue is potentially salvageable. However, the application of threshold values derived from stroke studies in TBI requires further validation. The burden of hypoperfusion or ischaemic brain demonstrated on perfusion CT has been shown to predict outcome following TBI, similar to the findings of earlier PET studies [20].

4.5 Summary and Context

Perfusion CT, according to the protocol used in this study, was unable to demonstrate BBB permeability related to brain contusions. The haemorrhagic core of contusions are associated with significantly reduced CBF and CBV to levels comparable with ischaemic thresholds and pericontusional brain has parameters similar to those observed in stroke penumbra.

4.5.1 Hypotheses

- H3: Dynamic contrast enhanced computed tomography can quantify the severity of BBB permeability in the vicinity of brain contusions.
  Based on the current evidence this hypothesis is not accepted

- H4: Maximal BBB permeability is observed at around 72h following injury.
  There was insufficient evidence to evaluate this hypothesis

Chapter 5

Study III - Pericontusional Inflammation: Cytokine, Chemokines, and Growth Factors

5.1 Overview

Cerebral contusions frequently enlarge over the several days following traumatic brain injury (TBI), involving a combination of haemorrhagic progression of the lesion core together with an expanding volume of vasogenic and cytotoxic oedema. These phenomena exacerbate local tissue destruction and cell loss, and also contribute to global secondary injury through raised intracranial pressure, brain shift, and ultimately uncal or transtentorial herniation [96].

The important contribution of inflammatory signalling to both secondary brain injury in the acute phase and later reparative processes has been increasingly recognised as the concept of central nervous system (CNS) immune privilege has been challenged and reconsidered over recent years. Evidence from in vitro and animal models has highlighted the role of cytokines, chemokine and growth factors in secondary injury following TBI [70].

Previous microdialysis studies have provided evidence for a canonical temporal sequence of immune mediators in patients with a diffuse pattern of TBI. Further, systemic administration of IL-1 receptor antagonist (IL1ra) modified the cerebral immune response in a pilot randomised controlled clinical trial of patients with diffuse TBI, suggesting potential as a novel pharmacological

intervention. However, it remains unclear whether a similar or distinct pattern of cytokine and chemokine expression is apparent in the pericontusional brain of focal TBI patients; characterising this localised response will be essential to successfully developing therapies directed at immune mediators.

Furthermore, specific cytokines and growth factors have been strongly implicated in the component of the inflammatory response that promote blood brain barrier permeability. In particular, Vascular Endothelial Growth Factor (VEGF) has been shown to disrupt the synthesis and formation of tight junction proteins, and VEGF antagonists reduce oedema following experimental TBI [179, 190]. The end effector of VEGF distrupting the BBB is MMP-9. Both VEGF and MMP-9 have been found at high concentrations in contusionectomy samples from TBI patients [74]. It has not been demonstrated in vivo whether there is spatially localised expression of VEGF in the vicinity of contusions.

In this study, I have undertaken targeted microdialysis monitoring of pericontusional brain regions in TBI patients to define the localised expression of selected cytokines, chemokines, and growth factors. To control for the contribution of catheter insertion to the immune response we have simultaneously monitored radiologically normal brain in each patient for comparison.

5.2 Methods

5.2.1 Recruitment and Monitoring

Adult patients with TBI requiring neurointensive care and invasive monitoring were eligible for recruitment to the study. Invasive neuromonitoring was inserted at two sites for each patient with the intention of having a microdialysis catheter within radiologically 'normal' white matter and another within pericontusional brain but avoiding the haemorrhagic core. On admission a triple-lumen cranial access device (Technicam, Newton Abbott, UK) was placed in the right or left frontal region as standard. An intracranial pressure (ICP) monitor (Codman, Raynham, MA, USA), a brain tissue oxygen probe (Licox Neurosciences, Andover, UK), and a microdialysis catheter (CMA 71, 100kDA molecular weight cut-off) perfused with 3.5% (w/v) Human Albumin Solution (Pharmacy Manufacturing Unit, Ipswich Hospital NHS Trust, Ipswich, UK) in central nervous system perfusion fluid, were introduced via the access device. Following assent, up to

three further invasive monitors, at least one of which was a microdialysis catheter (CMA 71 and perfused with 3.5% albumin solution, as above) were placed in proximity to a contusion, either via a second cranial access device or twist drill holes. If the first set of monitors happened to be placed adjacent to a contusion the second set were inserted in radiologically normal brain on the contralateral frontal region. In patients requiring an emergent craniotomy for an acute subdural haematoma the pericontusional monitoring was placed adjacent to underlying contusions under direct vision at the end of surgery, tunnelled through the scalp.

5.2.2 Sample Analysis

Hourly microdialysates were pooled into 8-hourly samples. All samples were analysed using the Milliplex Multi-Analyte Profiling Human Cytokine 42-plex analyte premixed kit (Millipore, St Charles, MI, USA) according to the manufacturers' instructions. All samples were assayed in duplicate wells (25 microL per well) and the mean of these results was used. The plates were read using a Luminex 200 analyser (Luminex Corporation, Austin, TX, USA) running STarStation software (Applied Cytometry Systems, Sheffield, UK). Protein concentrations were calculated by reference to an eight-point spline fit curve for each cytokine or chemokine.

5.2.3 Statistical Analysis

The temporal course of each cytokine was fitted with a generalised additive model including site of monitoring as a fixed factor and a random intercept for each patient. Ten-knot cubic spline bases were employed and the restricted maximum likelihood criterion was optimised to obtain the best fit. An F-test was performed for each cytokine to assess if there was a difference in concentration-time course between injured and non-injured brain. To examine the broader trends in cytokine expression and their relationship to time from injury and site of monitoring a multivariate dimension reduction technique, namely partial least squares analysis (PLS) based on further pooling the microdialysis samples into two groups: within 72h of injury and later than 72h. The PLS was performed with the non-linear iterative partial least squares (NIPALS) algorithm, which is tolerant of missing values in the data, using the *mixOmics* package (v6.1.0, https://cran.r-project.org/web/packages/mixOmics/index.html). This technique reduces the mulitvariate data to one or two 'principal' dimensions or factors that capture the dominant variation in the data and has previously been applied to cytokine assays from TBI patients [71]. To

assess how well the principal factors identified in the analysis discriminated between injured and non-injured brain a receiver-operating characteristic curve was used.

5.3 Results

5.3.1 Patients

Twelve patients (9 male; mean age 47.5 years, range 22-67 years) were enrolled (Table 5.1). Paired microdialysis monitoring was commenced a mean of 34 hours (range 16-44) following injury. Two patients died during their intensive care treatment due to refractory intracranial hypertension.

Age	Sex	Mechanism	GCS	Pupils	Marshall	Evacuated SDH	GOS
28	M	Fall	8	+/+	2d	-	4
67	M	Fall	6	+/+	5b	Right	3
67	M	Pedestrian RTA	10	+/+	2c	-	3
59	F	Fall	12	+/-	2d	-	1
65	M	Fall	11	+/+	2d	-	4
55	M	RTA	9	+/+	5b	Left	5
42	F	Fall	3	-/+	5b	Left	3
30	M	RTA	7	+/+	5b	Right	5
22	M	Assault	8	+/+	5b	Right	4
42	M	Fall	7	+/+	5b	Left	5
51	M	Fall	9	+/+	2d	-	1
42	F	Fall	5	-/+	2d	-	3

Table 5.1: Details of patients in the study. Marshall Category 2c indicates multiple unilateral contusions, 2d indicates bilateral contusions, category 3 indicates contusions with basal cistern effacement, and 5b indicates evacuated subdural haematoma. GCS: Glasgow Coma Scale, GOS: Glasgow Outcome Score (at 6 months following injury)

5.3.2 Univariate analysis

Generalised additive models for each of the 42 cytokines assayed, together with F-tests to compare the two monitoring sites for significant differences in time-concentration curves are shown in Fig 5.1. The majority of the cytokines exhibited largely monotonic time courses of decreasing concentration over the monitoring period. Exceptions to this pattern were IL-1a, IP-10, PDGFAA, and both IL-1ra and MCP-3 in pericontusional brain, all of which were observed to have a peak concentration between 48-96h following injury. EGF, FLT-3 ligand, Fractalkine, GM-CSF, IFN-g, IL-1a, IL-1b, IL-1ra, IL-3, IL-4, IL-6, IL-7, IL-9, IL-12p40, IL-12p70, IL-15, IL-17, IP-10, MDC, MIP-1a, MIP-1b, PDGFAA, PDGFABBB, sIL-2Ra, TGFa, TNFa, and TNFb were not found to have significant differences in either overall concentration or temporal profile between non-injured and injured brain. G-CSF, GRO, IL-2, IL-5, IL-10, RANTES, and sCD40L had significantly lower concentrations at the injured monitoring site but similar temporal profiles. In contrast, Eotaxin,

FGF-2, IFN-a, IL-8, IL-13, MCP-1 were higher in pericontusional brain but had comparable time-course as at the control site. Concentrations of MCP-3 were significantly higher in pericontusional brain and also appeared to have a delayed peak level compared to consistently decreasing concentrations in uninjured brain. VEGF was non-significantly elevated in peri-contusional brain in the 24-48h period but thereafter was lower in the injured tissue.

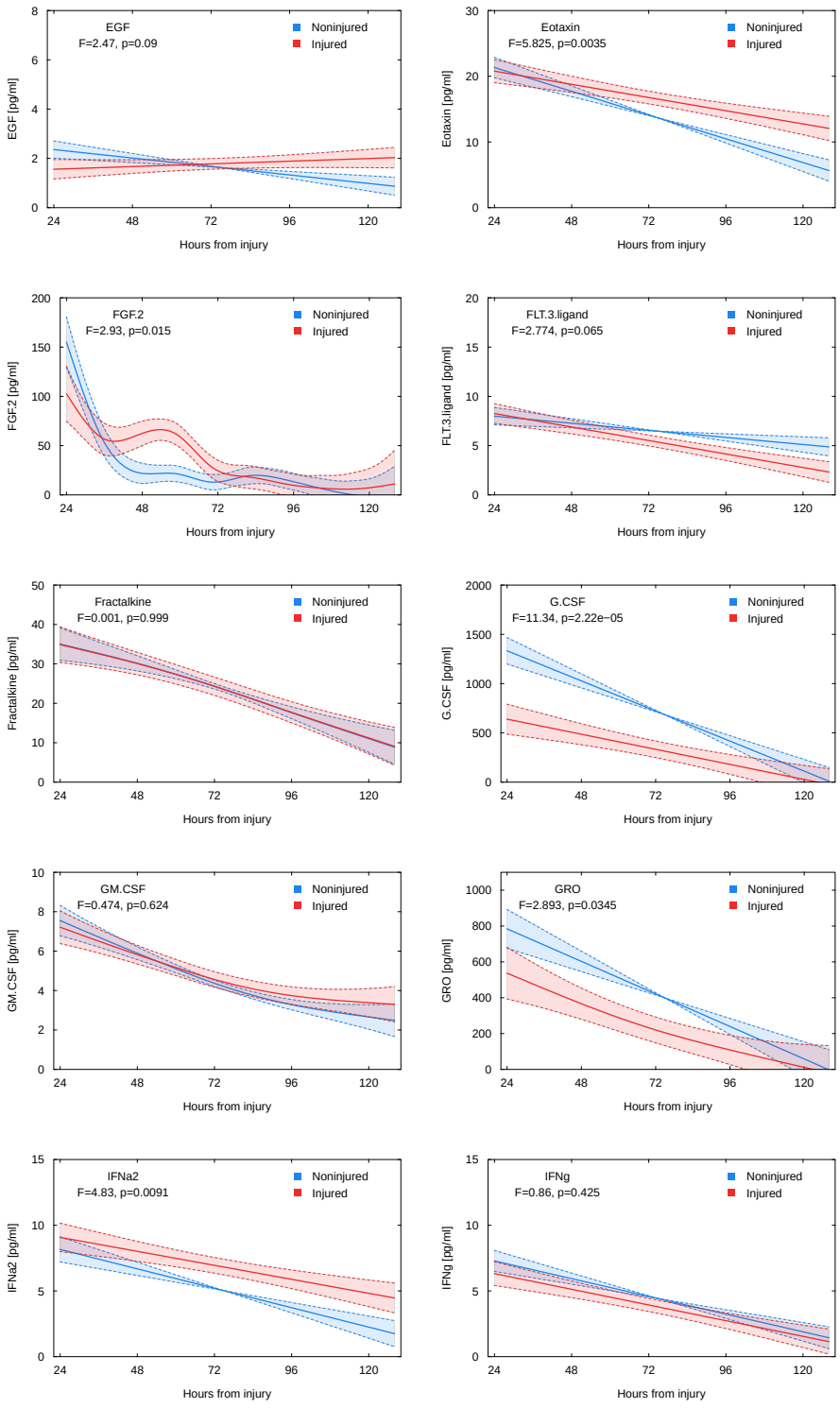

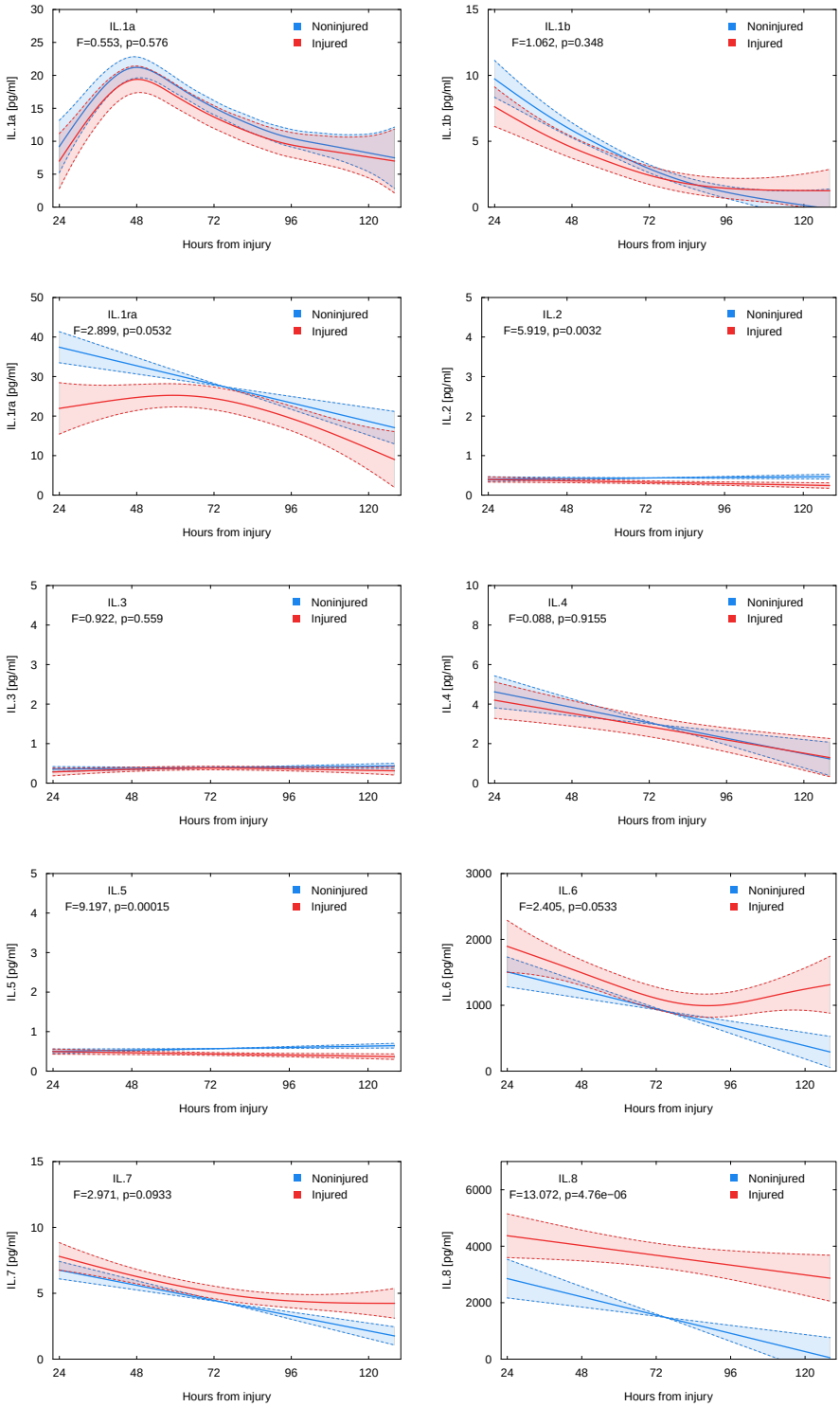
IL.1a
F=0.553, p=0.576
IL.1a [pg/ml]
IL.1b
F=1.062, p=0.348
IL.1b [pg/ml]
IL.1ra
F=2.899, p=0.0532
IL.1ra [pg/ml]
IL.2
F=5.919, p=0.0032
IL.2 [pg/ml]
IL.3
F=0.922, p=0.559
IL.3 [pg/ml]
IL.4
F=0.088, p=0.9155
IL.4 [pg/ml]
IL.5
F=9.197, p=0.00015
IL.5 [pg/ml]
IL.6
F=2.405, p=0.0533
IL.6 [pg/ml]
IL.7
F=2.971, p=0.0933
IL.7 [pg/ml]
IL.8
F=13.072, p=4.76e−06
IL.8 [pg/ml]
Noninjured
Injured
Hours from injury

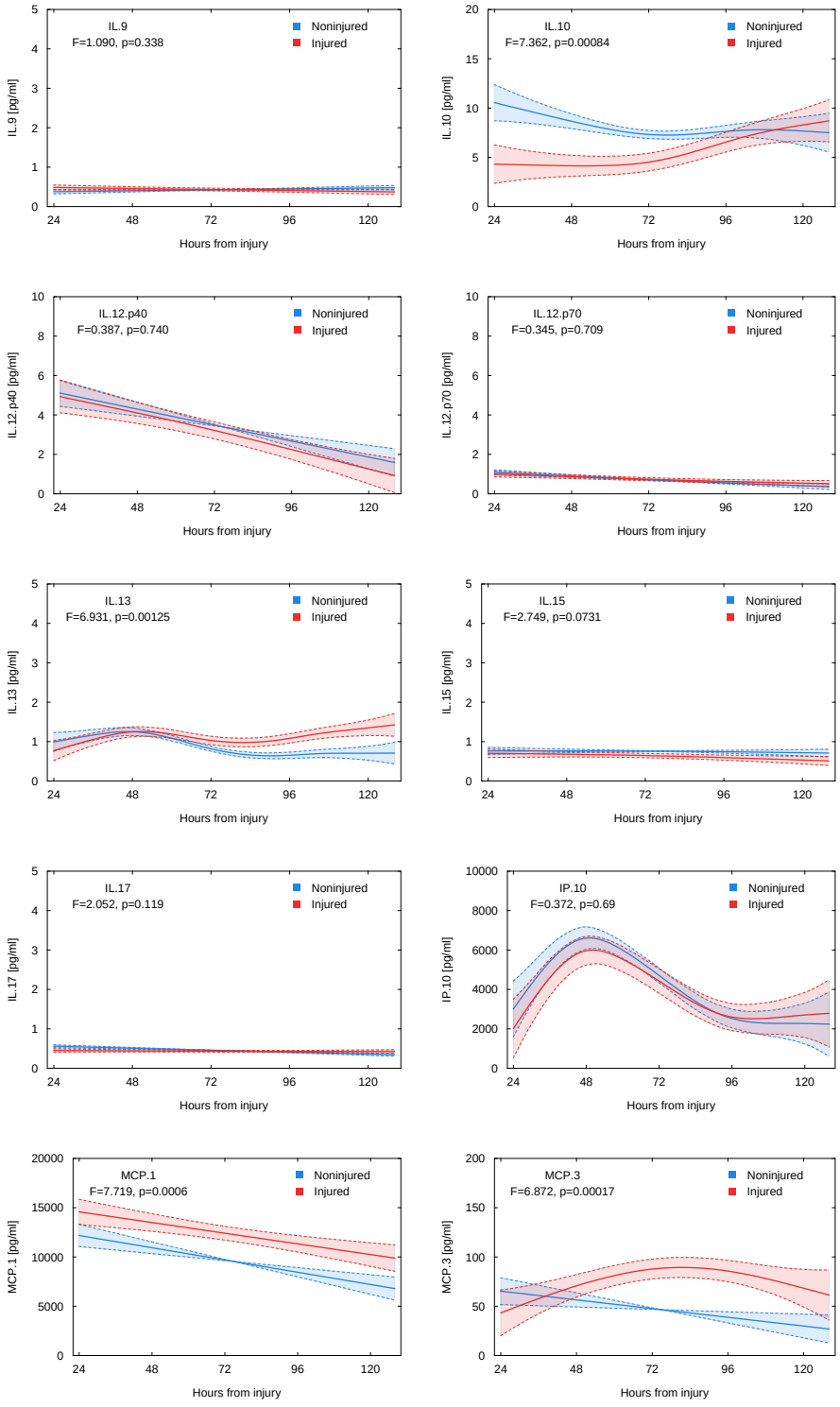
IL.9
F=1.090, p=0.338
Noninjured
Injured
IL.9 [pg/ml]
Hours from injury
IL.10
F=7.362, p=0.00084
IL.10 [pg/ml]
IL.12.p40
F=0.387, p=0.740
IL.12.p40 [pg/ml]
IL.12.p70
F=0.345, p=0.709
IL.12.p70 [pg/ml]
IL.13
F=6.931, p=0.00125
IL.13 [pg/ml]
IL.15
F=2.749, p=0.0731
IL.15 [pg/ml]
IL.17
F=2.052, p=0.119
IL.17 [pg/ml]
IP.10
F=0.372, p=0.69
IP.10 [pg/ml]
MCP.1
F=7.719, p=0.0006
MCP.1 [pg/ml]
MCP.3
F=6.872, p=0.00017
MCP.3 [pg/ml]

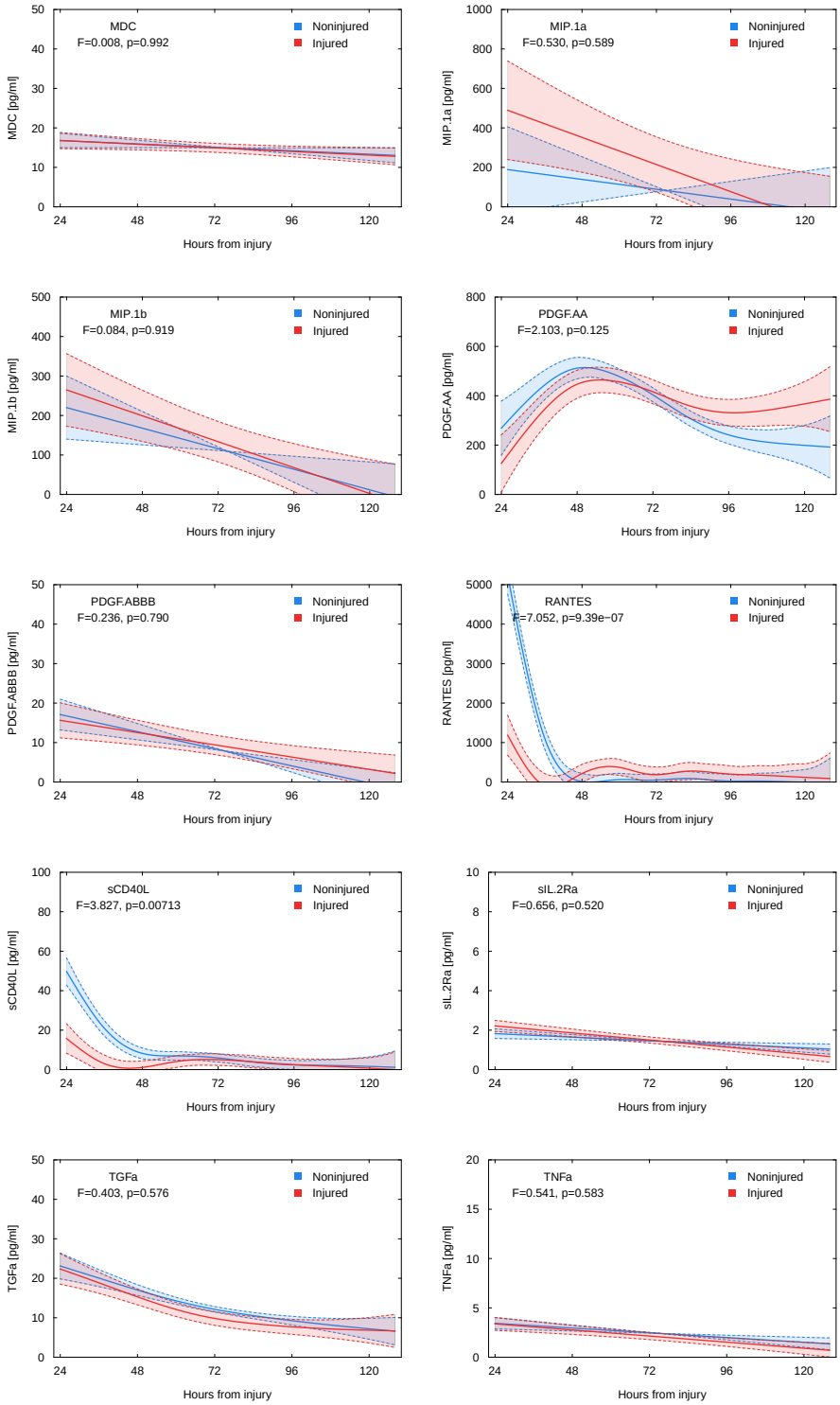
MDC
F=0.008, p=0.992
Noninjured
Injured
MDC [pg/ml]
Hours from injury
MIP.1a
F=0.530, p=0.589
MIP.1a [pg/ml]
MIP.1b
F=0.084, p=0.919
MIP.1b [pg/ml]
PDGF.AA
F=2.103, p=0.125
PDGF.AA [pg/ml]
PDGF.ABBB
F=0.236, p=0.790
PDGF.ABBB [pg/ml]
RANTES
F=7.052, p=9.39e−07
RANTES [pg/ml]
sCD40L
F=3.827, p=0.00713
sCD40L [pg/ml]
sIL.2Ra
F=0.656, p=0.520
sIL.2Ra [pg/ml]
TGFa
F=0.403, p=0.576
TGFa [pg/ml]
TNFa
F=0.541, p=0.583
TNFa [pg/ml]

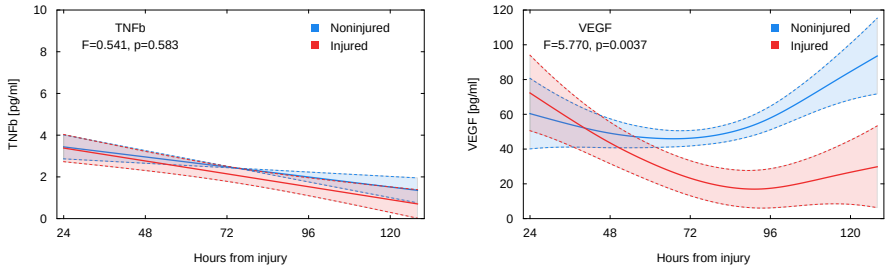

Figure 5.1: Generalised additive mixed models with cubic spline basis for each of the cytokines, with site of monitoring as a fixed factor and patient as a random factor. Test statistic and p-value in the upper left of each chart is the F-test comparing whether site of monitoring has a significant impact on the time-concentration curve of the respective cytokine.

5.3.3 Multivariate Analysis

As the temporal course of the cytokines was generally 'simple', i.e. monotonic or monophasic, the 8-hourly samples were pooled into pre- an post-72hr pools for the multivariate analysis. Partial least squares regression (PLS) of the largest component of variation (PC1, 29.2%) was related to time from injury, conversely PC2 (9.7%) tended to segregate samples from non-injured and injured monitoring sites. The mediators that most powerfully distinguished injured from non-injured brain were the chemokines MCP-1, MCP-3, and IL-8.

The normalisation of variance that is undertaken prior to performing PLS can inflate noise within the data. To examine whether cytokines/chemokines at very low abundance were biasing the data, a repeat analysis excluded all species with maximal concentrations <10pg/ml was conducted. PLS findings were substantively very similar, with no qualitative difference in the loading plot.

The discrminative power of the overall cytokine expression pattern was explored using a receiver-operating characteristics curve. The area under the curve (AUC) both for monitoring time (<72h vs >72h) and monitoring site ('normal' vs. injured) were approximately 0.8, which is generally considered good or excellent discrimination.

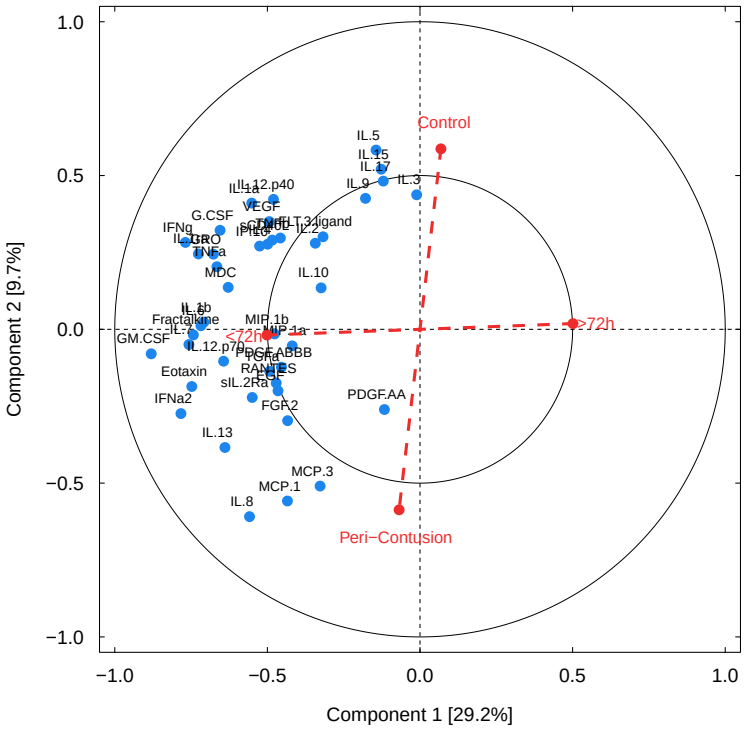

Figure 5.2: Loading plot of the partial least squares regression, demonstrating how each of the 42 cytokines assayed was expressed in relation to time and monitoring site

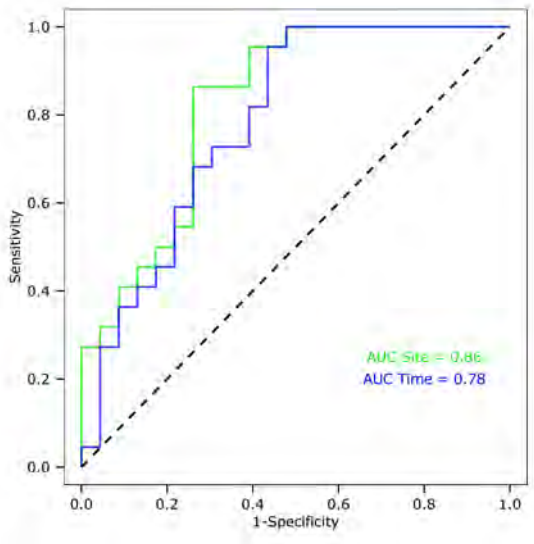

Figure 5.3: Receiver-operative characteristics curve for the first PLS component to discriminate Time and Site of monitoring

5.4 Discussion

This study has shown evidence a temporally and spatially segregated expression of cytokines and chemokine following focal TBI. In common with previous studies in diffuse TBI most cytokines were at their highest concentration either at the start of the monitoring period or during the first 72h from injury. Previous analysis has shown the rationale for the inference that the observed time courses of cytokine are a genuine injury-initiated cascade, rather than entirely a catheter insertion effect [69]. The present study, utilising control catheters in radiologically normal brain, provides further confirmatory evidence that, for at least a subset of cytokines and chemokines, the expression pattern is a consequence of the patients' injury rather than a localised response to the catheter. Nonetheless, for many of the cytokines demonstrating significantly different concentrations between injured and control brain, the temporal course of expression at both sites was similar. This would imply that there is a degree of global injury, even within radiologically normal tissue, but that differs in degree compared with regions of focal contusion. Alternatively this could also be inferred as evidence of a catheter insertion effect on top of which the inflammatory response to local TBI is observed.

It is important to note that the practicalities of TBI patient management and this study meant that we were only able to obtain two-site microdialysis samples within 24h from injury in a single patient. A number of the cytokine and chemokine time profiles show a broadly descending concentration from 24h onwards. It is impossible to extrapolate when these molecules will have been at their peak, whether there is a consistent sequence of expression within the first 24h, or whether those species that show little difference over the time period that was observed will have been significantly different between sites earlier following injury.

5.4.1 IL-1 family

The IL1 cytokine superfamily, which includes IL1alpha, IL1beta, IL1 receptor antagonist (ILra), has been extensively studied in both experimental and human TBI [70]. IL1b, produced by microglia, is the prototypical pro-inflammatory cytokine and elevated levels have been shown in blood, CSF, and ECF during the acute phase of injury, most prominently within 24h. Interestingly, there was not a significant difference in IL1b concentrations between injured and control monitoring sites, with the major caveat of having insufficient data to characterise the initial 24h from injury. In contrast, ILra was lower in pericontusional brain in the 24-48h period, thereafter

increasing to similar concentrations as control tissue. As has been suggested previously, it is likely that the balance between IL1b and ILra is the determinant of the degree or severity of the local inflammatory state. Correspondingly, in an earlier single-site microdialysis study IL1ra:IL1b ratio was found to be significantly higher amongst patients with favourable outcome [78]. The present investigation additionally suggests that, within individual patients, it is principally heterogeneity in IL1ra levels that is most marked between regions of injured and normal tissue. This would further support the hypothesis that ILra supplementation may be an effective therapy in TBI, and other acute brain injury conditions.

5.4.2 Chemokines

A further subset of the monitored chemokines that were notably at higher concentrations in pericontusional brain were those involved in promoting cellular infiltration. IL-8 (CXCL8), MCP-1 (CCL2), and MCP-3 (CCL7) are all all chemotactic factors that attract and induce migration of neutrophils (IL-8) and monocytes (MCP-1 and -3), and also regulate macrophage function. Both IL-8 and MCP-1 were significantly elevated from the start of monitoring, whereas MCP-3 showed a delayed response peaking at around 72h. MCP-1 has been shown previously to be elevated in plasma and CSF from TBI patients and in preclinical models is important in determining final lesion volume following focal injury [148, 75]. Similarly elevated IL-8 in CSF has previously been observed in TBI patients [93, 196]. These findings imply early cellular infiltration into pericontusional tissue, which would necessitate BBB dysfunction.

5.4.3 Anti-inflammatory cytokines

IL-10 plays a central role in moderating inflammatory response, and in general exerting anti-inflammatory effects by downregulating synthesis of pro-inflammatory cytokines and suppressing the expression and activation of respective cytokine receptors [165]. In turn, IL-10 reduces the attraction and infiltration of activated macrophages and T-cells. Furthermore, IL-10 is protective of endothelial cell function and BBB integrity. In pre-clinical TBI models an increase in IL-10 has been observed within hours of injury, with evidence for local cerebral production rather than influx through a permeable BBB. Studies with IL-10 knockout mice subjected to focal TBI have shown larger lesion volumes and poorer neurological function [10]. Correspondingly, intravenous administration of IL-10 found reduced lesion volume and improved motor and cognitive

recovery in both cortical impact and fluid percussion models [32]. Clinical studies of IL-10 in TBI have not shown consistent findings. Serum IL-10 has both been reported to have no association with severity of TBI whereas other groups have identified higher concentrations in patients with more severe TBI and with poorer outcome [56]. Similarly, IL-10 in CSF of TBI patients has been found to correlate with injury severity, raised intracranial pressure, and outcome, but in other series IL-10 concentrations, though elevated, do not exhibit a relationship with BBB permeability or mortality [56]. This heterogeneity of findings is undoubtedly multifactorial, and IL-10 levels in particular may be significantly confounded by the extent of extra-cranial injury. Furthermore, association of higher IL-10 concentrations with mortality and poor outcome does not necessarily imply a deleterious effect of this cytokine. In the present study there was a significantly higher concentration of IL-10 observed in the radiologically normal monitoring sites during the first 72h following injury, with concentrations at both monitoring sites becoming similar after this time. Alternative interpretations of this observation are that basal IL-10 synthesis is initially suppressed in pericontusional brain following injury, or that there is an injury response of increased IL-10 expression in radiologically normal brain that is absent in proximity to contusions. In either case, this is further evidence of a pro-inflammatory milieu localised to pericontusional brain and suggests that supplementing or potentiating IL-10 as a therapeutic target merits further investigation.

5.4.4 VEGF

VEGF was noted to be expressed at similar levels in peri-contusional and control monitoring sites in the first 48h following injury but thereafter was lower in pericontusional brain. This finding contrasts with the extensive evidence from pre-clinical and patient studies showing the elevated expression of VEGF in regions of focal injury as one of the key activators of BBB disruption [36, 155, 115, 69]. The expression of VEGF across the patients was heterogenous but the reasons for a lack of clear elevation of VEGF in pericontusional brain in the present study is unclear. One potential explanation may be the the lack of monitoring data from the initial 24h following injury during which higher concentrations of VEGF may have been observable in the pericontusional brain, although in animal TBI models VEGF generally peaks at day 4 from injury [36, 155, 120, 128]. Alternatively, it is conceivable that post-traumatic VEGF expression is highly localised to the edge of the haemorrhagic contusion and therefore even the pericontusional microdialysis catheters placed in adjacent brain were insufficiently close to detect this.

5.4.5 Multivariate analysis

The inflammatory response to injury comprises multiple redundant pathways and molecular interactions, and it is often by observing the concerted changes in a number of cytokines and chemokines that gives a better impression of the overall 'system state'. Further, individual mediators that do not show significant univariate differences between injured and control tissue may emerge as having more prominent roles in the context of examining covarying responses of groups of cytokines and chemokines. In this study we have employed principal components and partial least squares analysis, which are robust to data with a large number of observations in relatively few subjects. These techniques have been used previously to show the temporal pattern of inflammatory response in diffuse TBI, and also to examine the effect of intervention with recombinant IL1ra delivered subcutaneously in these patients. Rather than examining the response to intervention of a single mediator, PCA and PLS give a more general view of how the network of inflammatory pathways is perturbed, which also permits more nuanced interpretations as the role of individual cytokines may be pro- or anti- inflammatory depending on the covariation in changes of other cytokines.

In the present study the PLS analysis demonstrates that the pericontusional tissue exhibits a pro-inflammatory signature, with covarying increases in typical pro-inflammatory cytokines (e.g. IL-8) and concomitant reduction in anti-inflammatory cytokines (e.g. IL-10), Furthermore, this covariation in pro- and anti-inflammatory cascades is primarily seen in the early (<72h) phase of secondary injury.

Increased concentrations of pro-inflammatory cytokines and chemokines in pericontusional brain aligns with findings from experimental TBI models that these are the sites of predominant inflammatory cell invasion [70]. These data confirm that the inflammatory response in contusional TBI is spatially heterogenous in regions of radiologically normal and contusional/pericontusional brain. This is important in predicting the likely benefits of anti-inflammtory therapies such as IL-1ra [72].

5.4.6 Limitations

There are inherent statistical difficulties in examining large amounts of data collected from a relatively smaller number of subjects, and there is a risk of drawing spurious 'significant' findings

that are observed by chance. As such the cytokines and chemokines identified as significantly different between monitoring sites need corroboration in larger studies, but in general accord and are supported by findings in prior reports. The PLS analysis also goes some way to mitigating these statistical concerns and highlights the covarying changes of mutliple mediators at the sites of injury. As already mentioned, the absence of data from the first 24h following injury is a major limitation, particularly as it is likely during this period that a number of the signalling molecules will be at their highest concentrations.

5.5 Summary and Context

This study has demonstrated evidence for a localised, early, pro-inflammatory response within pericontusional brain typified by reduced IL1ra:IL1b ratio, increased expression of chemokines, and relatively lower concentrations of anti-inflammatory cytokines. The data did not show evidence for localised VEGF expression in pericontusional brain.

5.5.1 Hypotheses

- H5: Pericontusional brain exhibits a pro-inflammatory tissue signature following TBI.
  Based on the current evidence this hypothesis is accepted.

- H6: Vascular Endothelial Growth Factor exhibits higher expression in pericontusional brain following TBI.
  Based on the current evidence this hypothesis cannot be accepted.

Chapter 6

Study IV - Matrix Metalloproteinases in Pericontusional Brain

6.1 Overview

Matrix metalloproteinases (MMP) are a family of extracellular and cell-surface attached pro-enzymes that when activated target a wide range of protein substrates and are involved in diverse signalling pathways [121]. Preclinical models have demonstrated that MMPs have a central role initiating proteolysis of the tight junctions that bind the apical surface of brain endothelial cells and form the principal component of the blood brain barrier [202, 29]. Tissue obtained at contusionectomy surgery and post-mortem suggest increased expression of MMP-9 in pericontusional brain, but it is not clear if this is a consequence of tissue necrosis or an antecedent cause of contusion and brain oedema progression [186].

Early evidence from previous microdialysis studies indicates elevated expression of MMP-9 in the traumatised human brain, but it is not clear if this is a global response or concentrated in areas of contusional injury.

This is a further paired microdialysis study with catheters targeted at pericontusional brain and another placed in radiologically normal brain to assess whether MMP expression is localised in the pericontusional region *in vivo*.

6.2 Methods

6.2.1 Recruitment and Monitoring

Adult patients with TBI requiring neurointensive care and invasive monitoring were eligible for the study. Invasive neuromonitoring was inserted at two sites for each patient with the intention of having a microdialysis catheter within radiologically 'normal' white matter and another within pericontusional brain but avoiding the haemorrhagic core. Microdialysis catheters (CMA 71, 100kDA molecular weight cut-off) were perfused with 3.5% (w/v) Human Albumin Solution (Pharmacy Manufacturing Unit, Ipswich Hospital NHS Trust, Ipswich, UK) in central nervous system perfusion fluid. If the first set of monitors happened to be placed adjacent to a contusion the second set were inserted in radiologically normal brain on the contralateral frontal region. In patients requiring an emergent craniotomy for an acute subdural haematoma the pericontusional monitoring was placed adjacent to underlying contusions under direct vision at the end of surgery, tunnelled through the scalp.

6.2.2 Sample Analysis

Microdialysate was pooled 8-hourly and then assayed in duplicate for MMP-1, MMP-2, MMP-7, MMP-9, and MMP-10 using the five-plex Milliplex Multi-Analayte Profiling Human MMPII panel (Millipore, St. Charles, MI, USA) according to the manufacturers' instructions. All samples were assayed in duplicate wells (25 microL per well) and the mean of these results was used. The plates were read using a Luminex 200 analyser (Luminex Corporation, Austin, TX, USA) running STarStation software (Applied Cytometry Systems, Sheffield, UK). Protein concentrations were calculated by reference to an eight-point spline fit curve for each MMP.

6.2.3 Contusion Volume

The routinely performed CT scans for each patient were analysed with the stereological method, described earlier in this work, to determine the volume of haemorrhagic contusion and adjacent oedema using a 5mm grid spacing. The change in core, oedema, and total lesion volume over the initial 72h from injury was estimated by comparison of volumes on the scan performed closest to 72h from injury and the patient's baseline admission imaging.

6.2.4 Statistical Methods

To mitigate the effects of different monitoring periods in each patient the mean concentrations of each MMP in the first 72 hours following injury (<72h) and in the subsequent 72 hours (>72h) were calculated for each patient. Repeated measures analysis of variance (ANOVA) with MMP concentration as the dependent variable, and site of monitoring ('Normal' vs. Injured) and time (<72h vs. >72h) as the independent variables, was then applied for each MMP separately. Univariate subgroup comparisons were analysed with the independent samples T-test. All calculations were performed in R (v3.0.2, www.r-project.org) and considered significant at 5%.

6.3 Results

6.3.1 Patients

Twelve patients (10 male; mean age 46 years, range 21-65 years) were enrolled (10 in common with Study III). Paired microdialysis monitoring was commenced a mean of 36 hours (range 16-48) following injury. No complications attributable to the additional study monitoring were observed. Two patients died during their intensive care treatment due to refractory intracranial hypertension. Of the ten patients who survived, seven had a favourable outcome (GOS 4-5, moderate disability or good recovery) at six months follow-up and three were severely disabled (GOS 3)

Age	Sex	Mechanism	GCS	Pupils	Marshall	Evacuated SDH	GOS
28	M	Fall	8	+/+	2d	-	4
67	M	Fall	6	+/+	5b	Right	3
31	M	Fall	5	-/+	3	-	3
67	M	Pedestrian RTA	10	+/+	2c	-	3
59	F	Fall	12	+/-	2d	-	1
65	M	Fall	11	+/+	2d	-	4
55	M	RTA	9	+/+	5b	Left	5
42	F	Fall	3	-/+	5b	Left	3
30	M	RTA	7	+/+	5b	Right	5
22	M	Assault	8	+/+	5b	Right	4
42	M	Fall	7	+/+	5b	Left	5
48	M	Assault	10	+/+	2d	-	1

Table 6.1: Demographics of patients in the study. Marshall Category 2c indicates multiple unilateral contusions, 2d indicates bilateral contusions, category 3 indicates contusions with basal cistern effacement, and 5b indicates evacuated subdural haematoma. GCS: Glasgow Coma Scale, GOS: Glasgow Outcome Score (at 6 months following injury)

6.3.2 Temporal course of MMP expression

Mean time-concentration plots for each MMP assayed are shown in 6.1. Examples of catheter placement and corresponding individual time courses of the five MMPs assayed are shown in

6.2. Although in some patients MMP-2 concentrations gradually increased in pericontusional brain, overall concentrations of MMPs -1, -2, and -10 were similar at both sites during the monitoring period and did not demonstrate consistent temporal trends across the cohort of patients. There was a gradual increase in the concentration of MMP-7 at both monitoring sites, but this was not observed in all patients.

In contrast, MMP-9 concentrations were consistently higher in the injured brain compared with radiologically normal brain. The highest concentrations of MMP-9 were observed at the earliest monitoring times (i.e. <24 hours) within injured brain. Thereafter, MMP-9 concentrations decreased but remained higher within injured brain compared with radiologically normal brain to 72 hours post-injury, and beyond.

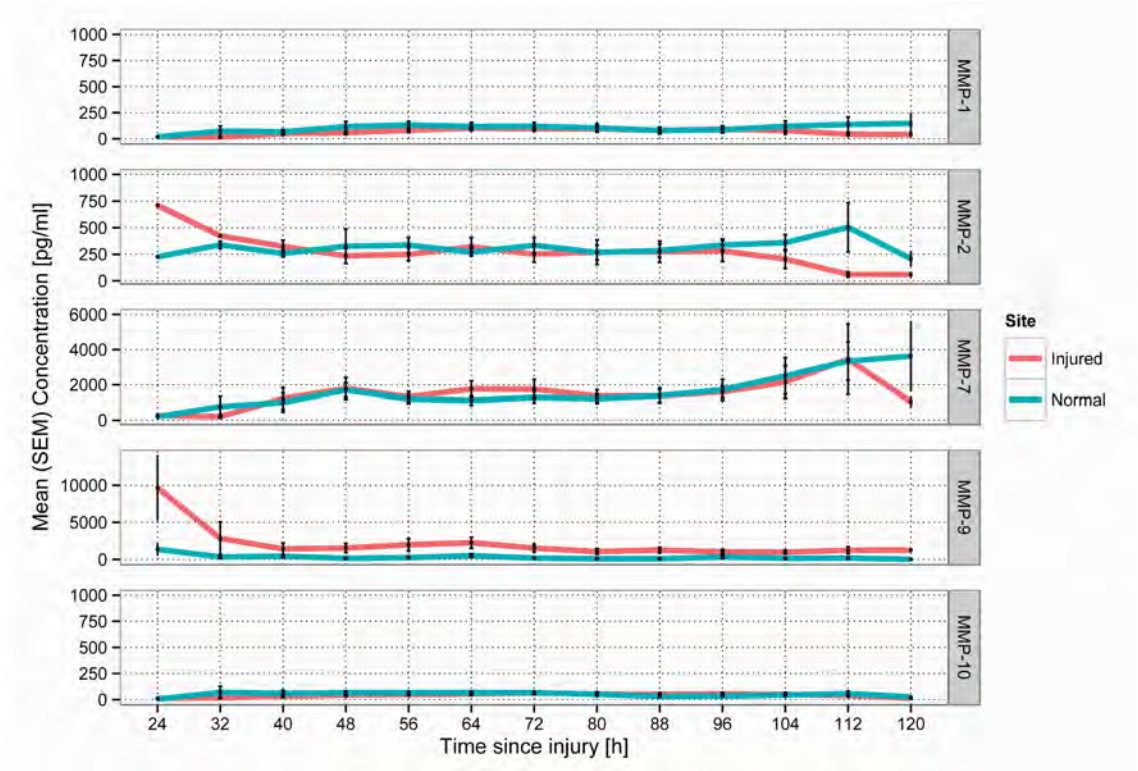

Figure 6.1: Mean time-concentration curves for each MMP across all patients. Error bars represent standard error of the mean (SEM)

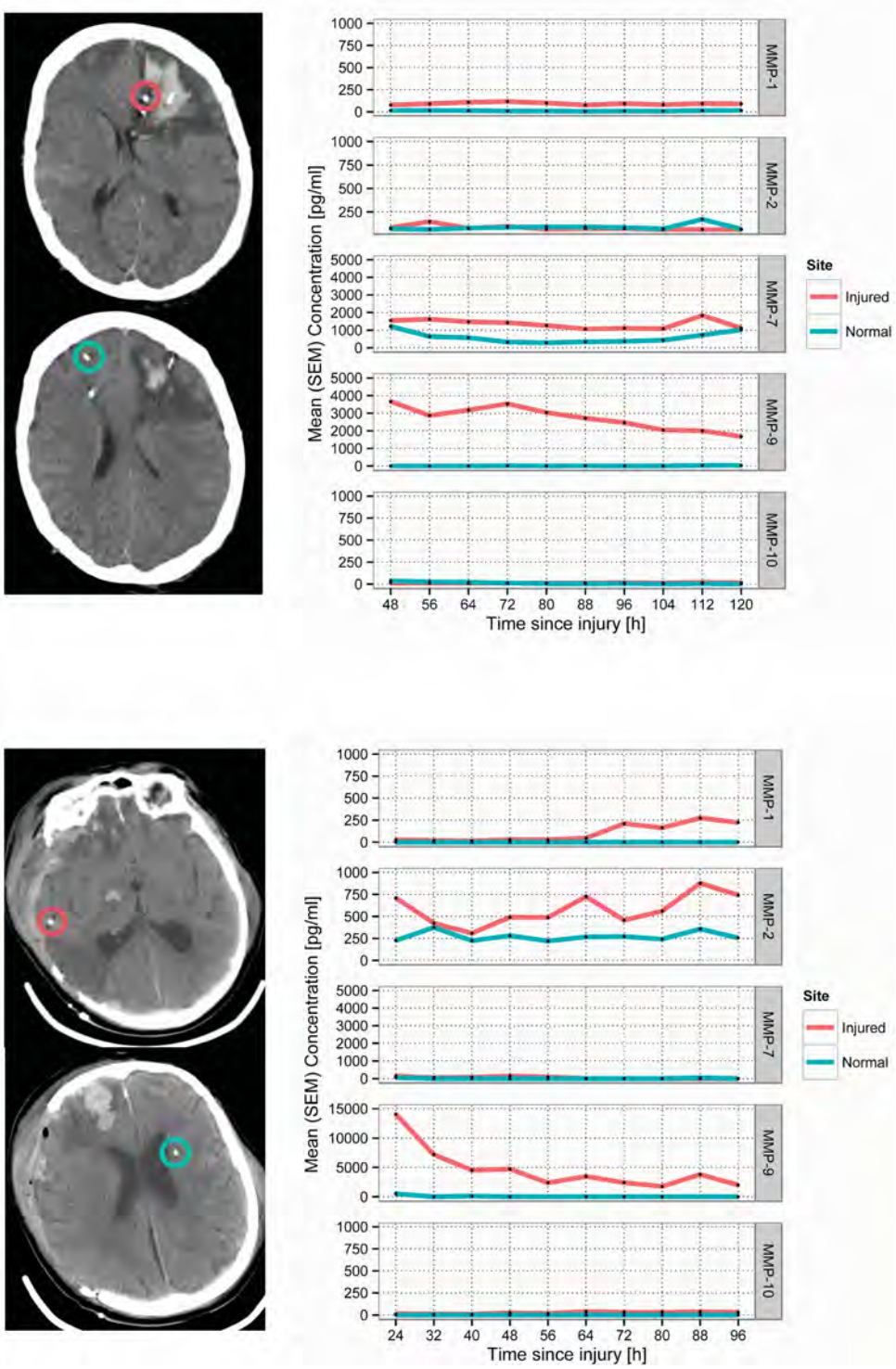

Figure 6.2: Representative examples of patient CT scans demonstrating catheter placement and corresponding time-concentrations curves for each MMP. Top: patient 5, bottom: patient 2. Red circles highlight the tip of the microdialysis catheter in pericontusional brain; green circles indicate the microdialysis catheter in 'normal' brain.

Mean concentrations of the five MMPs in normal and injured brain in the periods <72hrs and >72hrs following admission are shown in 6.3. Repeated measures ANOVA showed no significant difference in MMP-1, -2, -7, or -10 concentrations between normal or injured sites, and no effect

of time. However, MMP-9 concentrations were significantly higher in pericontusional brain compared with radiologically normal brain (p=0.03) and were also significantly higher in the early monitoring period (<72hrs) compared with later time-points (>72hrs, p=0.04).

There were no significant differences (p>0.05) in concentrations of any of the assayed MMPs when the cohort of patients was divided into two groups based either on presenting severity of TBI (GCS <8 vs. >8), whether or not the patient had a SDH evacuated, and functional outcome (GOS 1-3 vs. 4-5).

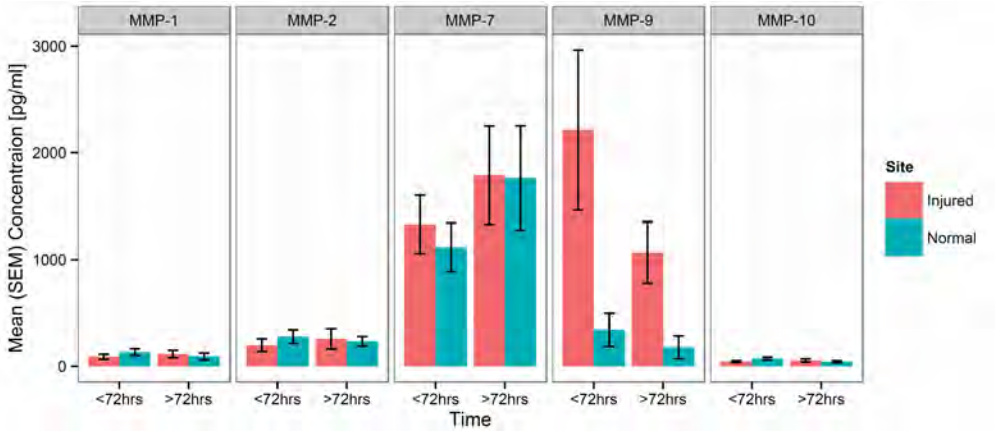

Figure 6.3: Group mean (SEM) concentration of each MMP at each monitoring site <72h following injury and >72h injury. Repeated measures ANOVA demonstrated significant differences between monitoring sites (p=0.03) and between monitoring periods (p=0.04) for MMP-9; no significant differences were observed for MMP-1, -2, -7 and -10 (see text for full details).

6.3.3 Pericontusional MMP-9 and contusion progression

Comparison of pericontusional MMP-9 expression and the volume change of the total contusion lesion (haemorrhagic core and oedema) is shown in Fig 6.4, and is suggestive of an association although there was no statistically significant correlation (r=0.48, p=0.112). Interestingly, the clear outlier in this plot (indicated by the highlighted point) represents a patient who developed marked cerebral oedema and refractory intracranial pressure as a consequence of extensive venous thrombosis rather than contusion progression per se. With this patient excluded there was a significant correlation between pericontusional MMP-9 expression and the magnitude of contusion volume expansion (r=0.72, p=0.013).

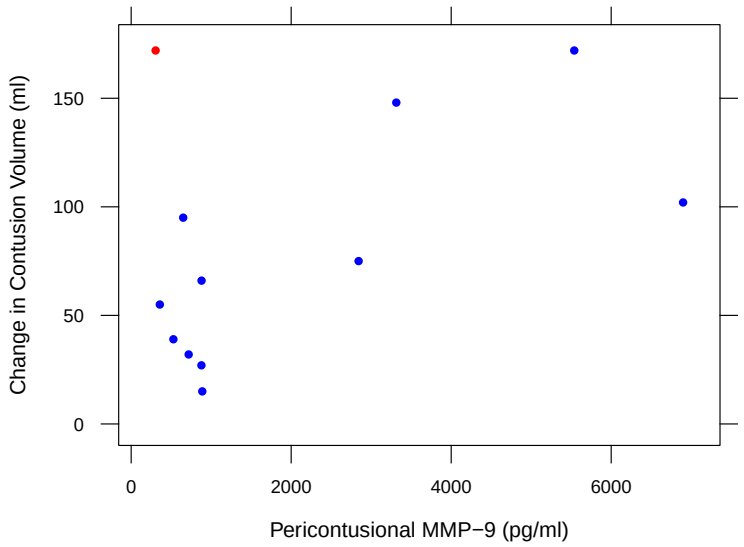

Figure 6.4: Scatter plot of pericontusional MMP-9 concentration and corresponding volume change of the total lesion (haemorrhagic core and oedema combined) over the initial 72h from injury. The red point indicates a patient with refractory cerebral oedema and intracranial pressure due to venous sinus thrombosis; with this patient excluded there is a significant correlation (r=0.72, p=0.013; see text)

6.4 Discussion

This study has demonstrated that there is a specific, early, and localised increase in MMP-9 concentrations within pericontusional brain following TBI. Although the concentration of MMP-7 appeared to gradually increase over the monitoring period in both injured and uninjured brain no significant differences were found in the concentrations of MMP-1, - 2, -7, -10 with respect to monitoring site or time. Comparing patient groups based on presenting GCS, presence of subdural haematoma requiring evacuation, and functional outcome, found no significant differences in MMP concentrations. It is unsurprising that in a relatively small cohort of patients there is no statistical relationship between interstitial MMP concentrations and clinical features that are dependent on a plurality of factors. However, there was provisional evidence for an association between MMP-9 expression and the degree of contusion expansion, albeit having excluded one patient with apparent confounding factors that were the cause of progressive cerebral oedema.

Our findings are in accordance with preclinical evidence that MMP-9 expression is increased in perilesional brain following experimental brain contusion, and in these models corresponds with the development of BBB permeability and expansion of the final lesion volume[153, 64]. Grosslete et al. and Zheng at el. have previously reported elevated levels of MMP-9 in CSF sampled acutely from TBI patients via ventriculostomy, with comparable temporal profiles demonstrating great-

est concentrations in the first sample at 24 hours post-injury followed by a decline, but remaining higher than control CSF for at least 72 hours [60, 192] Vilalta et al. studied four patients with diffuse brain injury using microdialysis and found similar early elevation of cerebral MMP-9 concentrations [187]. More recently, Roberts et al. conducted a single site microdialysis study of MMP-1, -2, -3, -7, -8, and -9 in eight TBI patients with a mixture of diffuse and focal injuries; similarly to the present study, they found MMP-9 was increased early following injury and thereafter declined [138].

The present data both corroborate these temporal MMP-9 profiles in a larger cohort of TBI patients, and adds the important new finding that in patients with predominantly focal or contusional injury the MMP-9 response is localised to perilesional brain. The paired catheter design means it is far less likely that the observed changes in MMP-9 are attributable to artefact from catheter insertion, as a similar effect would have been observed at both monitoring sites. The evidence from this study goes some way to supporting the hypothesis that the mechanisms of MMP-9 induced BBB disruption and oedema elucidated in animal models are also relevant in human TBI. The observed association between MMP-9 concentration and the increase in contusion and oedema volume further backs an important role for this enzyme in clinical TBI, though the finding is still insufficient to infer a causative role.

Both previous microdialysis studies have found evidence for increased cerebral expression of MMP-2 following TBI, although Vialta et al. identified an early peak similar to MMP-9, whereas in the later study by Roberts et al. MMP-2 concentration was initially low and increased at around 48 hours post-injury, with a subsequent decrease [187, 138] In the present study patients exhibited variable MMP-2 responses, with no consistent spatiotemporal pattern emerging on averaging across the cohort. Interestingly, an earlier study of contusion resection tissue also found MMP-2 concentrations that varied widely and the resulting overall difference in expression compared with control patient samples was modest [186]. Together, these findings suggest MMP-2 concentrations may be significantly elevated in only a subset of TBI patients; whether this is a function of injury severity or other patient-specific clinical factors will require larger studies to resolve. The relative importance of MMP-2 compared with MMP-9 in the pathogenesis of contusion expansion and brain oedema is unclear, and there is conflicting evidence on the role of MMP-2 in exacerbating lesion volume from different brain injury models [64, 201]. However, as both MMP-2 and -9 are gelatinases and act on similar substrates they may represent redundant pathways in post-traumatic proteolytic breakdown of the BBB. If interventions targeted at MMP activity are to be

successful a more complete understanding of the role of MMP-2 will be essential, particularly as evidence from preclinical TBI models suggests that MMP-2 and MMP-9 show different responses to current therapies such as hypothermia [176].

Induced hypothermia has been shown to attenuate MMP-9 expression in rodent TBI and stroke models but as yet this phenomenon has not been investigated in human patients [176, 103]. Despite a number of randomised trials, therapeutic hypothermia has not been conclusively shown to improve outcome following TBI, though its use to control intracranial pressure remains widespread [58, 163]. Conceivably, targeting hypothermia to patients with increased MMP-9 expression may be a method to select the subgroup of patients in which the benefits of this treatment outweigh its deleterious effects.

MMP inhibitors have been investigated as promising therapies for a number of diseases, most notably in metastatic cancer. However, despite successful preclinical findings, early phase clinical trials in cancer patients have proven disappointing due to lack of efficacy and excessive adverse effects [159]. Of interest, tetracycline antibiotics, most notably doxycycline, inhibit MMP-2 and -9 through chelation of the zinc ion in the catalytic site [157]. Doxycycline at sub-antimicrobial doses has been shown to be of benefit in periodontitis, likely via its effect on MMP-9 activity [133]. On the same basis, doxycycline has also been suggested as a treatment to stabilise the growth of abdominal aortic aneurysms, although the evidence to date is conflicting [107]. Currently available MMP inhibitors are not selective for specific subtypes but at the same time are not equally active on all members of the enzyme family; combined with redundancy in MMP pathways this may be an explanation for the limited efficacy of MMP inhibitors in clinical studies to date.

This study suggests that MMP-9 may be a therapeutic target to reduce lesion progression and brain swelling in contusional TBI. Investigating the efficacy of MMP inhibitors in this context will first require further detailed studies of the association between pericontusional MMP-9 concentration, contusion expansion and vasogenic oedema, intracranial pressure and treatment intensity, and cerebral metabolism, to establish robust measures of efficacy. Human studies to date indicate that the useful therapeutic window for MMP-9 inhibition following TBI may extend up to 72 hours from injury, but it is likely that any agent will be most effective at minimising brain oedema and contusion expansion if administered as acutely as possible. Defining the appropriate duration of MMP inhibition will also need to consider the later role these enzymes have in post-injury central nervous system repair.

6.4.1 Limitations

This study has a number of limitations. Firstly, no patient was monitored within the first 12 hours of injury and therefore the expression pattern of MMPs in the very acute stage remains uncertain. Secondly, MMP activity is regulated by endogenous Tissue Inhibitors of Metalloproteinase (TIMP) proteins which bind with latent and activated MMPs [121]. Although MMP-TIMP complexes would likely exceed the 100kDa cut-off of the CMA 71 microdialysis catheter, it cannot be determined from the present data whether all MMP-9 assayed was enzymatically active; future studies to address this question will be challenging due to low absolute amount of protein recovered with microdialysis. Third, the findings of the current study injury do not speak to whether MMP concentrations will display similar temporal profiles in patients with a predominantly diffuse axonal injury pattern on initial CT.

6.5 Summary and Context

This study has shown that MMP-9 is upregulated in pericontusional brain compared with radiologically normal brain and this expression occurs early following injury. The observed time course would suggest important upstream regulators of MMP-9, such as VEGF, are likely maximally expressed within the first few hours of injury and would be an explanation for why these were not observed in the cytokine study described in the previous chapter. The results provide preliminary evidence for an association between MMP-9 and the severity of contusion and oedema progression.

6.5.1 Hypotheses

- H7: MMP-9 shows increased expression early following TBI and is primarily localised to pericontusional brain.
  Based on this study this hypothesis is accepted.

- H8: MMP-2 shows delayed increase in expression following TBI that is also primarily localised to pericontusional brain. There was insufficient evidence to accept this hypothesis.

Chapter 7

Study V - Pericontusional Nitric Oxide

7.1 Overview

Nitric Oxide (NO) is a highly diffusable radical gas molecule that is synthesised from the amino acid L-arginine by the nitric oxide synthase (NOS) family of enzymes [57]. NO has a variety of roles in neurotransmission and synaptic modulation, intracellular signalling, neuroinflammatory cascades, and in the regulation of cerebrovascular tone and cerebral blood flow [57, 34]. Three NOS isoforms have been identified in humans: endothelial NOS (eNOS), neuronal NOS (nNOS), and inducible NOS (iNOS). Both eNOS and nNOS are constitutively expressed in the brain whereas iNOS is upregulated in response to injury [175, 57].

Broadly, cerebral autoregulation comprises mechanoregulation (maintenance of constant flow with varying systemic arterial blood pressure) and chemoregulation (maintenance of flow in response to changing CO_2 concentrations due to metabolic pertubations and during hypoxia) [57]. NO is a key mediator of both CO_2 chemoregulatory pathways [102] and is necessary for augmenting blood flow in response to hypoxia [166]. In the context of TBI this would suggest a beneficial role for NO in maintaining constant CBF under the stress conditions following injury, and that relative NO depletion may be a factor in post-injury ischaemia and loss of flow-metabolism coupling [57].

However, excess NO may be a factor in post-traumatic dysautoregulation, vasoplegia and va-

sodilatation, and hyperaemia, with consequent raised intracranial pressure, and has also been identified as a component of the pathway resulting in blood-brain barrier breakdown by VEGF [52, 34, 147, 188]. Furthermore, following cerebral insults, it has been shown that eNOS can become uncoupled from its cofactor tetrahydrobiopterin, resulting in the alternative production of superoxide, a radical that is neurotoxic. Superoxide may in turn react with NO to form peroxynitrite that is also neurotoxic and depletes available NO.

NO itself is difficult to assay in clinical samples owing to its short half life. However, assaying concentrations of stable NO metabolites nitrite and nitrate (NO_2 and NO_3, collectively NOx) is a validated method of indirectly quanitfying endogenous NO synthesis [137]. In humans, NOx have been assayed in CSF and microdialysate of diffuse-injury pattern TBI patients. A series of eleven TBI patients who underwent regular CSF sampling suggested a peak in NOx at approximately 24h following injury [178]. The concentration of NO was correlated with that of IL-8, suggesting that NO levels may reflect the degree of post-TBI inflammatory burden [178]. In a pilot study of twelve brain injury patients (11 TBI), studied with microdialysis, extracellular NOx concentration was found to be correlated with higher cerebral glucose and lower lactate/pyruvate ratio, suggesting a beneficial metabolic effect of higher NO concentrations [24]. However, a more recent microdialysis study in eleven TBI patients found significantly higher NO concentrations within the first 48h from injury amongst patients who died compared with survivors, suggesting that NO is a either a marker of more severe primary insult or that it potentially contributes to secondary injury and likelihood of poor outcome [174].

A number of factors may explain the contrasting findings in clinical TBI studies of NOx, including temporal and spatial heterogenity of NOx concentrations in relation to catheter placement. In this study we have examined whether there are spatiotemporal differences in NO production following contusional TBI using targeted pericontusional microdialysis catheters.

7.2 Methods

Adult patients with TBI requiring neurointensive care and invasive monitoring were enrolled. Neuromonitoring was inserted at two sites for each patient with the intention of having a microdialysis catheter within radiologically 'normal' white matter and another within pericontusional brain but avoiding the haemorrhagic core. On admission a triple-lumen cranial access device

(Technicam, Newton Abbott, UK) was placed in the right or left frontal region as standard. An intracranial pressure (ICP) monitor (Codman, Raynham, MA, USA), a brain tissue oxygen probe (Licox Neurosciences, Andover, UK), and a microdialysis catheter (CMA 71, 100kDA molecular weight cut-off) perfused with 3.5% (w/v) Human Albumin Solution (Pharmacy Manufacturing Unit, Ipswich Hospital NHS Trust, Ipswich, UK) in central nervous system perfusion fluid, were introduced via the access device. Following assent, up to three further invasive monitors, at least one of which was a microdialysis catheter (CMA 71 and perfused with 3.5% albumin solution, as above) were placed in proximity to a contusion, either via a second cranial access device or twist drill holes. If the first set of monitors happened to be placed adjacent to a contusion the second set were inserted in radiologically normal brain on the contralateral frontal region. In patients requiring an emergent craniotomy for an acute subdural haematoma the pericontusional monitoring was placed adjacent to underlying contusions under direct vision at the end of surgery, tunnelled through the scalp. Hourly microdialysates were pooled into 8-hourly samples.

7.2.1 NOx Assay

Nitric Oxide is a short lived molecule but its products NO_2 and NO_3 are stable and can be readily assayed. Collectively these are termed NOx. Total nitrate and nitrite (NOx) were determined by injection of 5microL of microdialysate into a purge vessel containing a solution of vanadium (III) chloride (50mmol/L) in hydrochloric acid (1 mol/L) at 95°C continuously purged with nitrogen gas. This chamber was connected to a Sievers 280i Nitric Oxide Analyser (GE Analytical Instruments, Boulder, CO, USA). The vanadium (III) chloride reconverts the NOx to nitric oxide which then reacts with ozone (O_3) within the analyser. This forms nitrogen dioxide which can be readily detected by chemiluminescence against standards of known concentration. This specialist assay was performed by Mr Richard Shannon. All samples were processed in duplicate.

7.2.2 Statistical Analysis

Paired NOx concentrations at each pooled time point within each patient were compared with a linear mixed model including a random effect for each patient. The temporal course of NOx concentrations were compared with generalised additive mixed models (GAMM) including a random effect for each patient. Smooth terms were composed of a ten-knot cubic regression spline basis and optimised using restricted maximum likelihood (REML). Metabolites assayed hourly

at the bedside (glucose, lactate, pyruvate, glycerol, and glutamate) were averaged to correspond with each pooled sample and then comparison of NOx with these metabolites was performed with similar statistical tests. All analysis was conducted in R v3.4.3 and statistical significance was set at $p<0.05$.

7.3 Results

Eleven patients (nine male) were included. Demographics are shown in Table 7.1. A total of 185 eight-hourly pooled samples were assayed for NOx concentration with overall mean 19.18 [SD 11.0] micromol/L, and median 16.64 micromol/L. Taking together all sample points, linear mixed model analysis showed that NOx concentration was moderately significantly higher in the radiologically 'normal' or uninjured sites (Figure 7.1 mean difference 2.43 micromol/L, 95% CI 0.04-4.82, p=0.047), with a significant effect of time ($p<0.001$).

Age	Sex	Mechanism	GCS	Pupils	Marshall	Evacuated SDH	GOS
28	M	Fall	8	+/+	2d	-	4
67	M	Fall	6	+/+	5b	Right	3
31	M	Fall	5	-/+	3	-	3
67	M	Pedestrian RTA	10	+/+	2c	-	3
59	F	Fall	12	+/-	2d	-	1
65	M	Fall	11	+/+	2d	-	4
55	M	RTA	9	+/+	5b	Left	5
42	F	Fall	3	-/+	5b	Left	3
30	M	RTA	7	+/+	5b	Right	5
22	M	Assault	8	+/+	5b	Right	4
42	M	Fall	7	+/+	5b	Left	5

Table 7.1: Demographics of patients in the study. Marshall Category 2c indicates multiple unilateral contusions, 2d indicates bilateral contusions, category 3 indicates contusions with basal cistern effacement, and 5b indicates evacuated subdural haematoma. GCS: Glasgow Coma Scal, GOS: Glasgow Outcome Score (at 6 months following injury)

To characterise the temporal trend a GAMM model was used with a fixed effect of monitoring site and smooth term for time, with per-patient random effect. The mean trend in NOx concentrations at each time point from the random-effect GAMM model at 'uninjured' and 'injured' monitoring sites is shown in Figure 7.2. NOx concentrations showed a significant decrease over time, a trend that was observed similarly at both monitoring sites. There was no significant difference in the temporal trends between paired noninjured and injured catheters. Binning the samples into <72h and >72h from injury showed a significant difference in time using a linear mixed model (mean difference 6.73 micros mol/L, 95% CI 4.08-9.38, $p<0.001$)

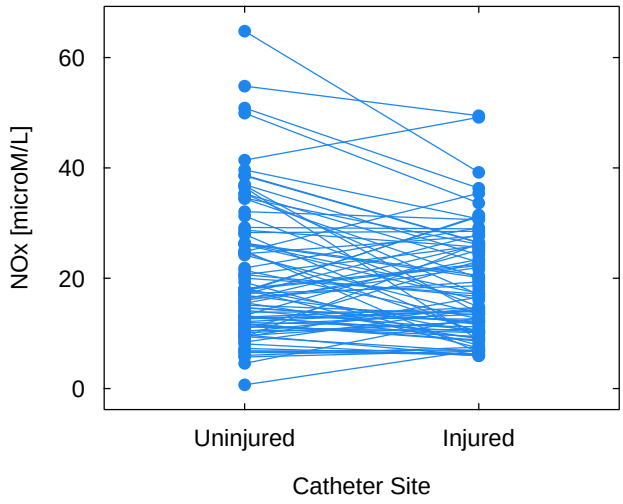

Figure 7.1: Comparison of NOx concentrations . Mean NOx concentration at each 8-hourly pooling period across the patients

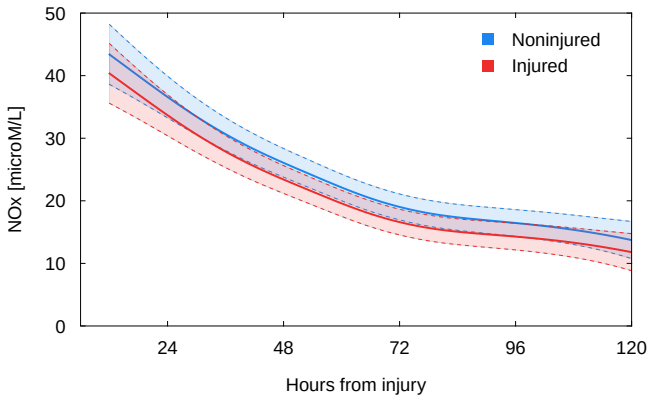

Figure 7.2: Time course of NOx concentrations. Smoothed mean NOx concentration at uninjured and injured monitoring sites from the GAMM model. Shaded region indicates pointwise standard error.

There were significant relationships between the concentrations of NOx and the other metabolites. The strongest association was seen with pyruvate (r=0.322, p<0.001), followed by lactate (r=0.258, p<0.001), and glucose (r=0.183, p=0.020). There was no significant correlation between NOx and either glycerol (r=-0.117, p=0.135) or glutamate (r=0.012, p=0.909). The functional relationship between NOx and glucose, pyruvate, and lactate was explored further with GAMM models including random effect terms for each patient. These models are shown in Figure 7.3. There was no significant difference between the association of NOx and glucose or pyruvate within noninjured and injured brain but there was a significant difference in trend for lactate, which increased for more rapidly with rising NOx at the injured monitoring sites compared with

the control catheters.

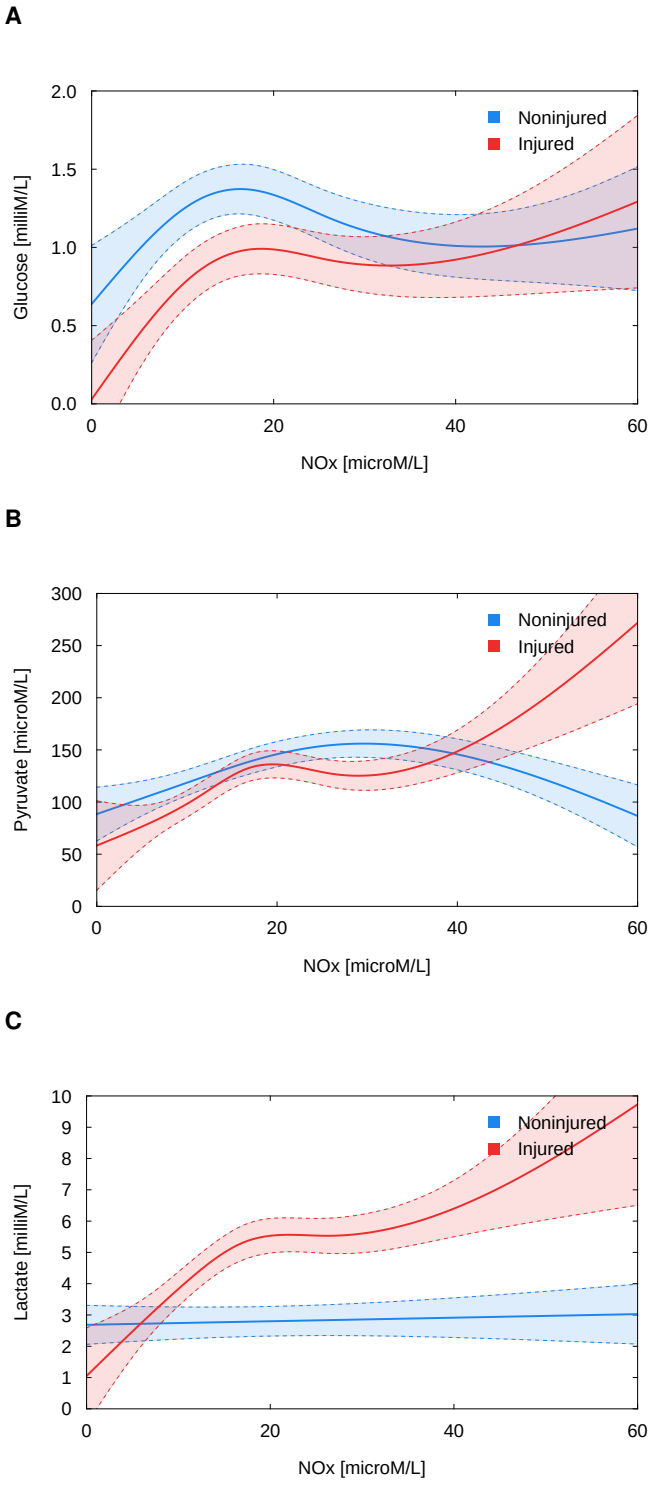

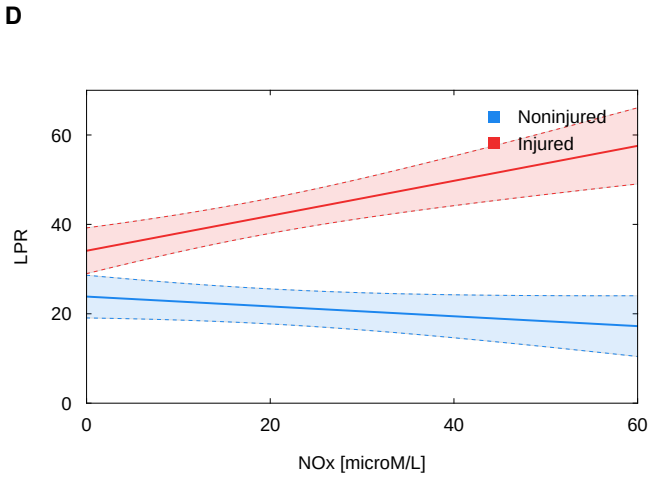

Figure 7.3: Functional relationship between NOx and energy metabolites. GAMM models of (**A**) glucose, (**B**) Pyruvate, (**C**) lactate, and (**D**) lactate/pyruvate ratio against NOx in noninjured and injured monitoring sites.

7.4 Discussion

This study has shown that interstitial or extracellular fluid concentrations of NOx are highest early following TBI and gradually reduce over the course of several days of monitoring. This finding is consistent with previous human microdialysis and CSF studies [24, 174]. The present data also show statistically significant lower concentrations of NOx in pericontusional brain throughout the period of monitoring but with a similar temporal course as in radiologically uninjured brain within the same patient.

Similarly, in agreement with previous microdialysis studies NOx was positively correlated with glucose, pyruvate, and lactate, but not glycerol or glutamate, both in noninjured and injured brain. However, lactate demonstrated a much stronger positive trend in association with NOx in pericontusional brain. Correspondingly, LPR - a measure of cellular redox state and the balance of aerobic and anaerobic metabolism - increased with higher NOx in pericontusional brain whereas LPR was either static or slightly decreased with increasing NOx in radiologically uninjured brain. The association of NOx and LPR in uninjured brain corresponds with the previous study in diffuse TBI, where catheters would typically be located in radiologically normal brain (as defined on computed tomography imaging)[24]. Therefore, the present study suggests potentially differing responses to NOx concentrations in contused brain compared with uninjured tissue or regions of diffuse injury. While catheter sites within radiologically normal brain have been termed 'uninjured' in this discussion, the fact that NOx followed a similar temporal course at both sites within individual patients suggests this may not necessarily be true. Explanations include a component

of diffuse injury affecting radiologically normal brain, a cerebral component of a systemic injury response, or lastly a catheter insertion artifact. By the same token, the correlation of NOx with energy metabolites and contrasting relationship with LPR may be an indirect association simply as a consequence of the difference in glucose, pyruvate, and lactate between pericontusional and radiologically normal brain.

Nonetheless, these data suggest the possibility that specific regions of the brain may have contrasting responses to NO supplementation following injury. Specifically, in radiologically normal brain increased NO levels are inferred to be beneficial and improve metabolic parameters as in the 'normal' physiological state. However, in pericontusional regions increasing NO appears to have a deleterious effect. This action might be hypothesised to be a consequence of NO action on potentiating blood brain barrier permeability, exacerbating local oedema and causing more profound microvascular ischaemia and inflammation [34, 57].

Animal studies in stroke and experimental contusional brain injury have shown that both inhaled and intravenous NO donors reduce final lesion volume and improve functional neurological assessments [86, 170]. However, there are conflicting findings that NOS inhibitors administered shortly after controlled cortical impact also reduced oedema and final lesion volume [169]. The present study further speaks to the fact that there is likely to be a heterogeneity of response to NO supplementation in TBI patients, and appropriate selection of patients for proposed clinical trials [127] based on timing and pattern of injury will be important to obtain beneficial effects rather than exacerbating secondary insults.

7.5 Limitations

This study was in a small number of patients and therefore the significant findings should be interpreted with some degree of caution. As discussed, the different associations between NOx and energy metabolites may have been observed by virtue of the difference in glucose, pyruvate, and lactate between monitoring sites. Lastly, the inference of NO synthesis from stable NOx concentrations does not account for NO diverted into alternative pathways, such as peroxynitrite formation, and therefore the true relationship between in vivo NO production and the assay results is not fully characterised.

7.6 Summary and Context

NO metabolites NO_2 and NO_3 are increased early following TBI in both radiologically normal and pericontusional brain and gradually reduced over several days. There is a slight but statistically significant lower mean NOx concentration in injured brain. NOx is positively correlated with pyruvate and lactate, but with heterogenous responses between uninjured and injured brain and resulting in contrasting relationships between LPR and NOx at radiologically normal and injured monitoring sites.

7.6.1 Hypotheses

- H9: NO concentrations are higher in pericontusional brain following TBI.
  Based on the current evidence this hypothesis is rejected.

- H10: NO is correlated with energy metabolites in both pericontusional and radiologically normal brain.
  Based on the current evidence this hypothesis is accepted.

Chapter 8

Study VI - Characterising the Dynamics of Cerebral Metabolism following Traumatic Brain Injury

8.1 Introduction

Cerebral metabolic dysfunction has been described in acute brain injury of various aetiology, including TBI, ischaemic stroke, and intracerebral haemorrhage, and has an important role in potentiating secondary injury cascades such as the induction of pro-inflammatory cytokine signalling and microvascular breakdown causing blood brain barrier permeability [111, 167]. Various states of metabolic dysfunction have been hypothesised and demonstrated from evidence accrued in cell culture and tissue models and from animal and human studies. Broadly, these can be classified as cellular substrate deficiency (as a consequence of tissue ischaemia or local diffusion barriers), aerobic glycolysis, or, lastly, a failure of oxidative phosphorylation that has been dubbed 'mitochondrial dysfunction' [27]. Distinguishing between these dynamic states within individual TBI patients *in vivo* is important for tailoring appropriate therapeutic interventions in an attempt to ameliorate the extent of secondary injury and improve neurological outcome.

Cerebral microdialysis is an invasive neuromonitoring technique that permits continuous real-time sampling of brain extracellular fluid and assessment of cerebral metabolism in the intensive care unit [79]. Standard metabolites assayed on bedside analyzers include glucose, lactate, pyruvate, glutamate, and glycerol. There is a body of observational evidence to support absolute

values, ratios, and temporal trends of specific metabolites as indicators of cerebral metabolic dysfunction. The most extensively studied parameter is the lactate/pyruvate ratio (LPR), generally accepted to be an index of cellular redox state and the balance between oxidative and anaerobic metabolism. Patients with average or prolonged LPR above thresholds of 25 or 40 are more likely to die or have unfavourable outcome following TBI [79]. Low cerebral glucose has similarly been associated with worse outcome both in observational series and interventional studies comparing alternative glycaemic control regimens [79]. Identically LPR values can potentially result from an infinite range of combinations of absolute lactate and pyruvate concentrations wherein one or both may be higher or lower than their respective normal range. Similar increases in LPR resulting from very different changes in lactate and/or pyruvate will likely reflect distinct states of energy compromise, for instance ischaemia or subtrate deficiency as opposed to aerobic hyperglycolysis [185, 21]. Thus, there as been much recent work on defining classifications of lactate, pyruvate, and LPR values that are proposed to map to various metabolic states. A further aspect crucial to interpreting glucose, pyruvate, and lactate concentrations, and their trends in vivo, is that they are not independent variables and display strong covariance, a fact that is often overlooked or not explicitly addressed in the microdialysis literature [123]. Characterising the functional form of the relationships between these metabolites is fundamental to understanding how they change in concert and in forecasting the response to therapeutic interventions.

Glycolysis is a series of enzymatic reactions, some of which are irreversible, and the detailed kinetics and metabolic control of the pathway are complex. However, the overall rate of glycolysis can be well approximated as a single-step irreversible reaction with Michaelis-Menten kinetics[124], i.e.:

$$J_{gly} = \frac{V_{gly}^{Max} \cdot G_c}{K_{gly}^{M} + G_c} \tag{8.1}$$

where J_{gly} is the rate of glycolysis, V_{gly}^{Max} is the (asymptotic) maximal rate, G_c is the cytosolic glucose concentration, and K_{gly}^{M} is the Michaelis rate constant. This implies that the rate of production and concentrations of the end products of glycolysis, including pyruvate, should exhibit a saturable increasing relationship with glucose concentrations. Lactate dehydrogenase (LDH) is the cytosolic enzyme that regulates the balance of the reversible interconversion of pyruvate and lactate together with NAD and NADH. A suitable rate equation for LDH is [152]:

$$J_{ldh} = \frac{V_{ldh}^{Max^F}\left(\frac{P_c \cdot NADH_c}{K_{ldh}^{M^F}}\right) - V_{ldh}^{Max^R}\left(\frac{L_c \cdot NAD_c}{K_{ldh}^{M^R}}\right)}{1 + \left(\frac{P_c \cdot NADH_c}{K_{ldh}^{M^F}}\right) - \left(\frac{L_c \cdot NAD_c}{K_{ldh}^{M^R}}\right)} \tag{8.2}$$

where J_{ldh} is the directional reaction rate, $V_{ldh}^{Max^F}$ and $V_{ldh}^{Max^R}$ are the maximal forward and reverse reaction rates, $K_{ldh}^{M^F}$ and $K_{ldh}^{M^R}$ are the respective rate constants, and P_c, L_c, NAD_c, and $NADH_c$ are the concentrations of pyruvate, lactate, NAD, and NADH, respectively. Assuming a steady-state reaction rate, rearrangement of this equation demonstrates that pyruvate and lactate concentrations should be linearly related. These rate equations therefore suggest hypothetical relationships between the metabolic parameters obtained with microdialysis that can be tested in TBI patients. Importantly, although microdialysis samples the extracellular concentrations, both glucose transport via the GLUT family of transporters (predominantly GLUT1), and pyruvate and lactate transport via monocarboxylate transporters (MCT) display linear relationships between extracellular and intracellular concentrations of the respective metabolites [61, 152]. Therefore, the functional form (i.e. linear, hyperbolic, etc) of the relationships between the extracellular concentrations of glucose, pyruvate, and lactate would be expected to mimic those of the intracellular compartment, albeit with different parameterisation.

In this study we have utilised microdialysis data from a large cohort of TBI patients with four principal objectives. Firstly, to quantify the independent effect of LPR and cerebral glucose on neurological outcome; secondly, to characterise the temporal course of metabolites following TBI; thirdly, to assess the functional relationships between metabolites and other monitoring variables, such as CPP; and finally to examine the functional inter-relationships of the key energy metabolites glucose, pyruvate, and lactate.

8.2 Methods

8.2.1 Patients

This is an observational study of 619 adult (>16 years) patients with TBI admitted for management on the neurocritical care unit (NCCU) at Addenbrooke's Hospital, Cambridge, UK over twenty years from 1997 to 2016. Data from the initial 223 patients in this cohort have been reported previously [172, 173].

All patients required intubation and mechanical ventilation and were managed according to a typical standardised tiered therapy protocol for TBI patients (Supplemental information). In brief, patients were sedated, paralysed, and mechanically ventilated to a target $PaCO_2$ of 4.5-5 kPa. Vasopressors are used to maintain a cerebral perfusion pressure (CPP) of 55-65mmHg. In response to elevated intracranial pressure there was a staged application of osmotherapy, external ventricular drainage, barbiturate coma, and ultimately decompressive craniectomy. Six month neurological outcome was assessed with the Glasgow Outcome Score, which was dichotomised into favourable (GOS 4-5) and unfavourable outcome (GOS 1-3) as appropriate.

8.2.2 Monitoring

Routine invasive neuromonitoring comprised of a triple lumen cranial access device (Technicam, Newton Abbott, UK) placed by default in the right frontal region unless contraindicated. An intracranial pressure (ICP) monitor (Codman, Raynham, MA, USA), a brain tissue oxygen ($PbtO_2$) probe (Licox Neurosciences, Andover, UK), and a microdialysis catheter (CMA 71, CMA/Mdialysis AB, Stockholm, Sweden; 100kDA molecular weight cut-off) were introduced via the access device and position with their tips in the white matter. Catheter location was confirmed on subsequent computed tomography and classified as pericontusional or within radiologically 'normal' brain based on their proximity to traumatic lesions.

Microdialysis catheters were perfused with standard crystalloid perfusate (CMA/MDialysis AB, Stockholm, Sweden) at 0.3μ l/min. Vials containing dialysate were changed at regular intervals as close to hourly as practicable and assayed on bedside analysers (CMA 600 and ISCUS models; CMA/Mdialysis AB, Stockholm, Sweden) for concentrations of lactate, pyruvate, glucose, glutamate, and glycerol.

Arterial blood pressure (ABP) was monitored continuously via a peripheral intra-arterial catheter. ICP, ABP, and $PbtO_2$ were digitised and recorded at 50-200Hz using ICM+ software (ICM+, Cambridge Enterprise/University of Cambridge, UK). In addition to storing the raw signals ICM+ has the facility for online calculation of secondary indices including the PRx metric of cerebral autoregulation. This is quantified as the Pearson correlation coefficient between thirty mean values of ICP and ABP calculated over 10 second windows [40]. A positive PRx value suggests ICP changing in concert with ABP, indicative of poor or absent autoregulation; PRx of approximately

zero or negative indicates intact autoregulation [40].

8.2.3 Data Processing

The raw data files from the microdialysis analysers were parsed and imported using custom scripts. Where the analyte is below the lower limit of detection of the assay and/or there is insufficient dialysate in a vial the datum is flagged as erroneous and these were excluded. As a further check the collated data were filtered of any values below the lower limits of detection of the analysers specified in the manufactuere's manual: glucose 0.1 mM, lactate 0.1mM, pyruvate 10 microM, glutamate 1 mM, glycerol 10 mM. To combine the high frequency ICP, CPP, PRx, and $PbtO_2$ signals with microdialysis data the former were exported in minute-by-minute format and then combined in epochs corresponding to the times of the sequential microdialysis assays and accounting for the 17 minute period that fluid takes to leave the semipermeable section of the microdialysis catheter and reach the collection vial.

To mitigate the effect of a small proportion extreme outliers when calculating summary statistics the data were Winsorized at the 0.00125 quantile, i.e. data that were either above or below the 99.875th and 0.125th quantile, respectively, were changed to be equal to the respective quantile threshold. This process does not remove data (compared with, for example, trimming) but allows more robust calculation of parametric statistics.

8.2.4 Statistical Analysis

All statistical analysis was performed in R (v.3.4.3; www.r-project.org) using the packages: *nlme, rms, mgcv, qgam, lattice, mice*. Ordinal proportional hazards regression was performed with the *lrm* function from the *rms* package. Due to the nature of the cohort a substantial proportion of patients had at least one missing data point which would result in exclusion from cohort-level regression and a potential source of bias. Therefore for these analysis the missing data were multiple imputed using the fully conditional chained equation model available in the *mice* R package.[180]. Missing data were treated as missing completely at random (MCAR) as the absence of data logging or recordings not being available for analysis was assumed not to be related to patients' prognosis or outcome. Continuous variables were imputed with predictive mean matching, and factors with logistic regression. Each of ten imputed datasets were then each entered into the re-

gression model(s) and the results pooled to obtain overall estimates of coefficients and standard errors.

For analysis of the hourly data linear mixed-effects (LME) and generalised additive mixed models (GAMM) were used.[199] The latter of these is an extension to the mixed modelling framework to include non-linear smooth functions of the independent variables being studied, represented in a choice of spline basis functions, in addition to categorical and/or linear (parametric) terms. This allows data-driven estimation of non-parametric non-linear relationships between variables. Whereas including polynomial or spline terms within standard least-squares regression or mixed-models is possible, these have a fixed degree of freedom and there is a tendency to overfit noise within the data. In the GAM(M) framework the degrees of freedom which determine the non-linearity or 'wiggliness' of the smooth terms is included as part of the model-fitting process by (restricted) maximum likelihood estimation and can be reduced to the null space of linear terms if that is all that is supported by the data. Furthermore, patient-level random effects and autoregressive error terms can also be included and they are therefore well served to analyse time-series/longitudinal data of differing duration from multiple individuals. For all analyses, unless otherwise stated, the basis for smooth terms was a cubic regression spline with ten knots. Random effects for each patient together with a first order autoregressive term (AR1) using the *gamm* and emphbam functions from the *mgcv* package was used with Restricted Maximum Likelihood (REML) as the fitting method. To evaluate smooth quantile relationships between variables the *qgam* package was used which extends the the mgcv GAM framework to include quantile regression[49].

8.3 Results

8.3.1 Demographics

Data for a total of 619 patients were collated for the study; baseline characteristics are summarised in Table 8.1. GCS and pupillary reaction at initial presentation were not available from electronic records for 42 (6.7%) and 112 (18.7%) of patients, respectively. Outcome could not be determined in 37 (6.0%) of patients. The median time to the initiation of microdialysis monitoring was 26.9 [16.5-50.1] hours and was continued for a median IQR] of 4.8 [2.7-7.8] days. In total there were 56,307 microdialysis epochs included, with a median sampling interval of 1.02[1.00-1.40] hours. In

addition to microdialysis, 461 (74.5%) patients had ICM+ data recording (the remaining patients would also have had ICP and $PbtO_2$ monitoring as standard clinical care, but high resolution data were not recorded for offline analysis).

Characteristic		Total N = 619
Age		*(median [IQR] years)*
		37 [24-52]
Sex		*(N [%])*
	Male	472 [76.3]
	Female	147 [23.7]
GCS		*(N [%])*
	3-8	387 [62.5]
	9-12	104 [16.8]
	13-15	86 [13.9]
	N.A.	42 [6.7]
Pupils		*(N [%])*
	Both reactive	417 [67.4]
	Unilateral unreactive	69 [11.1]
	Bilateral unreactive	21 [3.4]
	N.A.	112 [18.1]
Marshall CT Score		*(N [%])*
	Class II	298 [48.1]
	Class III	92 [14.9]
	Class IV	21 [3.4]
	Class V	96 [15.5]
	Class VI	36 [5.8]
	N.A.	76 [12.3]
Mechanism of Injury		*(N [%])*
	Assault	53 [8.6]
	Fall	200 [32.3]
	Cyclist	37 [6.0]
	Pedestrian RTA	51 [8.2]
	Occupant RTA	260 [44.9]
	Other and N.A.	18 [2.9]

Table 8.1: Admission baseline characteristics of the patient cohort.
IQR, interquartile range; GCS, Glasgow Coma Scale; CT, computed tomorgraphy; N.A., not available.

8.3.2 Lactate/Pyruvate Ratio and Outcome

Univariate comparison of individual mean LPR was not significantly different between unfavourable and favourable outcome groups when averaged over the first 24h from injury but was significantly different at 72h from injury (Figure 8.1 median [IQR]: 25.8 [11.0] vs. 24.2 [0.6], p=0.023) and significantly higher proportion of time at LPR>25 (median [IQR]: 50.6% [90.0] vs 29.8% [79.0], p=0.047). When averaged over the whole monitoring period there was again no significant difference between groups.

To examine the independent effect of LPR on outcome a proportional odds logistic regression of the five point GOS outcome scale against age, presenting GCS, pupillary reaction, Marshall CT score, and <24h to <168h mean values of glucose, LPR, ICP, CPP, PRx, and $PbtO_2$ was con-

ducted. Tenfold multiple imputation of missing data using chained equations was performed and the proportional odds regression repeated and pooled; the results are shown in Table 8.2. Outcome was missing for 37 (6.0%) patients. Among the independent predictor variables there was 22-27% missing values depending on the time period over which the physiological data were averaged. At all time points age, low GCS (<9), bilaterally unreactive pupils, and unevacuated mass lesion were significant predictors of outcome. Of the monitored variables, ICP, PRx, and LPR were significant predictors when averaged over 72h or longer. Cerebral glucose was also significantly associated with outcome when averaged over the first seven days from injury. As expected, the overall predictive power of the regression improved with time as evidenced by the increase in Harrell's C-statistic, equivalent to area under the receiver operating curve for binary logistic regression.

	≤24h	≤72h	≤120h	≤168h	All
Age	−0.032 (0.006)***	−0.033 (0.005)***	−0.031 (0.005)***	−0.031 (0.005)***	−0.031 (0.005)***
GCS 9-12	−0.221 (0.294)	−0.168 (0.275)	−0.163 (0.274)	−0.157 (0.280)	−0.171 (0.285)
GCS ≤ 8	−0.707 (0.246)**	−0.692 (0.227)**	−0.708 (0.229)**	−0.688 (0.236)**	−0.726 (0.238)**
Pupils (Unilateral)	−0.410 (0.271)	−0.461 (0.301)	−0.459 (0.290)	−0.454 (0.288)	−0.444 (0.282)
Pupils (Bilateral)	−1.728 (0.435)***	−1.791 (0.408)***	−1.712 (0.404)***	−1.661 (0.405)***	−1.623 (0.410)***
Marshall III	−0.314 (0.275)	−0.210 (0.254)	−0.260 (0.258)	−0.254 (0.262)	−0.248 (0.279)
Marshall IV	−0.638 (0.409)	−0.429 (0.460)	−0.404 (0.455)	−0.365 (0.456)	−0.339 (0.455)
Marshall V	0.029 (0.224)	−0.057 (0.214)	−0.088 (0.208)	−0.095 (0.210)	−0.117 (0.210)
Marshall VI	−1.015 (0.326)**	−0.893 (0.342)**	−0.814 (0.345)*	−0.876 (0.340)*	−0.854 (0.346)*
Glucose	−0.026 (0.074)	−0.082 (0.077)	−0.113 (0.071)	−0.147 (0.070)*	−0.186 (0.073)*
LPR	−0.006 (0.006)	−0.012 (0.006)*	−0.015 (0.007)*	−0.016 (0.007)*	−0.014 (0.007)*
Glutamate	−0.002 (0.003)	−0.004 (0.005)	−0.001 (0.005)	−0.002 (0.005)	−0.001 (0.005)
Glycerol	−0.000 (0.001)	−0.000 (0.001)	0.001 (0.001)	0.001 (0.001)	0.000 (0.001)
ICP	0.003 (0.028)	−0.061 (0.019)**	−0.057 (0.017)***	−0.064 (0.019)***	−0.078 (0.020)***
CPP	−0.001 (0.024)	−0.008 (0.012)	−0.002 (0.014)	0.000 (0.013)	0.009 (0.014)
PRx	−0.032 (0.574)	−1.668 (0.579)**	−1.921 (0.572)***	−2.215 (0.591)***	−2.602 (0.649)***
$PbtO_2$	0.003 (0.010)	0.008 (0.008)	0.008 (0.008)	0.006 (0.007)	0.003 (0.008)
C (AUROC)	0.681	0.694	0.695	0.701	0.709

$^{***}p < 0.001$, $^{**}p < 0.01$, $^{*}p < 0.05$

Table 8.2: Proportional odds regression against Glasgow Outcome Score (GOS) of baseline characteristics and monitoring data averaged over different intervals following injury. Numbers are regression coefficients with standard errors in parentheses; statistical significance indicated by asterix. Harrell's C statistic, equivalent to the area under the receiver operating curve (AUROC) is also included for each model.
GCS, Glasgow Coma Scale; LPR, lactate/pyruvate Ratio; ICP, intracranial pressure; CPP, cerebral perfusion pressure; PRx, measure of autoregulation (see text); $PbtO_2$, brain tissue oxygen tension.

8.3.3 Metabolism in Pericontusional Brain

Patients' CT scans, where available, were examined and microdialysis catheter location categorised as pericontusional if within 1cm of haemorrhage or pericontusional oedema. Overall, catheter location was determined to be pericontusional in 110 patients and in radiologically normal brain remote from obvious injury in 330. The remaining 179 patients did not have CT scans demonstrating catheter position. Mean LPR over the first 72h from injury was significantly higher

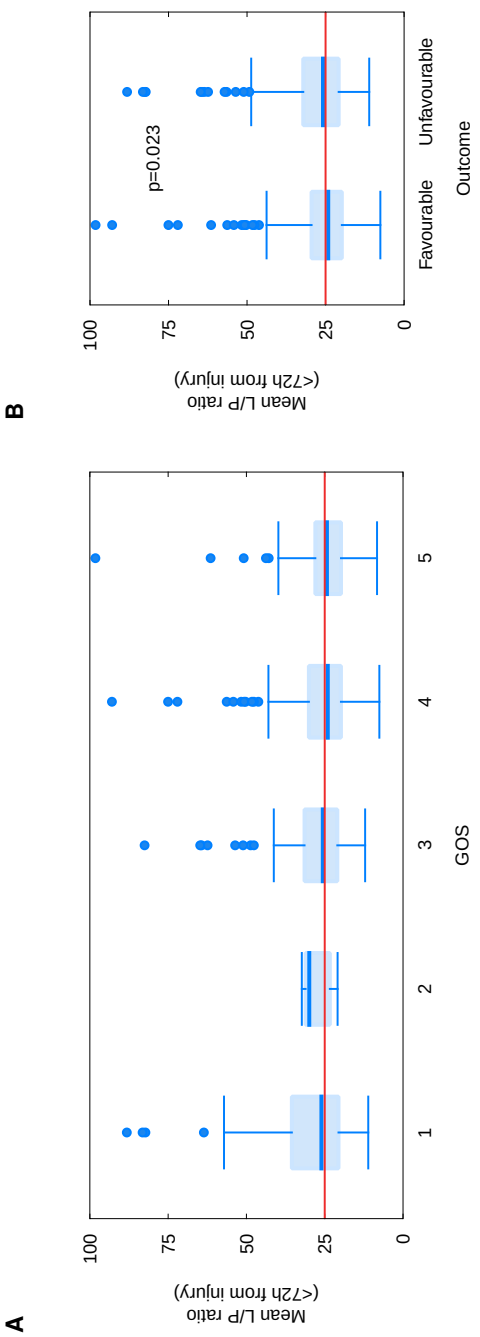

Figure 8.1: Boxplots of indivdual patients' mean lactate-pyruvate ratio (LPR) over the first 72h following injury, by (**A**) Glasgow Outcome Score (GOS) and (**B**) dichtomised GOS.

in pericontusional brain (29.1 vs 25.1, p=0.0038). There was no significant difference in glucose (1.84 vs 1.75, p=0.603)

8.3.4 Temporal trends

Generalized additive mixed models, including per-patient random effects and first-order autoregressive terms, were generated to fit data over first temporal profile of microdialysis analytes 14 days following injury. To ensure sufficient degrees of freedom to accurately reflect the temporal trends the smooth terms utilised a 14-knot cubic regression splines. Figure 8.2 shows the temporal profile of the monitored variables split by favourable and unfavourable outcome categories. Figure 8.3 demonstrates that, as expected, the data are highly autocorrelated and that the fitting a GAMM model including an AR1 term accounts for most of the autocorrelation in the residuals.

LPR showed an initial decreasing trend over the first c.48h and then generally increased to day 14; there were significant changes over time for both favourable ($F_{7.80}$=24.02 p<2e-16) and unfavourable ($F_{9.88}$=7.61 p=1.5e-10) outcome groups but with significant differences in both overall mean intercept (4.62 [1.38], T=3.35, p=0.00081) and trend between groups ($F_{2.16}$=3.94 p=0.015) was significantly different in the unfavourable outcome group, both in terms of mean value (2.52 [0.50]mM, t=5.02 p=5.1e-07) and temporal trend (F=18.04 p=2.16e-05); overall, LPR was on average higher in the unfavourable group until around day 10 following injury. Pyruvate exhibited a significant, and generally increasing, temporal trend ($F_{4.39}$=4.42 p=0.0011) but this did not differ significantly either in mean value or trend between outcome categories. Of interest, cerebral glucose was significantly lower over days five to eleven following injury in the favourable outcome group. Both glutamate and glycerol were generally higher in the unfavourable outcome group but not significantly different. The trends in mean intracranial pressure and PRx were significantly different between outcome groups throughout virtually the entire 14 day period, whereas the confidence intervals for CPP overlapped indicating no significant difference. $PbtO_2$ was similar between groups in the the first week after injury but then was lower in the those patients who ultimately had an unfavourable outcome.

8.3.5 Relationship between LPR and CPP, PRx, and $PbtO_2$

To assess the associations between CPP, PRx, and $PBtO_2$ and cerebral metabolism a further series of GAMMs were generated with LPR as the dependent variable, again including random

A

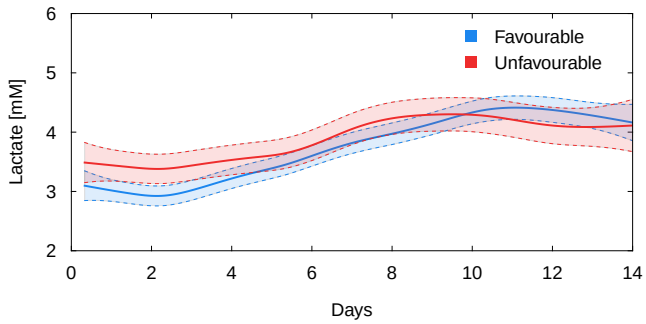
Lactate [mM]
Days
Favourable
Unfavourable
6
5
4
3
2
0
2
4
6
8
10
12
14

B

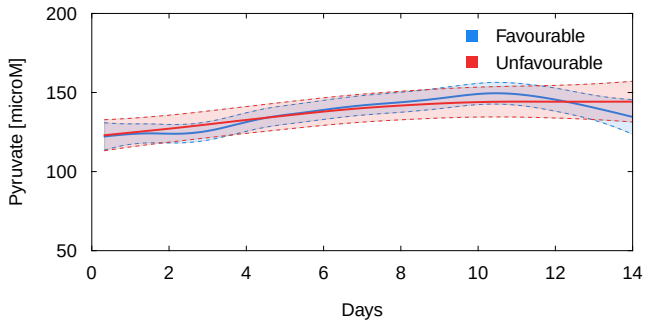
Pyruvate [microM]
Days
Favourable
Unfavourable
200
150
100
50
0
2
4
6
8
10
12
14

C

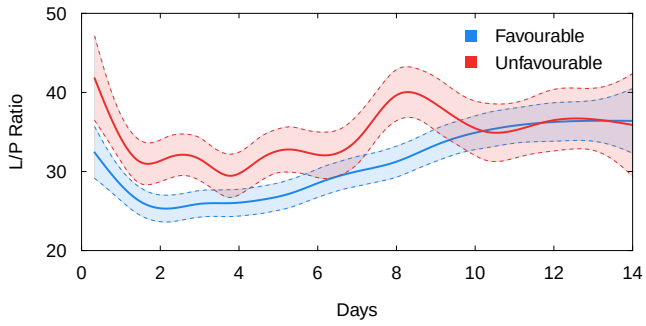
L/P Ratio
Days
Favourable
Unfavourable
50
40
30
20
0
2
4
6
8
10
12
14

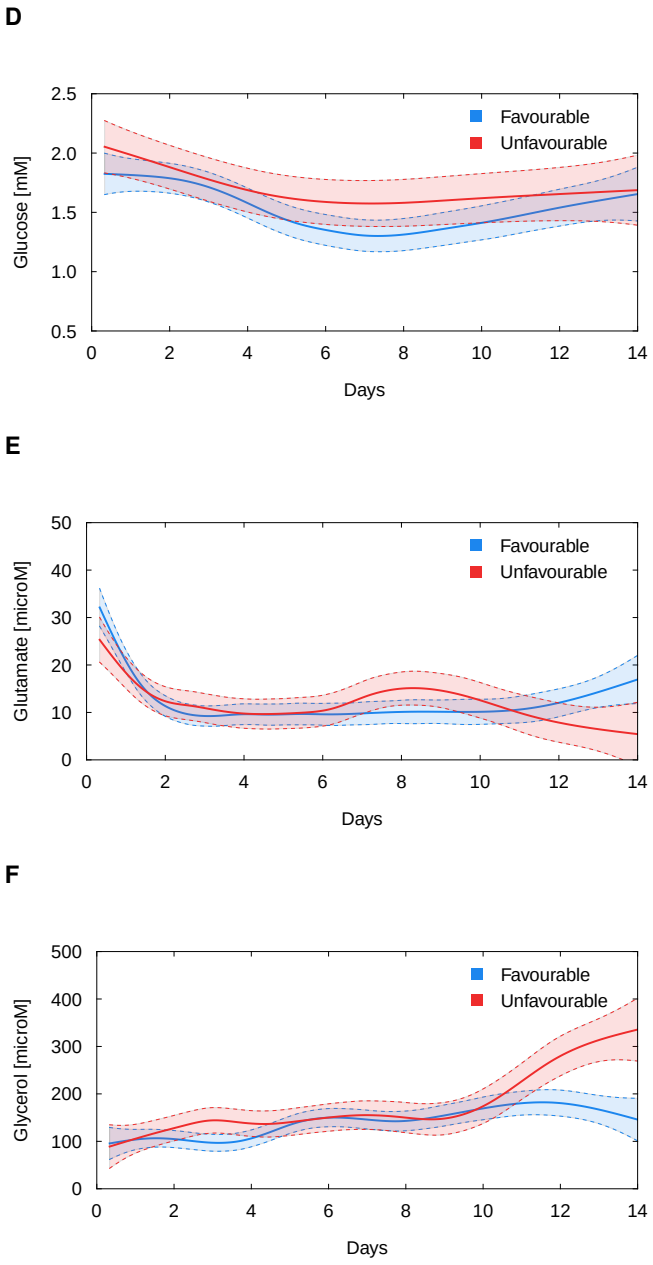

Figure 8.2: Fitted population mean time courses for microdialysis analytes using generalised additive mixed models, by dichomtomised Glasgow Outcome Score group.
Lactate (**A**), Pyurvate (**B**), Lactate-Pyruvate Ratio (LPR, **C**), Glucose (**D**), Glutamate (**E**), and Glycerol (**F**). Shaded areas indicated 95% intervals.

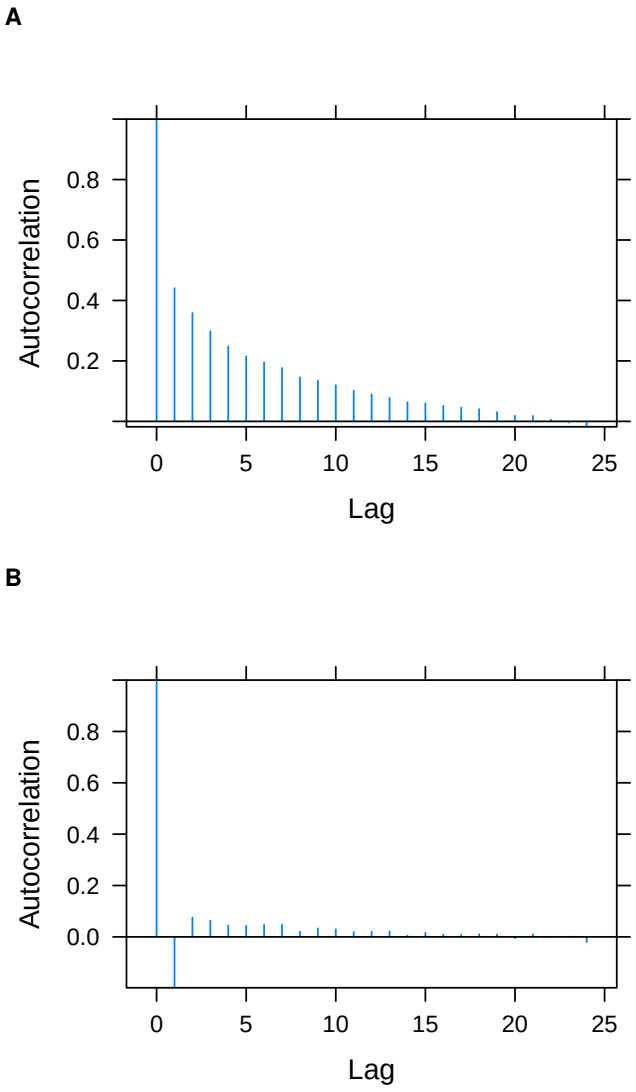

Figure 8.3: Autocorrelogram plots for the GAM model of LPR over time, **A** without including an AR1 autoregressive term and **B** including the autoregressive term (phi = 0.57). Strong autocorrelation in the residuals of the time series is evident and this is largely removed when the model includes the AR1 term.

effects and first-order autoregressive terms. All relationships were non-linear (Figure 8.4). Inspection of the GAMM models suggested thresholds of CPP below 60mmHg (2.21% of samples), PRx above 0.2 (24.21% of samples), and $PBtO_2$ below 20mmHg (29.26% of samples) were associated with increased LPR, although the confidence interval was wide and included zero effect for $PbtO_2$. Dichotomising the data based on these thresholds found significant differences in LPR with Wilcoxon tests (all p<1e-10). Comparison of the dichotomised groups with mixed models incorporating patient random-effects and autoregressive errors found significantly lower LPR for CPP >60mmHg (-1.42, t=-2.78, p=0.0055) and for PRx <0.2 (-0.80, t=4.27, p<1e-6), with borderline effect of $PbtO_2$ >20mmHg(-0.61, t=-1.91, p=0.056). Dichotomising $PbtO_2$ at a lower threshold of 10mmHg (7.04% of samples) did not find a significant difference.

8.3.6 Glucose and LPR

Figure 8.5 shows the nonlinear relationship between cerebral glucose concentration and LPR, demonstrating that LPR rapidly increases as glucose concentrations reduce below approximately 2mM; the confidence intervals are narrow indicating this was a robust feature amongst the patients in the cohort. Figure 8.6A shows the fitted GAMMs between lactate, pyruvate and glucose. Although low glucose was associated with a high LPR the absolute concentrations of lactate and pyruvate varied positively with glucose in an approximately hyperbolic pattern, as hypothesised. To confirm this relationship a double-reciprocal plot (Figure 8.6B) was examined as this should show a linear relationship, and indeed this was the case. Figure 8.6C shows the GAMM model between lactate and pyruvate and confirms the essentially linear relationship, as predicted by LDH rate equation. To test whether this finding was representative the pyruvate-lactate correlation was estimated for each individual patient (Figure 8.6D). Both Pearson and Spearman correlation coefficients were calculated; the former is a measure of linear association and the latter is additionally sensitive to non-linear monotonic associations. Correlation coefficient values were generally high (i.e. 0.8) and the distribution was similar with both coefficients lending weight to the contention that assumption of a linear trend was most appropriate. Lastly, a linear mixed model between lactate and pyruvate including random intercept and slope terms together with a first-order autoregressive term. Figure 8.6E displays the variation in the slope and intercept of the pyruvate-lactate relationship across patients in the cohort.

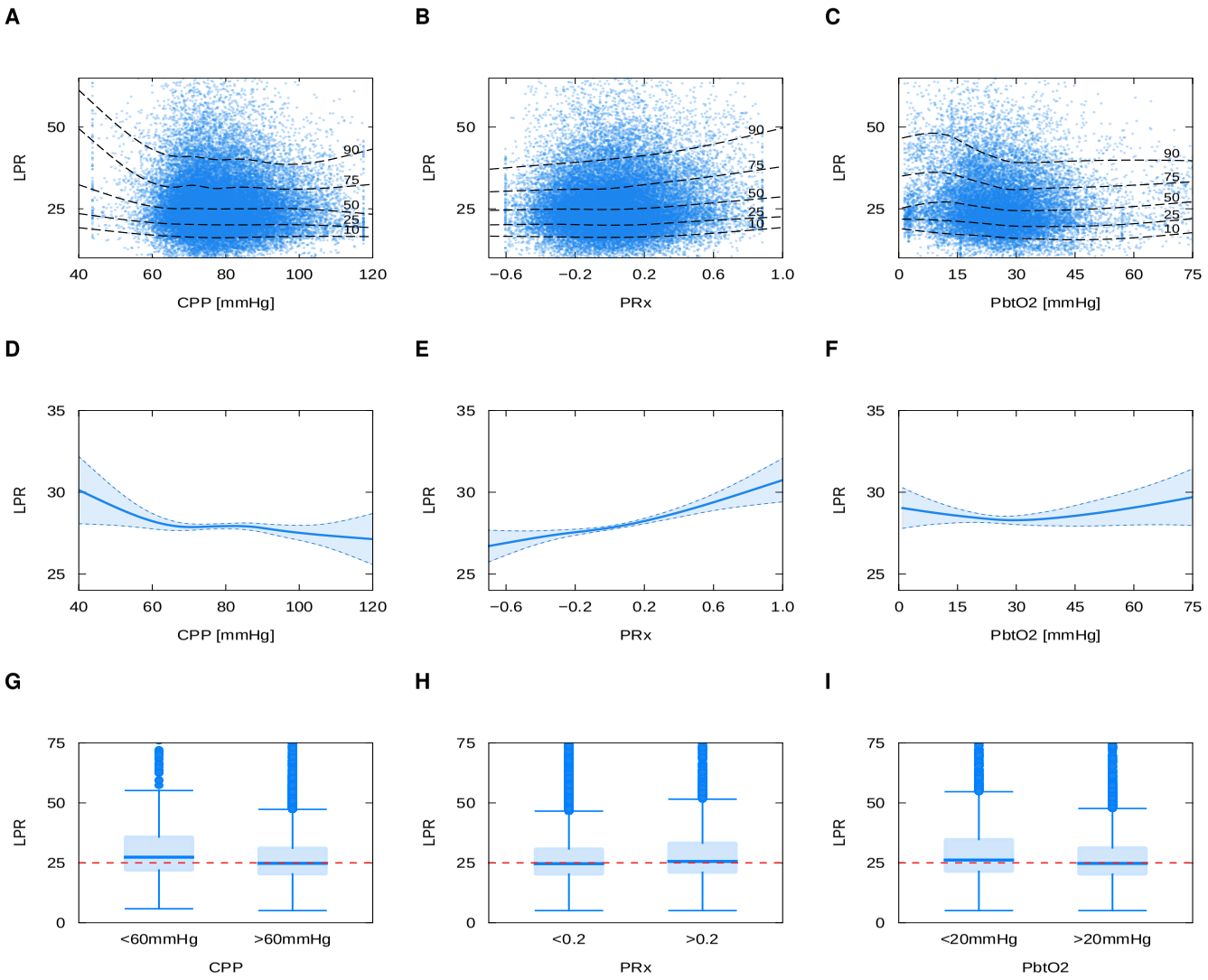

Figure 8.4: Relationship between lactate-pyruvate ratio (LPR) and cerebral perfusion pressure (CPP), autoregulation (PRx), and brain tissue oxygen tension ($PbtO_2$). Panels **A-C** show 10th, 25th, 50th, 75th, and 90th centiles of LPR for the whole cohort overlaid on scatter plot of all data. Panels **D-F** show fitted GAMM of mean relationship between respective variable and LPR, with 95% CI shaded. Panels **G-I** show boxplots of LPR with CPP, PRx, and $PbtO_2$ dichotomise; p-values for Wilcoxon signed ranks test.

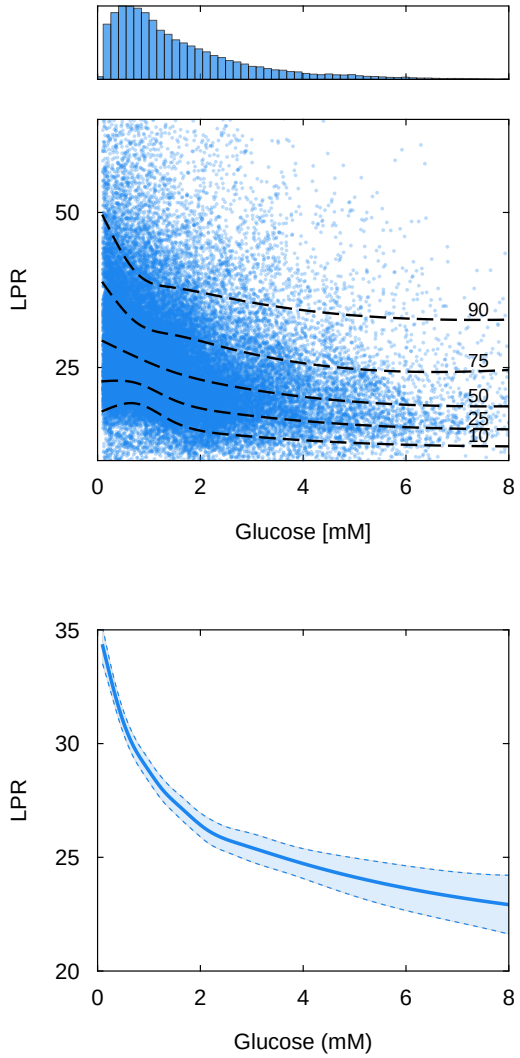

Figure 8.5: (top) density histogram indicating the distribution of cerebral glucose; (middle) bivariate scatter plot of glucose with LPR overlaid with 10th, 25th, 50th (median), 75th and 90th fitted quantiles (dashed lines); (bottom) mean trend from GAMM model with shaded 95% confidence interval.

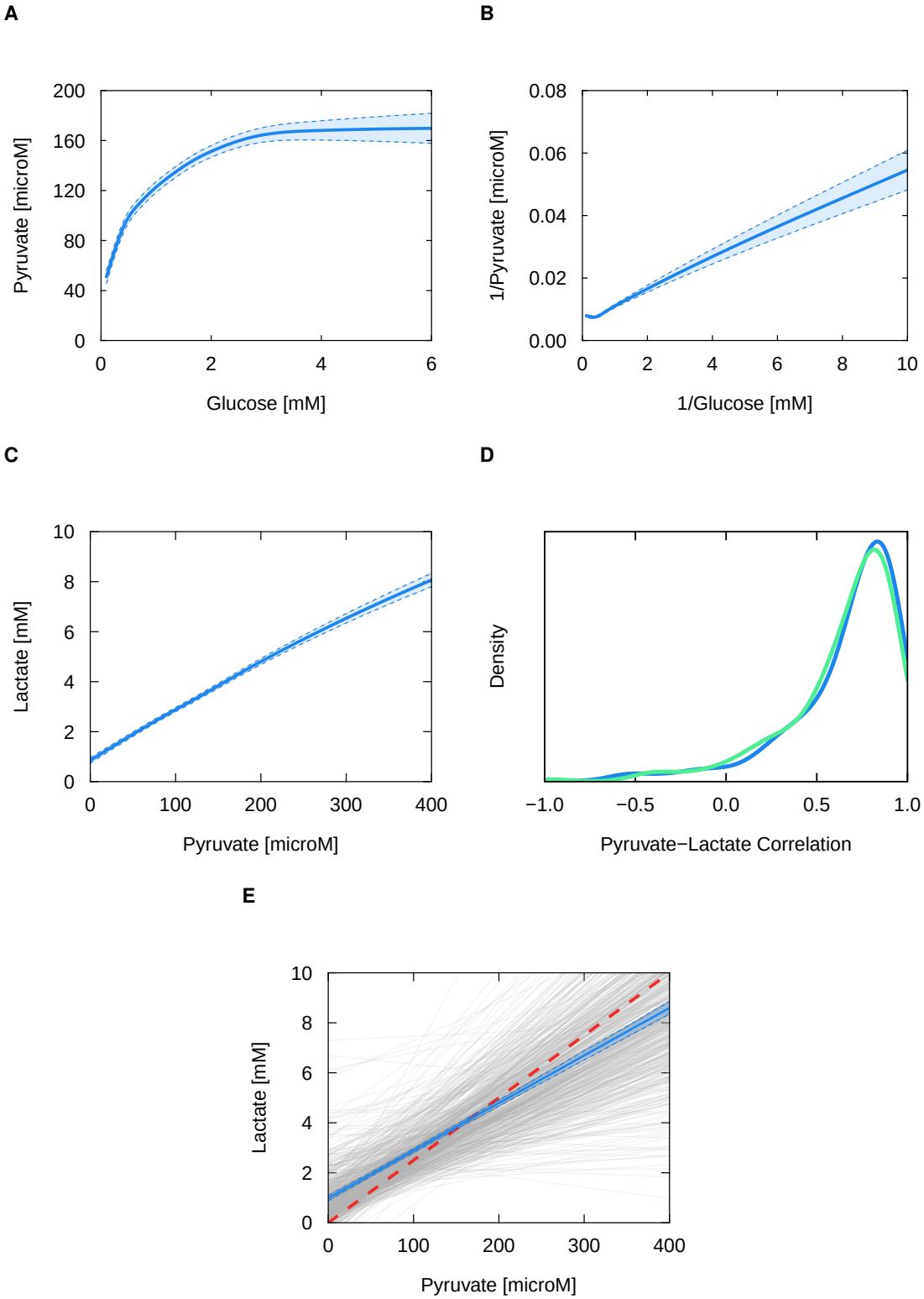

Figure 8.6: Inter-relationships between glucose, pyruvate, and lactate. **A**: GAMM model of microdialysis glucose and pyruvate. **B**: Double reciprocal GAMM model of glucose and pyruvate. **C**: GAMM model of pyruvate and lactate concentrations. **D**: Kernel density distribution estimate of Pearson (blue) and Spearman (green) correlation estimates for pyruvate-lactate association within each subject. **E**: linear mixed effect model of pyruvate and lactate with overall fixed effect (blue) and individual trends including the random effects for intercept and slope (gray lines). Red dashed line indicates reference line along which LPR=25. Shaded regions indicate 95% confidence intervals for all panels.

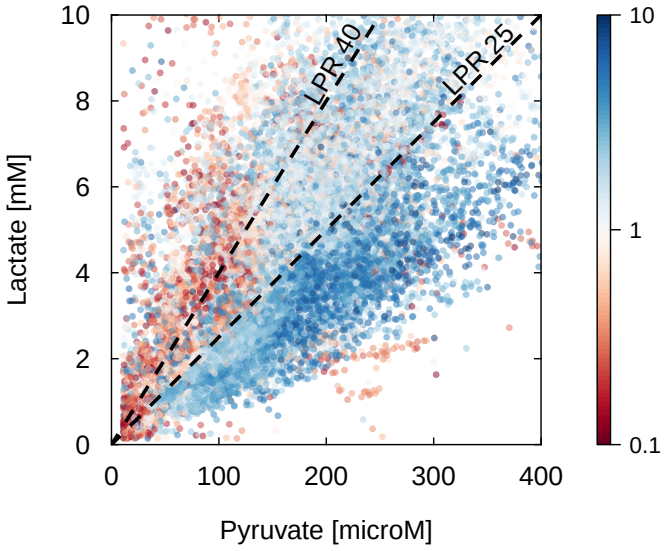

Figure 8.7: Bivariate plot of lactate and pyruvate colour coded by cerebral glucose concentration (colorbar, [mM]). Reference lines for LPR=25 and LPR=40 are overlaid.

8.3.7 Classifying metabolic dysfunction

Examination of the raw data in a bivariate plot of pyruvate and lactate suggests a potential classification of metabolic states based on LPR and glucose (Figure 8.7). The 'normal' state of LPR<25 and normal glucose concentrations (>1mM) is considered Type I. Type II is the situation of LPR<25 with glucose <1mM and Type III that of elevated LPR>25 and adequate cerebral glucose >1mM. Finally Type IV represents the most severely deranged state with both LPR>25 and glucose <1mM. The four metabolic states were then compared for differences in other microdialysis and neuromonitoring variables with a linear mixed model incorporating post-hoc pairwise comparisons between groups and a Bonferroni correction of the p-values (Figure 8.8). Glutamate was significantly higher in both Type I and III, corresponding with higher glucose. PRx was significantly impaired (i.e. worse autoregulation) and ICP higher during periods of Type III and IV metabolism. CPP and $PbtO_2$ was not different between any of the classes.

8.4 Discussion

8.4.1 Cerebral Metabolism and Outcome

This study of combined microdialysis and neuromonitoring data in 619 TBI patients represents the largest series in the literature and builds on the evidence from previous studies, including the findings from the initial 223 patients in the cohort [172]. Cerebral LPR averaged per patient over the first three, five, or seven days following injury was found to be independently associated with neurological condition at six months following injury, measured ordinally on the GOS scale. This affirms findings in previous studies [79]. The lack of association between LPR and outcome when averaged over the first 24 hours or the whole period of monitoring likely reflects the relative lack of data in the early period following injury and the confounding factors and selection bias in patients who where monitoring beyond seven days. It should be emphasised that the modelling presented here is not intended to motivate adoption of LPR (or any other microdialysis-derived parameter) as a specific or precise prognostic marker in the clinical management of individual TBI patients. Rather, the rationale for examining the association with outcome is to test the broad face-validity of the presumption that derangements of cerebral metabolism are related to outcome after TBI (and brain injury in general) and the corollary that therapy directed at normalising metabolism may have potential benefit.

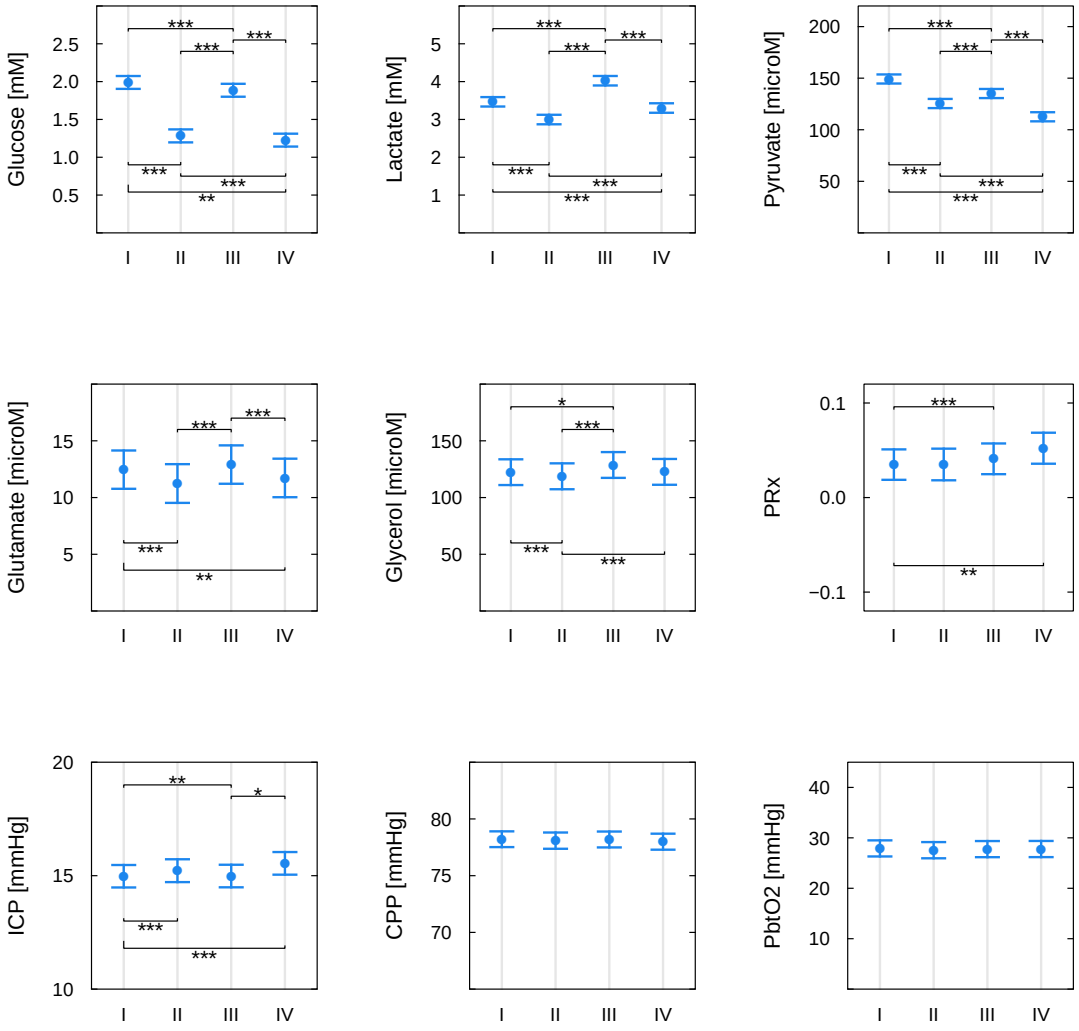

Figure 8.8: Marginal means and 95% confidence intervals for microdialysis and neuromonitoring variable between the four metabolic states. Type I: LPR<25, glucose >1mM; Type II: LPR<25, glucose <1mM; Type III: LPR>25, glucose >1mM; Type IV: LPR>25, glucose <1mM. Bars indicate significant pairwise comparisons: ***p<0.001, **p<0.01, *p<0.05; all Bonferroni corrected for multiple comparisons.

Consistent with the regression analysis, the mean temporal course of LPR was significantly different over the first several days from injury between dichotomised outcome groups. Both groups exhibited a decrease in LPR over the initial 48 hours following injury, possibly consistent with recovery from any acute derangements of ICP and cerebral blood flow together with physiological stabilisation in the intensive care unit [1]. Thereafter LPR increased, with a more pronounced and variable pattern in poor outcome patients. At a mean level, the secondary increase in LPR was due primarily to increasing lactate, whereas the trend for pyruvate was relatively flat. Impaired autoregulation (PRx >0.2), was strongly associated with increased LPR, suggesting techniques such as targeting 'optimal CPP' may be of substantial benefit in normalising metabolic derangements

following TBI [8]. Low CPP (<60mmHg) was also associated with raised LPR but the incidence of CPP below this threshold was very low. Somewhat surprisingly, the relationship between $PbtO_2$ and LPR was weak, with only a non-significant trend towards higher LPR at low brain oxygen tensions. Fewer patients in the cohort had brain tissue oxygen recordings compared with ICP and CPP, which may in part explain the lack of observed association.

8.4.2 Metabolic Dysfunction following TBI

The canonical model of cellular respiration commences with glucose entering the cytosol, proceeding along the series of enzymes of the glycolytic pathway to pyruvate (with net gain of two ATP molecules), which in turn enters the mitochondrion to feed the TCA cycle and the electron transport chain, producing a further 34 molecules of ATP. When oxygen is insufficient, pyruvate is converted to lactate to regenerate NAD and allow anaerobic glycolysis to continue. In the CNS there is evidence that glia and neurons are metabolically coupled in the so-called 'Astrocyte-Neuron Lactate Shuttle' (ANLS) [19, 130]. This model posits that neurons do not generally utilise glucose directly but predominantly generate pyruvate from lactate that is produced by glycolysis in astrocytes. During periods of greater neuronal activity and metabolic demand synaptic glutamate release increases, which is in turn taken up into surrounding astrocytes and upregulates glycolysis to generate further lactate that diffuses to neurons for utilisation in oxidative metabolism. Several compelling lines of evidence support the ANLS in animal models and humans but irrespective of the more complex arrangements, net brain metabolism remains predominantly oxidative in normal circumstances. As evidenced in the present study, frank cerebral ischaemia - i.e. low cerebral perfusion pressure and/or tissue hypoxia - is uncommon with modern critical care management of arterial blood pressure, intracranial pressure, and ventilation. Nonetheless, accumulated evidence suggests a number of other forms of metabolic dysfunction commonly manifest after TBI, and different types may coexist dynamically or be regionally localised within an individual patient [27, 26, 83]. Even if cerebral blood flow is adequate, substrate delivery may be impaired by local diffusion barriers that result from cell necrosis and matrix breakdown. Aerobic hyperglycolysis, wherein anaerobic glycolysis is upregulated despite sufficient oxygen availability, has been demonstrated to be a common early phenomenon in both preclinical models and human TBI patients [21]. Overlapping to some extent is the concept of 'mitochondrial dysfunction', a situation where oxidative respiration cannot proceed effectively due to deficiencies in the TCA cycle or electron transport chain, with an obligate increase in the rate of glycolysis to maintain ATP production.

Characterising the monitoring 'signature' of distinct aetiologies of metabolic dysfunction following TBI is a major goal of investigation and a key step in testing potential therapeutic strategies is reliable identification of the underlying pathophysiological state. Previously, LPR elevations have been loosely categorised as ischaemic/Type 1, corresponding with high lactate and normal or low pyruvate, and non-ischaemic/Type 2 reflecting normal lactate with low pyruvate. The latter of these states is suggested to reflect states of hyperglycolysis with excess substrate demand [101, 43]. The present study has shown that, within individuals, there is a strong linear relationship between pyruvate and lactate concentrations, and thus both change in concert. This association was demonstrated with flexible generalised additive mixed models, which do not impose a pre-determined functional form on the relationship between dependent and independent variables, and are able to account for the strong autocorrelation in biological time series that would otherwise risk overfitting. The parameters of the linear pyruvate-lactate relationship (i.e. the gradient coefficient) and hence the relative magnitude of changes in each metabolite was variable between patients. A key point to emphasise is that although lactate and pyruvate follow a linear relationship, if this is parameterised by a non-zero intercept then the LPR will change as the metabolite concentrations change. More precisely: if the equation of a straight line is $y = ax + b$ and $|b| > 0$, the ratio of variables will be $y/x = a + b/x$ and thus the ratio is *nonlinearly* dependent on the concentration. Only in the circumstance of an exactly zero intercept will the quotient of linearly-dependent variables remain constant (equal to the gradient m). Glucose was confirmed to have a strong nonlinear association with the concentration of pyruvate (and hence lactate), with features consistent with standard saturable Michaelis-Menten kinetics. As further evidence of this the relationship was linearised by examining a model of reciprocal concentrations of glucose and pyruvate. This is akin to a Lineweaver-Burke plot employed to estimate rate constants and maximal velocities of in enzyme kinetics [39]. Here the double reciprocal plot was used simply to characterise the functional relationship; parameters estimated from the plot are not readily interpretable, although may serve as a way of statistically comparing patient groups. Several further questions regarding the relationships between glucose, pyruvate, and lactate remain to be examined in further studies. For instance: do the parameters of the functional relationships differ significantly across the spectrum of TBI (i.e. diffuse vs focal) and is there regional heterogeneity within individual patients? Do the parameters follow a predictable temporal course following injury and does this differ between patients with favourable and unfavourable outcome?

Overall, these empirical findings of this study show that as glucose decreases, both pyruvate and lactate decrease, and LPR rises. Pyruvate, Lactate, and LPR exhibited most rapid rate of change

at glucose concentrations of approximately 1mM. Although cerebral metabolic derangement is likely a continuum of both type and degree, the present findings motivated an alternative classification of four metabolic states based on a threshold LPR of 25 and cerebral glucose of 1mM. Examining the mean lactate and pyruvate concentrations in the four classes, the group defined here as Type III would largely correspond with the previously defined 'ischaemic' or Type 1 LPR elevation, and the current Type IV would be defined as non-ischaemic/Type 2. The findings of no significant difference in CPP or $PBtO_2$ speak against frank cerebral ischaemia in either group but PRx was significantly higher in both Type III and Type IV classes, suggesting a possible mismatch in substrate demand and supply.

These results implicate glucose concentration as a key indicator or determinant of cerebral metabolic state, together with LPR. The natural question that follows is whether supplementing cerebral glucose improves LPR and has a beneficial effect on patient outcome. Target ranges for plasma glucose in the neurointensive care unit are a subject of much debate and several studies have shown that tight control with continuous insulin infusions, as used in general intensive care, have been associated with reduced cerebral glucose and elevated LPR in TBI patients when compared with more permissive glycaemic control[184, 132, 125]. However, early hyperglycaemia in TBI patients is associated with poor outcome [99] and intravenous glucose supplementation has not shown consistent benefit in TBI models [118, 33]. Thus, the role of active glucose administration in TBI patients remains an area for future study. Defining the parameters of individual patients' linear pyruvate-lactate relationship does potentially provide an indication of the likely cerebral metabolic response to additional glucose. For example, the subgroup of patients with a gradient >25 would be expected to have worsening of their LPR in response to increased pyruvate and lactate, whereas patients with a gradient <25 would be predicted to show improvement. This supposes that the linear pyruvate-lactate relationship is not altered by intervention, which is a further point that remains to be tested in future investigation.

8.4.3 Limitations

This study has a number of limitations inherent to observational investigations. Missing data was addressed with multiple imputation but this is imperfect and possibility of bias remains. Although the general management protocol for TBI patients at our institution is standardised, the specific interventions and their timing for each patient was not recorded and therefore potential

confounding effects on the data are not quantifiable. However, this is in part mitigated by the large number of patients included. Despite the strong associations between variables observed, extrapolation to the effects of manipulating, for example, glucose concentrations, are only hypothetical and speculative; further interventional studies are required.

8.5 Summary and Context

Cerebral metabolic dysfunction, as evidenced by raised LPR, is associated with patients' neurological outcome following TBI. Low CPP and $PbtO_2$ should be avoided as per current guidelines. Targeting CPP to minimise PRx (i.e. optimise autoregulation) may be beneficial in ameliorating metabolic dysfunction. The relationship between brain lactate and pyruvate is linear, with variable parameters between individual patients. Glucose is strongly related to both lactate and pyruvate concentrations and LPR; the benefit of supplementing glucose in patients with raised LPR and a favourable lactate-pyruvate relationship warrants further research.

8.5.1 Hypotheses

- H11: Cerebral metabolic parameters predict neurological outcome following TBI
  Based on the current evidence this hypothesis is accepted.

- H12: Derangements in LPR and cerebral glucose are different in radiologically normal and contused brain following TBI.
  Based on the current evidence this hypothesis is partially accepted.

- H13: There are defined functional relationships between the principal energy molecules assayed with microdialysis, namely glucose, pyruvate, and lactate.
  Based on the current evidence this hypothesis is accepted

Chapter 9

Summary and Future Directions

9.1 General summary

The overarching aim of this thesis was to detect BBB permeability in relation to brain contusions, characterise the temporal course of expansion and progression of contusions and associated brain oedema, and to identify signalling mediators and metabolic derangements in pericontusional brain that may be contributors to this process.

A robust and simple stereological technique for measuring contusion volume was validated and utilised in fifty-two patients to demonstrate that the majority of contusion expansion occurs within the first 72h of injury. The degree of contusion expansion was associated with severity of metabolic derangment measured by LPR.

Dynamic contrast enhanced perfusion CT imaging did not show evidence of BBB permeability in ten TBI patients imaged with a total of 16 scans. A number of possibilities may explain this finding but the utility of DCE-CT assessment of BBB dysfunction in the context of brain trauma remains unclear.

Using microdialysis catheters targeted to the vicinity of contusiuons and concomitantly placed in non-injured brain in twelve TBI patients, a spatially segregated pro-inflammatory pattern of cytokine production was observed in pericontusional brain that was most prominent within a similar time period from injury. Additionally, chemokines promoting cellular infiltration and matrix metalloproteinases with known activity against endothelial tight junctions were also preferentially expressed in pericontusional brain within the initial three days from injury. There was

some evidence for a correlation between MMP-9 expression and contusion expansion.

In a large cohort of over six hundred TBI patients managed with microdialysis, the associations between energy molecules and physiological parameters including ICP, CPP, PRx, and $PbtO_2$ were explored to better characterise their functional relationships. Non-linear associations between the principal measure of metabolic stress, namely LPR, and brain glucose, CPP, PRx, and oxygenation were identified. Glucose and PRx emerged as having the strongest association with LPR, suggesting that interventions to optimise these parameters may have the greatest likelihood of normalising deranged metabolism in the injured brain.

Put together, this work provides evidence for a localised pro-inflammatory response and metabolic derangement in peri-contusional brain, the severity of which is associated with subsequent magnitude of contusion and oedema progression.

9.1.1 Imaging of BBB permeability

Dynamic contrast enhance CT imaging was unable to show evidence of BBB permeability in contusional or pericontusional brain within five days from injury, despite observing clear evidence of contusion expansion and of local expression of mediators known to be associated with BBB breakdown, such as MMP-9. As discussed in the respective chapter, it is unclear whether this negative result implies that BBB permeability is not a feature of focal TBI in humans or if fundamentally the the DCE-CT technique or analysis is not sufficiently sensitive to detect it. Given the abundant evidence for BBB dysfunction in focal pre-clinical TBI models it is unlikely that this process is entirely absent in humans, although whether it is the primary mechanism of post traumatic brain oedema certainly is disputed [177]. On the other hand, given that DCE-CT has been shown to detect permeability related to stroke and other pathologies it is also unlikely that it should be unable to detect the same process in TBI [108].

Further studies with modified DCE-CT protocols (e.g. extended acquisition to improve sensitivity) are required, preferably incorporating multi-modality imaging with DCE-MRI or a radiotracer technique such as PET for comparison. Developing a reliable CT-based methodology for quantifying BBB permeability would not only be of great practical value in the management of TBI patients, but would be a useful surrogate end-point for early-phase interventional studies of therapeutic agents directed at reducing BBB permeability and brain oedema.

9.1.2 Measuring contusion progression

Commonly employed heuristic methods for quantifying the volume of intracerebral haematomas were shown to be progressively less accurate when the lesions being studied are increasingly irregular in shape. An alternative technique using unbiased stereology was found to have predictable accuracy and precision and was an efficient method for characterising the evolution of the haemorrhagic contusion and associated oedema on serial CT imaging. Consistent with clinical experience and evidence from pre-clinical studies, the most rapid phase of contusion expansion was in the initial 72h following injury, thereafter largely plateauing. Pericontusional tissue was shown to have more pronounced elevation of LPR and in turn higher LPR was shown to be associated with greater contusion expansion.

Although very simple, the stereological method is suitable for measuring volume of any type of object on cross-sectional imaging and can be adapted to estimate surface area. Although the systematic error associated with any grid spacing can be calculated precisely; further studies to assess inter-rater reliability for specific applications are required, particularly when lesion borders are ambiguous. For example, in the case of contusions that have matured over several days the the haemorrhagic core and surrounding oedema may become indistinct. However, this is similarly a difficulty that affects ABC/2 and associated methods, and more sophisticated automated and semi-automated segmentation algorithms. A reproducible technique for measuring volume of haemorrhage and oedema will also be an important surrogate measure of any proposed intervention to reduce contusion progression.

There has been much recent interest in the application of advanced machine learning algorithms based on deep convolution neural networks to medical imaging [150]. These techniques have been shown to be effective at both image labelling or categorisation, and segmentation of objects, including intracerebral haematomas and contusions [87, 5]. The main obstacles to employing this approach more widely are, firstly, the vast numbers (tens of thousands [5]) of labelled or segmented scans required for effective training. Secondly, the training process requires significant computational power and is often relatively slow therefore comparison and testing of alternative network architectures is time consuming. One application for an efficient manual segmentation technique such as stereology may be to generate the datasets required for training automated machine learning algorithms.

9.1.3 Pericontusional Inflammation and Signalling

Consistent with pre-clinical studies and human microdialysis investigations in diffuse TBI, the present study utilised targeted microdialysis and demonstrated localised increase in pro-inflammatory cytokines and chemokines (e.g. IL-8) and underexpression of anti-inflammtory mediators (e.g. IL-1ra and IL-10) in peri-contusional brain. In keeping with the finding of contusion expansion predominantly occurring during the 72h following injury, the pro-inflammatory 'signature' was most prominent during the same timeframe. The results implicate similar signalling cascades that are activated in patients with diffuse injury and hence that intervention with modulators such as recombinant IL1ra may have also have an effect in focal contusional TBI. However, although IL1ra no doubt does modify the cerebral inflammatory response, whether this is beneficial or ultimately deleterious to reparative processes is unclear.

This study found that there was significantly elevated localised expression of MMP-9 in peri-contusional brain, corroborating findings from in vitro and animal models which have heavily implicated this enzyme has having a prominent role in the proteolysis intercellular tight junctions and BBB permeability. As with the pro-inflammatory cytokines, MMP-9 concentrations were highest in the first hours of monitoring and thereafter declined. The canonical upstream regulator of MMP-9 expression and activation is VEGF and therefore this molecule had also been expected to have increased expression in pericontusional brain. However, the temporal profiles of VEGF in pericontusional and radiologically normal brain were similar during the initial 72h following injury and thereafter were lower in regions of injury. There is strong evidence for the role of VEGF in pre-clinical models [179] and it is possible that the practical limitations of monitoring in patients that prevented obtaining microdialysis samples prior to 24h from injury missed acute increases in VEGF (and other cytokines and chemokines) in pericontusional brain within hours of injury.

Nitric oxide has also been shown to be involved in the signalling cascade that leads to MMP-9 activation, and also has pleiotropic effects amongst numerous other pathways during normal physiology and following injury. Again using samples from targeted pericontusional microdialysis with paired control samples, in this study the combined concentration of NOx (NO_2 and NO_3 metabolites) was slightly higher in the non-injured brain and displayed very similar temporal profiles at both monitoring sites. There was a positive association between NOx at energy

molecules including glucose, pyruvate, and lactate within both injured and non-injured brain, but the increase in lactate, and consequently LPR, was more pronounced in pericontusional tissue. This finding suggests that while concentrations of NO may be similar at different sites its effects may be heterogenous.

9.1.4 Inter-relatonships between energy molecules

Glucose, puryvate, lactate, and the lactate/pyruvate ratio, are the primary parameters that are utilised for clinical microdialysis monitoring. Previous studies have highlighted that summary measures of glucose, lactate, and LPR all have relationships with outcome and are more deranged within perilesional tissue [172, 173]. However, there has been relatively little study of the raw hourly data to examine the temporal course of metabolic dysfunction and relationships between modifiable parameters, i.e. cerebral perfusion pressure, glucose, and oxygenation, to inform how these might be optimised to improve and normalise LPR and cerebral metabolism. In this study, LPR was shown to be most abnormal in the first 48-72h following injury, emphasising again that it is within this time period that the key events of secondary injury occur. Non-parametric regression with generalised additive mixed models, allowing for random effects between patients and accounting for the strong autocorrelation within patient time series, showed strongly non-linear associations between LPR and glucose, CPP, PRx, and $PbtO_2$. The importance of these results is that they immediately indicate thresholds for the respective parameters that could be targeted stepwise at the bedside to improve LPR. Moreover, brain glucose showed the strongest association with LPR suggesting that supplementing this substrate may be the first choice intervention in a patient with elevated LPR. The relationship between pyruvate and lactate within individual patients was found to be approximately linear, in accordance with expected kinetics of these molecules at equilibrium. However, the parameters of the linear relationship varied significantly between patients and with it the likelihood of LPR elevating above 25. Taking these results together suggests a classification of normal and disturbed metabolism into four states based on LPR < or >25 and brain glucose > or < 1mM and provides a conceptual framework to tailor interventions to correct metabolism specific to each circumstance.

9.2 General limitations

The studies described in this work have each been observational and extrapolation from correlative findings to mechanistic implications must be made with caution. However, the findings of pro-inflammatory cytokine and chemokine expression, and elevated MMP-9, in pericontusional brain are consistent with the body of in vitro, pre-clinical, and human in vivo studies, supporting the contention that these mediators are important in lesion progression and the development of brain swelling. Microdialysis is inherently a local monitor and there is a potential confounder of injury induced by insertion of the catheter into the brain. This study has addressed both these issues where possible by using two catheters to provide paired control data from pericontusional and radiologically normal brain. This approach was not associated with any complications for the enrolled patients but does present additional burdens in system maintenance and sample management that need to be considered. In the study of microdialysis data gathered from patients treated for TBI over twenty years there was inherently great heterogeneity in duration of monitoring, extent of missing microdialysis data, and availability of data from additional monitors (e.g. $PbtO_2$). To mitigate these challenges and draw out reliable findings the statistical analysis was designed to impute missing data where appropriate, to use the full statistical power of the hourly data whenever possible, and to take account of the specific characteristics of this type of physiological data, namely autocorrelation, together with random effects for individual patients.

9.3 Future Directions

9.3.1 Preventing Contusion Expansion and Oedema

Although the imaging technique employed in this work did not demonstrate BBB permeability associated with brain contusions, there was strong evidence indicating elevated expression of MMP-9 in pericontusional tissue. It remains possible that the VEGF-MMP-9 axis characterised in pre-clinical models is a major signalling pathway in human TBI. There are a number of existing pharmaceuticals that target this pathway that have been introduced for other pathologies. A monoclonal antibody directed at VEGF (Bevacizumab), primarily used for treatment of various cancers and macular degeneration, has been shown to rapidly reduce vasogenic oedema associated with intrinsic brain tumours such as glioblastoma in clinical trials [51, 90]. A pilot study of this agent in patients with contusional TBI, using contusion volume progression as the primary outcome, would be the logical next step.

Assuming MMP-9 is the common end effector of BBB disruption of multiple upstream activation pathways, an alternative option for interventional studies would be targeting MMP-9 directly. There are no specific inhibitors currently available but the antibiotic doxycycline does have some inhibitory activity against the enzyme and would be option for a preliminary mechanistic study [157]. A further option to develop more sensitive endpoints for these initial interventional studies would be developing suitable assays to quantify MMP-9 activity and the concentrations of tight junction proteins such as occludin and claudin in microdialysate.

9.3.2 Improving Cerebral Metabolism in TBI

Since the introduction of clinical microdialysis into the armamentarium of neuro-intensive care there has been much debate as to whether the metabolic parameters should form the basis of therapeutic targets, and if so which interventions should be used. The findings of the present study inform a hierarchical approach and natural targets to systematically try and correct LPR. The priorities in such a protocol would be ensuring adequate brain glucose by modifying systemic glycaemic control and potentially supplementation with intravenous boluses of glucose, aiming to maintain CPP within the individual's autoregulatory range (e.g. targeting optimal CPP [47]), and maintaining cerebral oxygenation. Designing a clinical study that can demonstrate efficacy of a care protocol comprising multiple interventions presents a number of challenges particularly when the magnitude of the marginal benefit of improving LPR on neurological outcome is uncertain. Identifying a good surrogate of clinical outcome, such as an imaging measure of neuronal loss, would be an alternative approach.

Bibliography

[1] H. Adams, J. Donnelly, M. Czosnyka, A. G. Kolias, A. Helmy, D. K. Menon, P. Smielewski, and P. J. Hutchinson. Temporal profile of intracranial pressure and cerebrovascular reactivity in severe traumatic brain injury and association with fatal outcome: An observational study. *PLoS Medicine*, 14(7): e1002353, July 2017.

[2] H. Alahmadi, S. Vachhrajani, and M. D. Cusimano. The natural history of brain contusion: An analysis of radiological and clinical progression. *Journal of Neurosurgery*, 112(5):1139–45, Aug. 2009.

[3] H. Alahmadi, S. Vachhrajani, and M. D. Cusimano. The natural history of brain contusion: an analysis of radiological and clinical progression. *Journal of Neurosurgery*, 112(5):1139–1145, May 2010.

[4] T. Aoki, T. Sumii, T. Mori, X. Wang, and E. H. Lo. Blood-brain barrier disruption and matrix metalloproteinase-9 expression during reperfusion injury: mechanical versus embolic focal ischemia in spontaneously hypertensive rats. *Stroke*, 33(11):2711–2717, Nov. 2002.

[5] M. R. Arbabshirani, B. K. Fornwalt, G. J. Mongelluzzo, J. D. Suever, B. D. Geise, A. A. Patel, and G. J. Moore. Advanced machine learning in action: identification of intracranial hemorrhage on computed tomography scans of the head with clinical workflow integration. *npj Digital Medicine*, 1(1):9, Apr. 2018.

[6] A. T. Argaw, Y. Zhang, B. J. Snyder, M. L. Zhao, N. Kopp, S. C. Lee, C. S. Raine, C. F. Brosnan, and G. R. John. IL-1 Regulates Blood-Brain Barrier Permeability via Reactivation of the Hypoxia-Angiogenesis Program. *The Journal of Immunology*, 177(8):5574–5584, Oct. 2006.

[7] A. T. Argaw, B. T. Gurfein, Y. Zhang, A. Zameer, and G. R. John. VEGF-mediated disruption of endothelial CLN-5 promotes blood-brain barrier breakdown. *Proceedings of the National Academy of Sciences*, 106(6):1977–1982, Feb. 2009.

[8] M. J. H. Aries, M. Czosnyka, K. P. Budohoski, L. A. Steiner, A. Lavinio, A. G. Kolias, P. J. Hutchinson, K. M. Brady, D. K. Menon, J. D. Pickard, and P. Smielewski. Continuous determination of optimal cerebral perfusion pressure in traumatic brain injury*. *Critical Care Medicine*, 40(8):2456–2463, Aug. 2012.

[9] C. Avolio, M. Ruggieri, F. Giuliani, G. M. Liuzzi, R. Leante, P. Riccio, P. Livrea, and M. Trojano. Serum MMP-2 and MMP-9 are elevated in different multiple sclerosis subtypes. *Journal of Neuroimmunology*, 136(1-2):46–53, Mar. 2003.

[10] V. Balasingam and V. W. Yong. Attenuation of astroglial reactivity by interleukin-10. *Journal of Neuroscience*, 16(9):2945–2955, May 1996.

[11] S. A. Baldwin, I. Fugaccia, D. R. Brown, L. V. Brown, and S. W. Scheff. Blood-brain barrier breach following cortical contusion in the rat. *Journal of Neurosurgery*, 85(3):476–481, Sept. 1996.

[12] P. Ballabh, A. Braun, and M. Nedergaard. The blood-brain barrier: an overview: structure, regulation, and clinical implications. *Neurobiology of Disease*, 16(1):1–13, June 2004.

[13] J. C. Baron. Perfusion thresholds in human cerebral ischemia: historical perspective and therapeutic implications. . *Cerebrovascular Diseases*, 11(1):2–8, Feb. 2001.

[14] P. Barzó, A. Marmarou, P. Fatouros, F. Corwin, and J. Dunbar. Magnetic resonance imaging—monitored acute blood-brain barrier changes in experimental traumatic brain injury. *Journal of Neurosurgery*, 85(6):1113–1121, Dec. 1996.

[15] P. Barzó, A. Marmarou, P. Fatouros, K. Hayasaki, and F. Corwin. Contribution of vasogenic and cellular edema to traumatic brain swelling measured by diffusion-weighted imaging. *Journal of Neurosurgery*, 87(6):900–907, Dec. 1997.

[16] A. T. Bauer, H. F. Bürgers, T. Rabie, and H. H. Marti. Matrix metalloproteinase-9 mediates hypoxia-induced vascular leakage in the brain via tight junction rearrangement. *Journal of Cerebral Blood Flow and Metabolism*, 30(4):837–848, Apr. 2010.

[17] A. Beaumont, A. Marmarou, K. Hayasaki, P. Barzo, P. Fatouros, F. Corwin, C. Marmarou, and J. Dunbar. The Permissive Nature of Blood Brain Barrier (BBB) Opening in Edema Formation Following Traumatic Brain Injury. In *Brain Edema XI*, pages 125–129. Springer Vienna, Vienna, 2000.

[18] A. Beaumont, P. Fatouros, T. Gennarelli, F. Corwin, and A. Marmarou. Bolus tracer delivery measured by MRI confirms edema without blood-brain barrier permeability in diffuse traumatic brain injury. *Acta Neurochirurgica Supplement*, 96:171–174, 2006.

[19] M. Bélanger, I. Allaman, and P. J. Magistretti. Brain Energy Metabolism: Focus on Astrocyte-Neuron Metabolic Cooperation. *Cell Metabolism*, 14(6):724–738, Dec. 2011.

[20] C. Bendinelli, A. Bivard, S. Nebauer, M. W. Parsons, and Z. J. Balogh. Brain CT perfusion provides additional useful information in severe traumatic brain injury. *Injury*, 44(9):1208–1212, Sept. 2013.

[21] M. Bergsneider, D. A. Hovda, E. Shalmon, D. F. Kelly, P. M. Vespa, N. A. Martin, M. E. Phelps, D. L. McArthur, M. J. Caron, J. F. Kraus, and D. P. Mecker. Cerebral hyperglycolysis following severe traumatic brain injury in humans: a positron emission tomography study. *Journal of Neurosurgery*, 86(2): 241–251, Feb. 1997.

[22] A. M. Blamire, D. C. Anthony, B. Rajagopalan, N. R. Sibson, V. H. Perry, and P. Styles. Interleukin-1beta -induced changes in blood-brain barrier permeability, apparent diffusion coefficient, and cerebral blood volume in the rat brain: a magnetic resonance study. *Journal of Neuroscience*, 20(21):8153–8159, Nov. 2000.

[23] J. P. Broderick, T. G. Brott, J. E. Duldner, T. Tomsick, and G. Huster. Volume of intracerebral hemorrhage. A powerful and easy-to-use predictor of 30-day mortality. *Stroke*, 24(7):987–993, July 1993.

[24] K. L. H. Carpenter, I. Timofeev, P. G. Al-Rawi, D. K. Menon, J. D. Pickard, and P. J. Hutchinson. Nitric oxide in acute brain injury: a pilot study of NO<Subscript><Emphasis Type="Italic">x</Emphasis></Subscript> concentrations in human brain microdialysates and their relationship with energy metabolism. In *Acta Neurochirurgica Supplement*, pages 207–213. Springer, Vienna, Vienna, 2008.

[25] K. L. H. Carpenter, I. Jalloh, C. N. Gallagher, P. Grice, D. J. Howe, A. Mason, I. Timofeev, A. Helmy, M. P. Murphy, D. K. Menon, P. J. Kirkpatrick, T. A. Carpenter, G. R. Sutherland, J. D. Pickard, and P. J. Hutchinson. 13C-labelled microdialysis studies of cerebral metabolism in TBI patients. *European Journal of Pharmaceutical Sciences*, 57:87–97, June 2014.

[26] K. L. H. Carpenter, I. Jalloh, and P. J. Hutchinson. Glycolysis and the significance of lactate in traumatic brain injury. *Frontiers in Neuroscience*, 9, Apr. 2015.

[27] K. L. H. Carpenter, A. M. Young, and P. J. Hutchinson. Advanced monitoring in traumatic brain injury: microdialysis. *Current Opinion in Critical Care*, 23(2):103–109, Apr. 2017.

[28] Y. Chassidim, R. Veksler, S. Lublinsky, G. S. Pell, A. Friedman, and I. Shelef. Quantitative imaging assessment of blood-brain barrier permeability in humans. *Fluids and Barriers of the CNS*, 10(1):9, Dec. 2013.

[29] F. Chen, N. Ohashi, W. Li, C. Eckman, and J. H. Nguyen. Disruptions of occludin and claudin-5 in brain endothelial cells in vitro and in brains of mice with acute liver failure. *Hepatology*, 50(6):1914–1923, Aug. 2009.

[30] H. Chen, N. Liu, Y. Li, F. Chen, and G. Zhu. Permeability imaging in cerebrovascular diseases: applications and progress in research. *Neurovascular Imaging*, 2(1):1, Dec. 2016.

[31] J. Chen, F. Braet, S. Brodsky, T. Weinstein, V. Romanov, E. Noiri, and M. S. Goligorsky. VEGF-induced mobilization of caveolae and increase in permeability of endothelial cells. *American Journal of Physiology: Cell Physiology*, 282(5):C1053–63, May 2002.

[32] X. Chen, X. S. Duan, L. J. Xu, J. J. Zhao, Z. F. She, W. W. Chen, Z. J. Zheng, and G. D. Jiang. Interleukin-10 mediates the neuroprotection of hyperbaric oxygen therapy against traumatic brain injury in mice. *Neuroscience*, 266:235–243, Apr. 2014.

[33] L. Cherian, J. C. Goodman, and C. S. Robertson. Effect of Glucose Administration on Contusion Volume After Moderate Cortical Impact Injury in Rats. *Journal of Neurotrauma*, 15(12):1059–1066, Dec. 1998.

[34] L. Cherian, R. Hlatky, and C. S. Robertson. Nitric oxide in traumatic brain injury. *Brain Pathology*, 14 (2):195–201, Apr. 2004.

[35] R. M. Chesnut, L. F. Marshall, M. R. Klauber, B. A. Blunt, N. Baldwin, H. M. Eisenberg, J. A. Jane, A. Marmarou, and M. A. Foulkes. The role of secondary brain injury in determining outcome from severe head injury. *The Journal of Trauma: Injury, Infection, and Critical Care*, 34(2):216–222, Feb. 1993.

[36] A. Chodobski, I. Chung, E. Koźniewska, T. Ivanenko, W. Chang, J. F. Harrington, J. A. Duncan, and J. Szmydynger-Chodobska. Early neutrophilic expression of vascular endothelial growth factor after traumatic brain injury. *Neuroscience*, 122(4):853–867, 2003.

[37] A. Chodobski, B. J. Zink, and J. Szmydynger-Chodobska. Blood–Brain Barrier Pathophysiology in Traumatic Brain Injury. *Translational Stroke Research*, 2(4):492–516, Nov. 2011.

[38] C. S. Cobbs, J. Chen, D. A. Greenberg, and S. H. Graham. Vascular endothelial growth factor expression in transient focal cerebral ischemia in the rat. *Neuroscience Letters*, 249(2-3):79–82, June 1998.

[39] A. Cornish-Bowden. *Fundamentals of enzyme kinetics. 4th ed.* Wiley-Blackwell, 2012.

[40] M. Czosnyka, Z. Czosnyka, and P. Smielewski. Pressure reactivity index: journey through the past 20 years. *Acta Neurochirurgica*, 159(11):2063–2065, Aug. 2017.

[41] J. W. Dankbaar, J. Hom, T. Schneider, S. C. Cheng, B. C. Lau, I. van der Schaaf, S. Virmani, S. Pohlman, W. P. Dillon, and M. Wintermark. Dynamic Perfusion CT Assessment of the Blood-Brain Barrier Permeability: First Pass versus Delayed Acquisition. *American Journal of Neuroradiology*, 29(9):1671–1676, Oct. 2008.

[42] H. E. de Vries, M. C. Blom-Roosemalen, M. van Oosten, A. G. de Boer, T. J. van Berkel, D. D. Breimer, and J. Kuiper. The influence of cytokines on the integrity of the blood-brain barrier in vitro. *Journal of Neuroimmunology*, 64(1):37–43, Jan. 1996.

[43] G. A. Dienel. Lactate shuttling and lactate use as fuel after traumatic brain injury: metabolic considerations. *Journal of Cerebral Blood Flow & Metabolism*, 34(11):1736–1748, Nov. 2014.

[44] A. A. Divani, S. Majidi, X. Luo, F. G. Souslian, J. Zhang, A. Abosch, and R. P. Tummala. The ABCs of Accurate Volumetric Measurement of Cerebral Hematoma. *Stroke*, 42(6):1569–1574, June 2011.

[45] D. N. Doll, H. Hu, J. Sun, S. E. Lewis, J. W. Simpkins, and X. Ren. Mitochondrial Crisis in Cerebrovascular Endothelial Cells Opens the Blood–Brain Barrier. *Stroke*, 46(6):1681–1689, June 2015.

[46] J. J. Donkin and R. Vink. Mechanisms of cerebral edema in traumatic brain injury: therapeutic developments. *Current Opinion in Neurology*, 23(3):293–299, 2010.

[47] J. Donnelly, M. Czosnyka, H. Adams, C. Robba, L. A. Steiner, D. Cardim, B. Cabella, X. Liu, A. Ercole, P. J. Hutchinson, D. K. Menon, M. J. H. Aries, and P. Smielewski. Individualizing Thresholds of Cerebral Perfusion Pressure Using Estimated Limits of Autoregulation. *Critical Care Medicine*, 45(9): 1464–1471, Sept. 2017.

[48] N. Eriksen, E. Rostrup, K. Andersen, M. J. Lauritzen, M. Fabricius, V. A. Larsen, J. P. Dreier, A. J. Strong, J. A. Hartings, and B. Pakkenberg. Application of stereological estimates in patients with severe head injuries using CT and MR scanning images. *The British Journal of Radiology*, 83(988):307–317, Apr. 2010.

[49] M. Fasiolo, Y. Goude, R. Nedellec, and S. N. Wood. Fast calibrated additive quantile regression. *arXiv*, July 2017.

[50] N. Ferrara. Vascular Endothelial Growth Factor: Basic Science and Clinical Progress. *Endocrine Reviews*, 25(4):581–611, Aug. 2004.

[51] N. Ferrara, K. J. Hillan, H.-P. Gerber, and W. Novotny. Discovery and development of bevacizumab, an anti-VEGF antibody for treating cancer. *Nature Reviews Drug Discovery*, 3(5):391–400, May 2004.

[52] S. Fischer, M. Clauss, M. Wiesnet, D. Renz, W. Schaper, and G. F. Karliczek. Hypoxia induces permeability in brain microvessel endothelial cells via VEGF and NO. *American Journal of Physiology: Cell Physiology*, 276(4):C812–C820, Apr. 1999.

[53] L. E. Folkerson, D. Sloan, B. A. Cotton, J. B. Holcomb, J. S. Tomasek, and C. E. Wade. Predicting progressive hemorrhagic injury from isolated traumatic brain injury and coagulation. *Surgery*, 158(3): 655–661, Sept. 2015.

[54] M. E. Fuentes, S. K. Durham, M. R. Swerdel, A. C. Lewin, D. S. Barton, J. R. Megill, R. Bravo, and S. A. Lira. Controlled recruitment of monocytes and macrophages to specific organs through transgenic expression of monocyte chemoattractant protein-1. *The Journal of Immunology*, 155(12):5769–5776, Dec. 1995.

[55] B. J. Gabbe, R. A. Lyons, F. E. Lecky, O. Bouamra, M. Woodford, T. J. Coats, and P. A. Cameron. Comparison of Mortality Following Hospitalisation for Isolated Head Injury in England and Wales, and Victoria, Australia. *PLoS One*, 6(5):e20545, May 2011.

[56] J. M. Garcia, S. A. Stillings, J. L. Leclerc, H. Phillips, N. J. Edwards, S. A. Robicsek, B. L. Hoh, S. Blackburn, and S. Doré. Role of Interleukin-10 in Acute Brain Injuries. *Frontiers in Neurology*, 8:e28, June 2017.

[57] P. S. Garry, M. Ezra, M. J. Rowland, J. Westbrook, and K. T. S. Pattinson. The role of the nitric oxide pathway in brain injury and its treatment — From bench to bedside. *Experimental Neurology*, 263: 235–243, Jan. 2015.

[58] A. P. Georgiou and A. R. Manara. Role of therapeutic hypothermia in improving outcome after traumatic brain injury: a systematic review. . *British Journal of Anaesthesia*, 110(3):357–367, Mar. 2013.

[59] J. M. Gidday, Y. G. Gasche, J.-C. Copin, A. R. Shah, R. S. Perez, S. D. Shapiro, P. H. Chan, and T. S. Park. Leukocyte-derived matrix metalloproteinase-9 mediates blood-brain barrier breakdown and is proinflammatory after transient focal cerebral ischemia. *American Journal of Physiology: Heart and Circulatory Physiology*, 289(2):H558–H568, Aug. 2005.

[60] M. Grossetete, J. Phelps, L. Arko, H. Yonas, and G. A. Rosenberg. Elevation of MMP-3 and MMP-9 in CSF and Blood in Patients with Severe Traumatic Brain Injury. *Neurosurgery*, 65(4):702–708, Oct. 2009.

[61] R. Gruetter, K. Ugurbil, and E. R. Seaquist. Steady-state cerebral glucose concentrations and transport in the human brain. *Journal of Neurochemistry*, 70(1):397–408, Jan. 1998.

[62] M. Guilfoyle, I. Timofeev, and P. Hutchinson. Microdialysis. In *Gupta and Gelb's Essentials of Neuroanesthesia and Neurointensive Care*, pages 342–348. Cambridge University Press, June 2018.

[63] M. D. Habgood, N. Bye, K. M. Dziegielewska, C. J. Ek, M. A. Lane, A. Potter, C. Morganti-Kossmann, and N. R. Saunders. Changes in blood-brain barrier permeability to large and small molecules following traumatic brain injury in mice. . *European Journal of Neuroscience*, 25(1):231–238, Jan. 2007.

[64] O. Hadass, B. N. Tomlinson, M. Gooyit, S. Chen, J. J. Purdy, J. M. Walker, C. Zhang, A. B. Giritharan, W. Purnell, C. R. Robinson, D. Shin, V. A. Schroeder, M. A. Suckow, A. Simonyi, G. Y Sun, S. Mobashery, J. Cui, M. Chang, and Z. Gu. Selective Inhibition of Matrix Metalloproteinase-9 Attenuates Secondary Damage Resulting from Severe Traumatic Brain Injury. *PLoS One*, 8(10):e76904, Oct. 2013.

[65] G. Haraldsen, D. Kvale, B. Lien, I. N. Farstad, and P. Brandtzaeg. Cytokine-regulated expression of E-selectin, intercellular adhesion molecule-1 (ICAM-1), and vascular cell adhesion molecule-1 (VCAM-1) in human microvascular endothelial cells. *The Journal of Immunology*, 156(7):2558–2565, Apr. 1996.

[66] S. J. Harper and D. O. Bates. VEGF-A splicing: the key to anti-angiogenic therapeutics? *Nature Reviews Cancer*, 8(11):880–887, Oct. 2008.

[67] B. T. Hawkins. The Blood-Brain Barrier/Neurovascular Unit in Health and Disease. *Pharmacological Reviews*, 57(2):173–185, June 2005.

[68] A. Helmy, K. L. H. Carpenter, J. N. Skepper, P. J. Kirkpatrick, J. D. Pickard, and P. J. Hutchinson. Microdialysis of cytokines: methodological considerations, scanning electron microscopy, and determination of relative recovery. *Journal of Neurotrauma*, 26(4):549–561, Apr. 2009.

[69] A. Helmy, K. L. H. Carpenter, D. K. Menon, J. D. Pickard, and P. J. A. Hutchinson. The cytokine response to human traumatic brain injury: temporal profiles and evidence for cerebral parenchymal production. *Journal of Cerebral Blood Flow and Metabolism*, 31(2):658–670, Aug. 2010.

[70] A. Helmy, M.-G. De Simoni, M. R. Guilfoyle, K. L. H. Carpenter, and P. J. Hutchinson. Cytokines and innate inflammation in the pathogenesis of human traumatic brain injury. *Progress in Neurobiology*, 95 (3):352–372, Nov. 2011.

[71] A. Helmy, C. A. Antoniades, M. R. Guilfoyle, K. L. H. Carpenter, and P. J. Hutchinson. Principal component analysis of the cytokine and chemokine response to human traumatic brain injury. *PLoS One*, 7(6):e39677, 2012.

[72] A. Helmy, M. R. Guilfoyle, K. L. Carpenter, J. D. Pickard, D. K. Menon, and P. J. Hutchinson. Recombinant human interleukin-1 receptor antagonist promotes M1 microglia biased cytokines and chemokines following human traumatic brain injury. *Journal of Cerebral Blood Flow and Metabolism*, page 0271678X15620204, Dec. 2015.

[73] A. K. Heye, R. D. Culling, M. d. C. Valdés Hernández, M. J. Thrippleton, and J. M. Wardlaw. Assessment of blood–brain barrier disruption using dynamic contrast-enhanced MRI. A systematic review. *NeuroImage: Clinical*, 6:262–274, Jan. 2014.

[74] T. Hirose, N. Matsumoto, O. Tasaki, H. Nakamura, F. Akagaki, and T. Shimazu. Delayed Progression of Edema Formation Around a Hematoma Expressing High Levels of VEGF and MMP-9 in a Patient With Traumatic Brain Injury: Case Report. *Neurologia Medico-Chirurgica*, 53(9):609–612, Sept. 2013.

[75] L. Ho, W. Zhao, K. Dams-O'Connor, C. Y. Tang, W. Gordon, E. R. Peskind, S. Yemul, V. Haroutunian, and G. M. Pasinetti. Elevated Plasma MCP-1 Concentration Following Traumatic Brain Injury as a Potential "Predisposition" Factor Associated with an Increased Risk for Subsequent Development of Alzheimer's Disease. *Journal of Alzheimer's Disease*, 31(2):301–313, 2012.

[76] J. Hom, J. W. Dankbaar, B. P. Soares, T. Schneider, S. C. Cheng, J. Bredno, B. C. Lau, W. Smith, W. P. Dillon, and M. Wintermark. Blood-brain barrier permeability assessed by perfusion CT predicts symptomatic hemorrhagic transformation and malignant edema in acute ischemic stroke. *American Journal of Neuroradiology*, 32(1):41–48, Jan. 2011.

[77] A. P.-H. Huang, C.-W. Lee, H.-J. Hsieh, C.-C. Yang, Y.-H. Tsai, F.-Y. Tsuang, L.-T. Kuo, Y.-S. Chen, Y.-K. Tu, S.-J. Huang, H.-M. Liu, and J.-C. Tsai. Early Parenchymal Contrast Extravasation Predicts Subsequent Hemorrhage Progression, Clinical Deterioration, and Need for Surgery in Patients With Traumatic Cerebral Contusion. *The Journal of Trauma: Injury, Infection, and Critical Care*, 71(6):1593–1599, Dec. 2011.

[78] P. J. Hutchinson, M. T. O'Connell, N. J. Rothwell, S. J. Hopkins, J. Nortje, K. L. H. Carpenter, I. Timofeev, P. G. Al-Rawi, D. K. Menon, and J. D. Pickard. Inflammation in Human Brain Injury: Intracerebral

Concentrations of IL-1 α, IL-1 β, and Their Endogenous Inhibitor IL-1ra. *Journal of Neurotrauma*, 24 (10):1545–1557, Oct. 2007.

[79] P. J. Hutchinson, I. Jalloh, A. Helmy, K. L. H. Carpenter, E. Rostami, B.-M. Bellander, M. G. Boutelle, J. W. Chen, J. Claassen, C. Dahyot-Fizelier, P. Enblad, C. N. Gallagher, R. Helbok, L. Hillered, P. D. Le Roux, S. Magnoni, H. S. Mangat, D. K. Menon, C.-H. Nordström, K. H. O'Phelan, M. Oddo, J. P. Barcena, C. Robertson, E. Ronne-Engström, J. Sahuquillo, M. Smith, N. Stocchetti, A. Belli, T. A. Carpenter, J. P. Coles, M. Czosnyka, N. Dizdar, J. C. Goodman, A. K. Gupta, T. H. Nielsen, N. Marklund, A. Montcriol, M. T. O'Connell, M. A. Poca, A. Sarrafzadeh, R. J. Shannon, J. Skjøth-Rasmussen, P. Smielewski, J. F. Stover, I. Timofeev, P. Vespa, E. Zavala, and U. Ungerstedt. Consensus statement from the 2014 International Microdialysis Forum. *Intensive Care Medicine*, 41(9):1517–1528, July 2015.

[80] H. B. Huttner, T. Steiner, M. Hartmann, M. Kohrmann, E. Juettler, S. Mueller, J. Wikner, U. Meyding-Lamade, P. Schramm, S. Schwab, and P. D. Schellinger. Comparison of ABC/2 estimation technique to computer-assisted planimetric analysis in warfarin-related intracerebral parenchymal hemorrhage. . *Stroke*, 37(2):404–408, Jan. 2006.

[81] C. Iaccarino, P. Schiavi, E. Picetti, M. Goldoni, D. Cerasti, M. Caspani, and F. Servadei. Patients with brain contusions: predictors of outcome and relationship between radiological and clinical evolution. *Journal of Neurosurgery*, 120(4):908–918, Apr. 2014.

[82] J. Ito, A. Marmarou, P. Barzó, P. Fatouros, and F. Corwin. Characterization of edema by diffusion-weighted imaging in experimental traumatic brain injury. *Journal of Neurosurgery*, 84(1):97–103, Jan. 1996.

[83] I. Jalloh, K. L. H. Carpenter, A. Helmy, T. A. Carpenter, D. K. Menon, and P. J. Hutchinson. Glucose metabolism following human traumatic brain injury: methods of assessment and pathophysiological findings. *Metabolic Brain Disease*, 30(3):615–632, Nov. 2014.

[84] X. Jiang, S. Namura, and I. Nagata. Matrix metalloproteinase inhibitor KB-R7785 attenuates brain damage resulting from permanent focal cerebral ischemia in mice. *Neuroscience Letters*, 305(1):41–44, June 2001.

[85] B. N. Joe, J. Suh, C. F. Hildebolt, D. M. Hovsepian, B. Johnston, and K. T. Bae. MR Volumetric Measurements of the Myomatous Uterus. *Academic Radiology*, 14(4):455–462, Apr. 2007.

[86] K. H. Jung, K. Chu, S. Y. Ko, S. T. Lee, D. I. Sinn, D. K. Park, J. M. Kim, E. C. Song, M. Kim, and J. K. Roh. Early intravenous infusion of sodium nitrite protects brain against in vivo ischemia-reperfusion injury. . *Stroke*, 37(11):2744–2750, Oct. 2006.

[87] K. Kamnitsas, C. Ledig, V. F. J. Newcombe, J. P. Simpson, A. D. Kane, D. K. Menon, D. Rueckert, and B. Glocker. Efficient multi-scale 3D CNN with fully connected CRF for accurate brain lesion segmentation. *Medical Image Analysis*, 36:61–78, Feb. 2017.

[88] T. Kasahara, N. Mukaida, K. Yamashita, H. Yagisawa, T. Akahoshi, and K. Matsushima. IL-1 and TNF-alpha induction of IL-8 and monocyte chemotactic and activating factor (MCAF) mRNA expression in a human astrocytoma cell line. *Immunology*, 74(1):60–67, Sept. 1991.

[89] T. Kawamata, T. Mori, S. Sato, and Y. Katayama. Tissue hyperosmolality and brain edema in cerebral contusion. *Neurosurgical Focus*, 22(5):E5, 2007.

[90] G. M. Keating. Bevacizumab: a review of its use in advanced cancer. . *Drugs*, 74(16):1891–1925, Oct. 2014.

[91] K. Kinoshita. Traumatic brain injury: pathophysiology for neurocritical care. *Journal of Intensive Care*, 4(1):1028, Apr. 2016.

[92] A. A. Konstas, G. V. Goldmakher, T. Y. Lee, and M. H. Lev. Theoretic Basis and Technical Implementations of CT Perfusion in Acute Ischemic Stroke, Part 1: Theoretic Basis. *American Journal of Neuroradiology*, 30(4):662–668, Apr. 2009.

[93] T. Kossmann, P. F. Stahel, P. M. Lenzlinger, H. Redl, R. W. Dubs, O. Trentz, G. Schlag, and M. C. Morganti-Kossmann. Interleukin-8 Released into the Cerebrospinal Fluid after Brain Injury is Associated with Blood–Brain Barrier Dysfunction and Nerve Growth Factor Production. *Journal of Cerebral Blood Flow and Metabolism*, 17(3):280–289, Aug. 2016.

[94] R. U. Kothari, T. Brott, J. P. Broderick, W. G. Barsan, L. R. Sauerbeck, M. Zuccarello, and J. Khoury. The ABCs of measuring intracerebral hemorrhage volumes. *Stroke*, 27(8):1304–1305, Aug. 1996.

[95] Z. Kovács, K. Ikezaki, K. Samoto, T. Inamura, and M. Fukui. VEGF and flt. Expression time kinetics in rat brain infarct. *Stroke*, 27(10):1865–72– discussion 1872–3, Oct. 1996.

[96] D. Kurland, C. Hong, B. Aarabi, V. Gerzanich, and J. M. Simard. Hemorrhagic Progression of a Contusion after Traumatic Brain Injury: A Review. *Journal of Neurotrauma*, 29(1):19–31, Jan. 2012.

[97] H. Kushi, Y. Katayama, T. Shibuya, T. Tsubokawa, and T. Kuroha. Gadolinium DTPA-enhanced magnetic resonance imaging of cerebral contusions. *Acta Neurochirurgica Supplement*, 60:472–474, 1994.

[98] H. Kushi, T. Saito, K. Makino, and N. Hayashi. L-8 is a key mediator of neuroinflammation in severe traumatic brain injuries. In *Brain Edema XII*, pages 347–350. Springer, Vienna, Vienna, 2003.

[99] A. M. Lam, H. R. Winn, B. F. Cullen, and N. Sundling. Hyperglycemia and neurological outcome in patients with head injury. *Journal of Neurosurgery*, 75(4):545–551, Oct. 1991.

[100] D. A. Lang, D. M. Hadley, G. M. Teasdale, P. Macpherson, and E. Teasdale. Gadolinium DTPA enhanced magnetic resonance imaging in acute head injury. *Acta Neurochirurgica*, 109(1-2):5–11, 1991.

[101] D. B. Larach, W. A. Kofke, and P. Le Roux. Potential non-hypoxic/ischemic causes of increased cerebral interstitial fluid lactate/pyruvate ratio: a review of available literature. *Neurocritical Care*, 15(3):609–622, Feb. 2011.

[102] S. Lavi. Role of Nitric Oxide in the Regulation of Cerebral Blood Flow in Humans: Chemoregulation Versus Mechanoregulation. *Circulation*, 107(14):1901–1905, Mar. 2003.

[103] J. E. Lee, Y. J. Yoon, M. E. Moseley, and M. A. Yenari. Reduction in levels of matrix metalloproteinases and increased expression of tissue inhibitor of metalloproteinase—2 in response to mild hypothermia therapy in experimental stroke. *Journal of Neurosurgery*, 103(2):289–297, Aug. 2005.

[104] Q. Li, Q. Zhang, M. Wang, S. Zhao, J. Ma, N. Luo, N. Li, Y. Li, G. Xu, and J. Li. Interferon-γ and tumor necrosis factor-α disrupt epithelial barrier function by altering lipid composition in membrane microdomains of tight junction. *Clinical Immunology*, 126(1):67–80, Jan. 2008.

[105] W. Li, J. A. Long, L. T. Watts, Z. Jiang, Q. Shen, Y. Li, and T. Q. Duong. A Quantitative MRI Method for Imaging Blood-Brain Barrier Leakage in Experimental Traumatic Brain Injury. *PLoS One*, 9(12): e114173, Dec. 2014.

[106] S. Liebner, R. M. Dijkhuizen, Y. Reiss, K. H. Plate, D. Agalliu, and G. Constantin. Functional morphology of the blood–brain barrier in health and disease. *Acta Neuropathologica*, 135(3):311–336, Feb. 2018.

[107] J. H. N. Lindeman, H. Abdul-Hussien, J. H. van Bockel, R. Wolterbeek, and R. Kleemann. Clinical Trial of Doxycycline for Matrix Metalloproteinase-9 Inhibition in Patients With an Abdominal Aneurysm. *Circulation*, 119(16):2209–2216, Apr. 2009.

[108] N. Liu, H. Chen, B. Wu, Y. Li, M. Wintermark, A. Jackson, J. Hu, Y. Zhang, Z. Su, G. Zhu, and W. Zhang. CT Permeability Imaging Predicts Clinical Outcomes in Acute Ischemic Stroke Patients Treated with Intra-arterial Thrombolytic Therapy. *Molecular Neurobiology*, 54(4):2539–2546, Mar. 2016.

[109] G. Lotocki, J. P. de Rivero Vaccari, E. R. Perez, J. Sanchez-Molano, O. Furones-Alonso, H. M. Bramlett, and W. D. Dietrich. Alterations in Blood-Brain Barrier Permeability to Large and Small Molecules and Leukocyte Accumulation after Traumatic Brain Injury: Effects of Post-Traumatic Hypothermia . *Journal of Neurotrauma*, 26(7):1123 –1134, July 2009.

[110] J. Mankertz, S. Tavalali, H. Schmitz, A. Mankertz, E. O. Riecken, M. Fromm, and J. D. Schulzke. Expression from the human occludin promoter is affected by tumor necrosis factor alpha and interferon gamma. *Journal of cell science*, 113 (Pt 11):2085–2090, June 2000.

[111] H. S. Markus. Cerebral perfusion and stroke. *J Neurology Neurosurgery and Psychiatry*, 75(3):353–361, Mar. 2004.

[112] A. Marmarou, S. Signoretti, G. Aygok, P. Fatouros, and G. Portella. Traumatic brain edema in diffuse and focal injury: cellular or vasogenic? *Acta Neurochirurgica. Supplement*, 96:24–29, 2006.

[113] A. Marmarou, S. Signoretti, P. P. Fatouros, G. Portella, G. A. Aygok, and M. R. Bullock. Predominance of cellular edema in traumatic brain swelling in patients with severe head injuries. *Journal of Neurosurgery*, 104(5):720–730, May 2006.

[114] M. Mazonakis, S. Karampekios, J. Damilakis, A. Voloudaki, and N. Gourtsoyiannis. Stereological estimation of total intracranial volume on CT images. *European Radiology*, 14(7):1285–1290, July 2004.

[115] P. Mellergård MD, PHD, F. Sjögren PHD, and J. Hillman. Release of VEGF and FGF in the extracellular space following severe subarachnoidal haemorrhage or traumatic head injury in humans. *British Journal of Neurosurgery*, 24(3):276–282, May 2010.

[116] Z. Metting, L. A. RÃ diger, R. E. Stewart, M. Oudkerk, J. De Keyser, and J. van der Naalt. Perfusion computed tomography in the acute phase of mild head injury: Regional dysfunction and prognostic value. *Annals of Neurology*, 66(6):809–816, Dec. 2009.

[117] S. Michinaga and Y. Koyama. Pathogenesis of Brain Edema and Investigation into Anti-Edema Drugs. *International Journal of Molecular Sciences*, 16(12):9949–9975, Dec. 2015.

[118] N. Moro, S. Ghavim, N. G. Harris, D. A. Hovda, and R. L. Sutton. Glucose administration after traumatic brain injury improves cerebral metabolism and reduces secondary neuronal injury. *Brain Research*, 1535:124–136, Oct. 2013.

[119] P. Mouton. *Unbiased Stereology: A Concise Guide*. Johns Hopkins University Press, Baltimore, 2011.

[120] S. Nag, J. L. Takahashi, and D. W. Kilty. Role of vascular endothelial growth factor in blood-brain barrier breakdown and angiogenesis in brain trauma. *Journal of Neuropathology and Experimental Neurology*, 56(8):912–921, Aug. 1997.

[121] H. Nagase, R. Visse, and G. Murphy. Structure and function of matrix metalloproteinases and TIMPs. *Cardiovascular Research*, 69(3):562–573, Feb. 2006.

[122] R. K. Narayan, A. I. R. Maas, F. Servadei, B. E. Skolnick, M. N. Tillinger, L. F. Marshall, and Traumatic Intracerebral Hemorrhage Study Group. Progression of traumatic intracerebral hemorrhage: a prospective observational study. *Journal of Neurotrauma*, 25(6):629–639, June 2008.

[123] D. W. Nelson, B. Thornquist, R. M. MacCallum, H. Nyström, A. Holst, A. Rudehill, M. Wanecek, B.-M. Bellander, and E. Weitzberg. Analyses of cerebral microdialysis in patients with traumatic brain injury: relations to intracranial pressure, cerebral perfusion pressure and catheter placement. *BMC Medicine*, 9(1):21, Dec. 2011.

[124] A. Neves, R. Costalat, and L. Pellerin. Determinants of Brain Cell Metabolic Phenotypes and Energy Substrate Utilization Unraveled with a Modeling Approach. *PLoS Computational Biology*, 8(9):e1002686, Sept. 2012.

[125] M. Oddo, J. M. Schmidt, E. Carrera, N. Badjatia, E. S. Connolly, M. Presciutti, N. D. Ostapkovich, J. M. Levine, P. Le Roux, and S. A. Mayer. Impact of tight glycemic control on cerebral glucose metabolism after severe brain injury: a microdialysis study. *Critical Care Medicine*, 36(12):3233–3238, Dec. 2008.

[126] M. Oertel, D. F. Kelly, D. McArthur, W. J. Boscardin, T. C. Glenn, J. H. Lee, T. Gravori, D. Obukhov, D. Q. McBride, and N. A. Martin. Progressive hemorrhage after head trauma: predictors and consequences of the evolving injury. *Journal of Neurosurgery*, 96(1):109–116, Jan. 2002.

[127] T. J. Papadimos. The beneficial effects of inhaled nitric oxide in patients with severe traumatic brain injury complicated by acute respiratory distress syndrome: a hypothesis. *Journal of Trauma Management and Outcomes*, 2(1):1, Jan. 2008.

[128] E. Papavassiliou, N. Gogate, M. Proescholdt, J. D. Heiss, S. Walbridge, N. A. Edwards, E. H. Oldfield, and M. J. Merrill. Vascular endothelial growth factor (vascular permeability factor) expression in injured rat brain. *Journal of Neuroscience Research*, 49(4):451–460, Aug. 1997.

[129] C. S. Patlak, R. G. Blasberg, and J. D. Fenstermacher. Graphical Evaluation of Blood-to-Brain Transfer Constants from Multiple-Time Uptake Data. *Journal of Cerebral Blood Flow and Metabolism*, 3(1):1–7, June 2016.

[130] L. Pellerin and P. J. Magistretti. Sweet Sixteen for ANLS. *Journal of Cerebral Blood Flow and Metabolism*, 32(7):1152–1166, May 2012.

[131] I. Pineau and S. Lacroix. Endogenous signals initiating inflammation in the injured nervous system. *Glia*, 57(4):351–361, Mar. 2009.

[132] M. P. Plummer, N. Notkina, I. Timofeev, P. J. Hutchinson, M. E. Finnis, and A. K. Gupta. Cerebral metabolic effects of strict versus conventional glycaemic targets following severe traumatic brain injury. *Critical Care*, 22(1):47, 2018.

[133] P. M. Preshaw, A. F. Hefti, S. Jepsen, D. Etienne, C. Walker, and M. H. Bradshaw. Subantimicrobial dose doxycycline as adjunctive treatment for periodontitis. *Journal of Clinical Periodontology*, 31(9):697–707, Sept. 2004.

[134] J. Puig, G. Blasco, P. Daunis-i Estadella, C. van Eendendburg, M. Carrillo-García, C. Aboud, M. Hernández-Pérez, J. Serena, C. Biarnés, K. Nael, D. S. Liebeskind, G. Thomalla, B. K. Menon, A. Demchuk, M. Wintermark, S. Pedraza, and M. Castellanos. High-permeability region size on perfusion CT predicts hemorrhagic transformation after intravenous thrombolysis in stroke. *PLoS One*, 12(11):e0188238, Nov. 2017.

[135] A. I. Qureshi, A. D. Mendelow, and D. F. Hanley. Intracerebral haemorrhage. *The Lancet*, 373(9675): 1632–1644, May 2009.

[136] P. Reinstrup, N. Ståhl, P. Mellergård, T. Uski, U. Ungerstedt, and C.-H. Nordström. Intracerebral microdialysis in clinical practice: baseline values for chemical markers during wakefulness, anesthesia, and neurosurgery. *Neurosurgery*, 47(3):701–710, Sept. 2000.

[137] K. Rejdak, A. Petzold, M. A. Sharpe, A. D. Kay, M. Kerr, G. Keir, E. J. Thompson, and G. Giovannoni. Cerebrospinal fluid nitrite/nitrate correlated with oxyhemoglobin and outcome in patients with subarachnoid hemorrhage. *Journal of the Neurological Sciences*, 219(1-2):71–76, Apr. 2004.

[138] D. J. Roberts, C. N. Jenne, C. Léger, A. H. Kramer, C. N. Gallagher, S. Todd, I. F. Parney, C. J. Doig, V. W. Yong, P. Kubes, and D. A. Zygun. A Prospective Evaluation of the Temporal Matrix Metalloproteinase Response after Severe Traumatic Brain Injury in Humans. *Journal of Neurotrauma*, 30(20):1717–1726, Oct. 2013.

[139] B. Roozenbeek, A. I. R. Maas, and D. K. Menon. Changing patterns in the epidemiology of traumatic brain injury. *Nature Reviews Neurology*, 9(4):231–236, Feb. 2013.

[140] A. Rosell and E. Lo. Multiphasic roles for matrix metalloproteinases after stroke. *Current Opinion in Pharmacology*, 8(1):82–89, Feb. 2008.

[141] G. A. Rosenberg and M. Navratil. Metalloproteinase inhibition blocks edema in intracerebral hemorrhage in the rat. *Neurology*, 48(4):921–626, Apr. 1997.

[142] G. A. Rosenberg, E. Y. Estrada, and J. E. Dencoff. Matrix Metalloproteinases and TIMPs Are Associated With Blood-Brain Barrier Opening After Reperfusion in Rat Brain. *Stroke*, 29(10):2189–2195, Oct. 1998.

[143] E. Rostami, H. Engquist, and P. Enblad. Imaging of Cerebral Blood Flow in Patients with Severe Traumatic Brain Injury in the Neurointensive Care. *Frontiers in Neurology*, 5:4, July 2014.

[144] J. Sahuquillo, M.-A. Merino, A. Sánchez-Guerrero, F. Arikan, M. Vidal-Jorge, T. Martínez-Valverde, A. Rey, M. Riveiro, and M.-A. Poca. Lactate and the Lactate-to-Pyruvate Molar Ratio Cannot Be Used as Independent Biomarkers for Monitoring Brain Energetic Metabolism: A Microdialysis Study in Patients with Traumatic Brain Injuries. *PLoS One*, 9(7):e102540, July 2014.

[145] K. E. Sandoval and K. A. Witt. Blood-brain barrier tight junction permeability and ischemic stroke. *Neurobiology of Disease*, 32(2):200–219, Nov. 2008.

[146] S. Schwarzmaier, S.-W. Kim, R. Trabold, and N. Plesnila. Temporal Profile of Thrombogenesis in the Cerebral Microcirculation after Traumatic Brain Injury in Mice. *Journal of Neurotrauma*, 27(1):121–130, Jan. 2010.

[147] S. Schwarzmaier, N. Terpolilli, A. Dienel, M. Gallozzi, R. Schinzel, F. Tegtmeier, and N. Plesnila. Endothelial Nitric Oxide Synthase Mediates Arteriolar Vasodilatation after Traumatic Brain Injury in Mice. *Journal of Neurotrauma*, 32(10):731–738, May 2015.

[148] B. D. Semple, N. Bye, M. Rancan, J. M. Ziebell, and M. C. Morganti-Kossmann. Role of CCL2 (MCP-1) in Traumatic Brain Injury (TBI): Evidence from Severe TBI Patients and CCL2 -/- Mice. *Journal of Cerebral Blood Flow and Metabolism*, 30(4):769–782, Apr. 2010.

[149] R. J. Shannon, K. L. H. Carpenter, M. R. Guilfoyle, A. Helmy, and P. J. Hutchinson. Cerebral microdialysis in clinical studies of drugs: pharmacokinetic applications. *Journal of Pharmacokinetics and Pharmacodynamics*, 40(3):343–358, June 2013.

[150] D. Shen, G. Wu, and H.-I. Suk. Deep Learning in Medical Image Analysis. *Annual Review of Biomedical Engineering*, 19(1):221–248, June 2017.

[151] F. Shen, H. Su, Y. Fan, Y. Chen, Y. Zhu, W. Liu, W. L. Young, and G.-Y. Yang. Adeno-associated viral-vector-mediated hypoxia-inducible vascular endothelial growth factor gene expression attenuates ischemic brain injury after focal cerebral ischaemia in mice. *Stroke*, 37(10):2601–2606, Oct. 2006.

[152] A. A. Shestov, X. Liu, Z. Ser, A. A. Cluntun, Y. P. Hung, L. Huang, D. Kim, A. Le, G. Yellen, J. G. Albeck, and J. W. Locasale. Quantitative determinants of aerobic glycolysis identify flux through the enzyme GAPDH as a limiting step. *eLife*, 3:e03342, July 2014.

[153] Y. Shigemori, Y. Katayama, T. Mori, T. Maeda, and T. Kawamata. Matrix metalloproteinase-9 is associated with blood-brain barrier opening and brain edema formation after cortical contusion in rats. In *Brain Edema XIII*, pages 130–133. Springer, Vienna, Vienna, 2006.

[154] D. Shlosberg, M. Benifla, D. Kaufer, and A. Friedman. Blood–brain barrier breakdown as a therapeutic target in traumatic brain injury. *Nature Reviews Neurology*, 6(7):393–403, July 2010.

[155] M. K. Sköld, C. V. Gertten, A.-C. Sandbergnordqvist, T. Mathiesen, and S. Holmin. VEGF and VEGF receptor expression after experimental brain contusion in rat. *Journal of Neurotrauma*, 22(3):353–367, Mar. 2005.

[156] M. Slevin, J. Krupinski, A. Slowik, P. Kumar, A. Szczudlik, and J. Gaffney. Serial Measurement of Vascular Endothelial Growth Factor and Transforming Growth Factor-β1 in Serum of Patients With Acute Ischemic Stroke. *Stroke*, 31(8):1863–1870, Aug. 2000.

[157] G. N. Smith Jr, E. A. Mickler, K. A. Hasty, and K. D. Brandt. Specificity of inhibition of matrix metalloproteinase activity by doxycycline: Relationship to structure of the enzyme. *Arthritis & Rheumatism*, 42(6):1140–1146, June 1999.

[158] S. P. Sourbron and D. L. Buckley. Classic models for dynamic contrast-enhanced MRI. *NMR in Biomedicine*, 26(8):1004–1027, May 2013.

[159] J. A. Sparano, P. Bernardo, P. Stephenson, W. J. Gradishar, J. N. Ingle, S. Zucker, and N. E. Davidson. Randomized Phase III Trial of Marimastat Versus Placebo in Patients With Metastatic Breast Cancer Who Have Responding or Stable Disease After First-Line Chemotherapy: Eastern Cooperative Oncology Group Trial E2196. *Journal of Clinical Oncology*, 22(23):4683–4690, Dec. 2004.

[160] S. M. Stamatovic. Potential role of MCP-1 in endothelial cell tight junction 'opening': signaling via Rho and Rho kinase. *Journal of cell science*, 116(22):4615–4628, Nov. 2003.

[161] S. M. Stamatovic, P. Shakui, R. F. Keep, B. B. Moore, S. L. Kunkel, N. Van Rooijen, and A. V. Andjelkovic. Monocyte Chemoattractant Protein-1 Regulation of Blood–Brain Barrier Permeability. *Journal of Cerebral Blood Flow and Metabolism*, 25(5):593–606, Mar. 2005.

[162] S. C. Stein, X.-H. Chen, G. P. Sinson, and D. H. Smith. Intravascular coagulation: a major secondary insult in nonfatal traumatic brain injury. *Journal of Neurosurgery*, 97(6):1373–1377, 2002.

[163] N. Stocchetti, M. Carbonara, G. Citerio, A. Ercole, M. B. Skrifvars, P. Smielewski, T. Zoerle, and D. K. Menon. Severe traumatic brain injury: targeted management in the intensive care unit. *The Lancet Neurology*, 16(6):452–464, June 2017.

[164] M. G. Stovell, M. O. Mada, A. Helmy, T. A. Carpenter, E. P. Thelin, J.-L. Yan, M. R. Guilfoyle, I. Jalloh, D. J. Howe, P. Grice, A. Mason, S. Giorgi-Coll, C. N. Gallagher, M. P. Murphy, D. K. Menon, P. J. Hutchinson, and K. L. H. Carpenter. The effect of succinate on brain NADH/NAD+ redox state and high energy phosphate metabolism in acute traumatic brain injury. *Scientific Reports*, 8(1):1, July 2018.

[165] K. Strle, J. H. Zhou, W. H. Shen, S. R. Broussard, R. W. Johnson, G. G. Freund, R. Dantzer, and K. W. Kelley. Interleukin-10 in the brain. *Critical Reviews in Immunology*, 21(5):427–449, 2001.

[166] H. Takuwa, T. Matsuura, R. Bakalova, T. Obata, and I. Kanno. Contribution of nitric oxide to cerebral blood flow regulation under hypoxia in rats. *The Journal of Physiological Sciences*, 60(6):399–406, Oct. 2010.

[167] C. Tao, X. Hu, H. Li, and C. You. White Matter Injury after Intracerebral Hemorrhage: Pathophysiology and Therapeutic Strategies. *Frontiers in Human Neuroscience*, 11:5877, Aug. 2017.

[168] A. Tennant. Admission to hospital following head injury in England: Incidence and socio-economic associations. *BMC Public Health*, 5(1):21, 2005.

[169] N. A. Terpolilli, K. Zweckberger, R. Trabold, L. Schilling, R. Schinzel, F. Tegtmeier, and N. Plesnila. The novel nitric oxide synthase inhibitor 4-amino-tetrahydro-L-biopterine prevents brain edema formation and intracranial hypertension following traumatic brain injury. *Journal of Neurotrauma*, 26(11): 110306202455053–1975, Mar. 2011.

[170] N. A. Terpolilli, S.-W. Kim, S. C. Thal, W. M. Kuebler, and N. Plesnila. Inhaled Nitric Oxide Reduces Secondary Brain Damage after Traumatic Brain Injury in Mice. *Journal of Cerebral Blood Flow and Metabolism*, 33(2):311–318, Dec. 2012.

[171] E. P. Thelin, K. L. H. Carpenter, P. J. Hutchinson, and A. Helmy. Microdialysis Monitoring in Clinical Traumatic Brain Injury and Its Role in Neuroprotective Drug Development. *The AAPS Journal*, 19(2): 367–376, Jan. 2017.

[172] I. Timofeev, K. L. H. Carpenter, J. Nortje, P. G. Al-Rawi, M. T. O'Connell, M. Czosnyka, P. Smielewski, J. D. Pickard, D. K. Menon, P. J. Kirkpatrick, A. K. Gupta, and P. J. Hutchinson. Cerebral extracellular chemistry and outcome following traumatic brain injury: a microdialysis study of 223 patients. *Brain*, 134(2):484–494, Jan. 2011.

[173] I. Timofeev, M. Czosnyka, K. L. H. Carpenter, J. Nortje, P. J. Kirkpatrick, P. G. Al-Rawi, D. K. Menon, J. D. Pickard, A. K. Gupta, and P. J. Hutchinson. Interaction between Brain Chemistry and Physiology after Traumatic Brain Injury: Impact of Autoregulation and Microdialysis Catheter Location. *Journal of Neurotrauma*, 28(6):849–860, June 2011.

[174] M. M. Tisdall, K. Rejdak, N. D. Kitchen, M. Smith, and A. Petzold. The prognostic value of brain extracellular fluid nitric oxide metabolites after traumatic brain injury. *Neurocritical Care*, 19(1):65–68, Oct. 2011.

[175] N. Toda, K. Ayajiki, and T. Okamura. Cerebral blood flow regulation by nitric oxide in neurological disorders. *Canadian Journal of Physiology and Pharmacology*, 87(8):581–594, Aug. 2009.

[176] J. S. Truettner, O. F. Alonso, and W. D. Dietrich. Influence of Therapeutic Hypothermia on Matrix Metalloproteinase Activity after Traumatic Brain Injury in Rats. *Journal of Cerebral Blood Flow and Metabolism*, 25(11):1505–1516, May 2005.

[177] A. W. Unterberg, J. Stover, B. Kress, and K. L. Kiening. Edema and brain trauma. *Neuroscience*, 129(4): 1019–1027, Jan. 2004.

[178] M. Uzan, N. Tanriover, H. Bozkus, K. Gumustas, O. Guzel, and C. Kuday. Nitric Oxide (NO) metabolism in the cerebrospinal fluid of patients with severe head injury. *Surgical Neurology*, 56(6): 350–356, Dec. 2001.

[179] N. van Bruggen, H. Thibodeaux, J. T. Palmer, W. P. Lee, L. Fu, B. Cairns, D. Tumas, R. Gerlai, S.-P. Williams, M. v. L. Campagne, and N. Ferrara. VEGF antagonism reduces edema formation and tissue damage after ischemia/reperfusion injury in the mouse brain. *The Journal of Clinical Investigation*, 104 (11):1613–1620, Dec. 1999.

[180] S. van Buuren and K. Groothuis-Oudshoorn. mice: Multivariate Imputation by Chained Equations in R. *Journal of Statistical Software*, 45(1):1–67, Dec. 2011.

[181] J. Vandooren, P. E. Van den Steen, and G. Opdenakker. Biochemistry and molecular biology of gelatinase B or matrix metalloproteinase-9 (MMP-9): the next decade. *Critical Reviews in Biochemistry and Molecular Biology*, 48(3):222–272, May 2013.

[182] R. Veksler, I. Shelef, and A. Friedman. Blood-Brain Barrier Imaging in Human Neuropathologies. *Archives of Medical Research*, 45(8):646–652, Nov. 2014.

[183] R. Veltkamp, D. A. Siebing, L. Sun, S. Heiland, K. Bieber, H. H. Marti, S. Nagel, S. Schwab, and M. Schwaninger. Hyperbaric oxygen reduces blood-brain barrier damage and edema after transient focal cerebral ischemia. *Stroke*, 36(8):1679–1683, Aug. 2005.

[184] P. Vespa, R. Boonyaputthikul, D. L. McArthur, C. Miller, M. Etchepare, M. Bergsneider, T. Glenn, N. Martin, and D. Hovda. Intensive insulin therapy reduces microdialysis glucose values without altering glucose utilization or improving the lactate/pyruvate ratio after traumatic brain injury. *Critical Care Medicine*, 34(3):850–856, Mar. 2006.

[185] P. M. Vespa, K. O'Phelan, D. McArthur, C. Miller, M. Eliseo, D. Hirt, T. Glenn, and D. A. Hovda. Pericontusional brain tissue exhibits persistent elevation of lactate/pyruvate ratio independent of cerebral perfusion pressure*. *Critical Care Medicine*, 35(4):1153–1160, Apr. 2007.

[186] A. Vilalta, J. Sahuquillo, M. A. Poca, J. De Los Rios, E. Cuadrado, A. Ortega-Aznar, M. Riveiro, and J. Montaner. Brain contusions induce a strong local overexpression of MMP-9. Results of a pilot study. In *Acta Neurochirurgica Supplements*, pages 415–419. Springer, Vienna, Vienna, 2008.

[187] A. Vilalta, J. Sahuquillo, A. Rosell, M. A. Poca, M. Riveiro, and J. Montaner. Moderate and severe traumatic brain injury induce early overexpression of systemic and brain gelatinases. *Intensive Care Medicine*, 34(8):1384–1392, Mar. 2008.

[188] N. Villalba, S. K. Sonkusare, T. A. Longden, T. L. Tran, A. M. Sackheim, M. T. Nelson, G. C. Wellman, and K. Freeman. Traumatic Brain Injury Disrupts Cerebrovascular Tone Through Endothelial Inducible Nitric Oxide Synthase Expression and Nitric Oxide Gain of Function. *Journal of the American Heart Association*, 3(6):e001474–e001474, Dec. 2014.

[189] R. Wada, R. I. Aviv, A. J. Fox, D. J. Sahlas, D. J. Gladstone, G. Tomlinson, and S. P. Symons. CT Angiography "Spot Sign" Predicts Hematoma Expansion in Acute Intracerebral Hemorrhage. *Stroke*, 38(4):1257–1262, Apr. 2007.

[190] W. Wang, W. L. Dentler, and R. T. Borchardt. VEGF increases BMEC monolayer permeability by affecting occludin expression and tight junction assembly. *American Journal of Physiology: Heart and Circulatory Physiology*, 280(1):H434–40, Jan. 2001.

[191] Y. Wang. VEGF overexpression induces post-ischaemic neuroprotection, but facilitates haemodynamic steal phenomena. *Brain*, 128(1):52–63, Nov. 2004.

[192] Z. Wang, K. Zheng, P. Zheng, W. Fan, C. Li, H. Liu, and X. Shan. Matrix metalloproteinases and their tissue inhibitors in serum and cerebrospinal fluid of patients with moderate and severe traumatic brain injury. *Neurology India*, 61(6):606–609, 2013.

[193] X.-E. Wei, D. Wang, M.-H. Li, Y.-Z. Zhang, Y.-H. Li, and W.-B. Li. A Useful Tool for the Initial Assessment of Blood–Brain Barrier Permeability After Traumatic Brain Injury in Rabbits: Dynamic Contrast-Enhanced Magnetic Resonance Imaging. *The Journal of Trauma: Injury, Infection, and Critical Care*, 71(6): 1645–1651, Dec. 2011.

[194] X.-E. Wei, Y.-Z. Zhang, Y.-H. Li, M.-H. Li, and W.-B. Li. Dynamics of Rabbit Brain Edema in Focal Lesion and Perilesion Area after Traumatic Brain Injury: A MRI Study . *Journal of Neurotrauma*, 29(14): 2413 –2420, Sept. 2012.

[195] X.-E. Wei, Y.-Z. Zhang, Y.-H. Li, M.-H. Li, and W.-B. Li. Dynamics of Rabbit Brain Edema in Focal Lesion and Perilesion Area after Traumatic Brain Injury: A MRI Study. *Journal of Neurotrauma*, 29(14): 2413–2420, Sept. 2012.

[196] M. J. Whalen, T. M. Carlos, P. M. Kochanek, S. R. Wisniewski, M. J. Bell, R. S. Clark, S. T. DeKosky, D. W. Marion, and P. D. Adelson. Interleukin-8 is increased in cerebrospinal fluid of children with severe head injury. *Critical Care Medicine*, 28(4):929–934, Apr. 2000.

[197] B. Wójciak-Stothard, A. Entwistle, R. Garg, and A. J. Ridley. Regulation of TNF-α-induced reorganization of the actin cytoskeleton and cell-cell junctions by Rho, Rac, and Cdc42 in human endothelial cells. *Journal of Cellular Physiology*, 176(1):150–165, July 1998.

[198] D. Wong and K. Dorovini-Zis. Regulation by Cytokines and Lipopolysaccharide of E-selectin Expression by Human Brain Microvessel Endothelial Cells in Primary Culture. *Journal of Neuropathology and Experimental Neurology*, 55(2):225–235, Feb. 1996.

[199] S. N. Wood. Fast stable restricted maximum likelihood and marginal likelihood estimation of semi-parametric generalized linear models. *Journal of the Royal Statistical Society. Series B: Statistical Methodology*, 73(1):3–36, Jan. 2011.

[200] T. Woodcock and C. Morganti-Kossmann. The Role of Markers of Inflammation in Traumatic Brain Injury. *Frontiers in Neurology*, 4, Mar. 2013.

[201] M. Yamaguchi, V. Jadhav, A. Obenaus, A. Colohan, and J. H. Zhang. Matrix metalloproteinase inhibition attenuates brain edema in an in vivo model of surgically-induced brain injury. *Neurosurgery*, 61 (5):1067–1076, Nov. 2007.

[202] Y. Yang, E. Y. Estrada, J. F. Thompson, W. Liu, and G. A. Rosenberg. Matrix Metalloproteinase-Mediated Disruption of Tight Junction Proteins in Cerebral Vessels is Reversed by Synthetic Matrix

Metalloproteinase Inhibitor in Focal Ischemia in Rat. *Journal of Cerebral Blood Flow and Metabolism*, 27 (4):697–709, Aug. 2006.

[203] W. L. Yeh, D. Y. Lu, C. J. Lin, H. C. Liou, and W. M. Fu. Inhibition of Hypoxia-Induced Increase of Blood-Brain Barrier Permeability by YC-1 through the Antagonism of HIF-1 Accumulation and VEGF Expression. *Molecular Pharmacology*, 72(2):440–449, July 2007.

[204] Q. Yuan, Y.-r. Sun, X. Wu, J. Yu, Z.-q. Li, Z.-y. Du, X.-h. Wu, L.-f. Zhou, and J. Hu. Coagulopathy in Traumatic Brain Injury and Its Correlation with Progressive Hemorrhagic Injury: A Systematic Review and Meta-Analysis. *Journal of Neurotrauma*, 33(14):1279–1291, July 2016.

[205] Z. G. Zhang, L. Zhang, Q. Jiang, R. Zhang, K. Davies, C. Powers, N. v. Bruggen, and M. Chopp. VEGF enhances angiogenesis and promotes blood-brain barrier leakage in the ischemic brain. *The Journal of Clinical Investigation*, 106(7):829–838, Oct. 2000.

[206] B.-Q. Zhao, E. Tejima, and E. H. Lo. Neurovascular Proteases in Brain Injury, Hemorrhage and Remodeling After Stroke. *Stroke*, 38(2):748–752, Feb. 2007.

[207] K.-J. Zhao, Y. Liu, R.-Y. Zhang, X.-Q. Wang, C. Gao, and J.-K. Shen. A precise, simple, convenient and new method for estimation of intracranial hematoma volume – the formula 2/3Sh. *Neurological Research*, 31(10):1031–1036, July 2013.

[208] K.-J. Zhao, R.-Y. Zhang, Q.-F. Sun, X.-Q. Wang, X.-Y. Gu, Q. Qiang, C. Gao, and J.-K. Shen. Comparisons of 2/3Sh estimation technique to computer-assisted planimetric analysis in epidural, subdural and intracerebral hematomas. *Neurological Research*, 32(9):910–917, July 2013.

[209] L. Zhao, M. M. Zhang, and K.-y. Ng. Effects of Vascular Permeability Factor on the Permeability of Cultured Endothelial Cells from Brain Capillaries. *Journal of Cardiovascular Pharmacology*, 32(1):1, July 1998.